

COMMUNAL CELL DEATH AND
P53 MEDIATED TRANSCRIPTIONAL CONTROL IN
DROSOPHILA MELANOGASTER

APPROVED BY SUPERVISORY COMMITTEE

John M. Abrams, Ph.D. (Mentor) _____

Melanie Cobb, Ph.D. _____

James F. Amatruda, M.D., Ph.D. _____

Joachim Seemann, Ph.D. _____

DEDICATION

This is dedicated to Kathy Montgomery.

COMMUNAL CELL DEATH AND
P53 MEDIATED TRANSCRIPTIONAL CONTROL IN
DROSOPHILA MELANOGASTER

BY

NICHOLE LINK

DISSERTATION

Presented to the Faculty of the Graduate School of Biomedical Sciences

The University of Texas Southwestern Medical Center at Dallas

In Partial Fulfillment of the Requirements

For the Degree of

DOCTOR OF PHILOSOPHY

The University of Texas Southwestern Medical Center at Dallas

Dallas, Texas

January, 2011

Copyright

by

NICHOLE LINK, 2011

All Rights Reserved

COMMUNAL CELL DEATH AND
P53 MEDIATED TRANSCRIPTIONAL CONTROL IN
DROSOPHILA MELANOGASTER

Publication No. _____

NICHOLE LINK, Ph.D.

The University of Texas Southwestern Medical Center at Dallas, 2011

Supervising Professor: John M. Abrams, Ph.D.

Apoptosis is essential for all metazoan development. The key component that functions in apoptosis, the apoptosome, is a molecular machine that initiates caspase activation and is conserved throughout the animal kingdom. *Drosophila* strains that are mutated for genes encoding the apoptosome show pronounced defects in programmed

cell death (PCD). Using a characteristic phenotype associated with mosaic animals, we conducted a screen in *Drosophila* to discover new regulators or effectors of the apoptosome. Using this model, we also discovered a unique communal form of cell death where large regions of epithelial cells are eliminated within minutes.

We also produced ‘saturation tile’ arrays by digital optical chemistry for an unbiased sampling of transcriptional activity in the *Drosophila* genome. We found that the scope of unannotated transcriptional activity is extensive and widespread. A dominant population of noncanonical transcripts was stress-responsive and required p53, a master regulator of conventional stress-responsive target genes in vertebrates and invertebrates. This prompted us to examine stimulus dependent activity surrounding a single p53 enhancer in our tiled region. Through genetic analyses, we showed that this enhancer coordinates stimulus dependent induction of multiple genes spanning over 300kb throughout the Reaper region. Surprisingly, this same enhancer regulated a gene positioned across the centromere at distances over 20Mb and also controlled at least one gene mapping to a different chromosome. Chromosome conformation capture analyses placed this enhancer in close proximity to these distant targets *in vivo* through specific DNA looping and these interactions were influenced by p53. Therefore, a single p53 enhancer is necessary and sufficient for long range, multigenic regulation in *cis* and in *trans*.

ACKNOWLEDGEMENTS

I thank my mentor, Dr. John M. Abrams, who is an exceptionally brilliant scientist and a kind and supportive man. I am a bit more fragile than I should be, and he adapted his mentoring to help me develop professionally and personally. He has made an enormous effort to help me grow from an ignorant young scientist to what I am today. I am incredibly lucky to have found John as a mentor. I admire you, sir.

I also thank my thesis committee members Drs. James Amatruda, Woody Wright, Melanie Cobb, and previous member Matthew Porteus for their support and suggestions regarding my project.

Collaboration with Skip Garner's lab was essential for array design and experimentation.

In addition, I acknowledge former and current members of the Abrams lab: Anna Christich, Su Kit Chew, Kathleen Galindo, Po Chen, Melissa O'Neal, Mahesh Vaishnav, Alex D'brot, Sophie Tu, and Wan-Jin Lu. Thanks to Margaret Allen, Amy Haughey and Charlotte Roberson for their administrative assistance.

Finally, I thank my family for their continued support and Oliver for scientific discussions and understanding as I completed this long journey.

TABLE OF CONTENTS

ACKNOWLEDGEMENTS	vii
TABLE OF CONTENTS	viii
Prior Publications	x
List of Figures	xi
List of Tables	xiv
List of Abbreviations	xv
Forward	17
Characterization of communal cell death and identification of novel programmed cell death mutations in <i>Drosophila melanogaster</i>	20
SUMMARY	20
INTRODUCTION	21
MATERIALS AND METHODS	26
RESULTS	32
DISCUSSION	45
PERSPECTIVES AND FUTURE DIRECTIONS	49
Stimulus-responsive noncanonical transcription in <i>Drosophila melanogaster</i>	93
SUMMARY	93
INTRODUCTION	94
MATERIALS AND METHODS	96
RESULTS	100
DISCUSSION	107
PERSPECTIVES AND FUTURE DIRECTIONS	109
Multigenic regulation through a single p53 enhancer in <i>cis</i> and in <i>trans</i>	130

SUMMARY	130
INTRODUCTION	131
MATERIAL AND METHODS	133
RESULTS	138
DISCUSSION	143
PERSPECTIVES AND FUTURE DIRECTIONS	147
Bibliography	174

PRIOR PUBLICATIONS

1. Link N, Chen P, Lu WJ, Pogue K, Chuong A, Mata M, Checketts J, and J. M. Abrams. (2007) A collective form of cell death requires homeodomain interacting protein kinase. ***Journal of Cell Biology*** 178: 567-574. [[Pubmed](#)]
2. Chew SK, Chen P, Link N, Galindo K A, Pogue K, and J.M. Abrams. (2009) Genome-wide silencing in Drosophila captures conserved apoptotic effectors. ***Nature*** 460: 123-127.

LIST OF FIGURES

Figure 1-1. Apoptosis is conserved throughout evolution.	51
Figure 1-2. Canonical cell death mutations display a progressive blemish phenotype. .	52
Figure 1-3. Apoptosis in the wing requires the canonical cell death pathway.	53
Figure 1-4. Epithelial wing cells are removed by apoptosis.	54
Figure 1-5. Collective cell death eliminates the wing epithelium	55
Figure 1-6. Rational for clonal analysis of communal cell death in the wing	56
Figure 1-7. Communal cell death is cell autonomous.	57
Figure 1-8. Screen for cell death defective mutations.....	58
Figure 1-9. Classification of wing phenotypes.....	59
Figure 1-10. Generation of a null mutation in <i>homeodomain interacting protein kinase</i> .	60
Figure 1-11. HIPK is required for communal cell death in the wing	61
Figure 1-12. <i>hipk</i> null mutants display developmental defects.....	62
Figure 1-13. HIPK displays normal developmental cell death in the embryo	63
Figure 1-14. Without HIPK, excessive neurons and cells are retained.	64
Figure 1-15. HIPK displays normal stress-induced cell death.....	65
Figure 1-16. I(3)S141405 displays cell death defects in the wing	66
Figure 1-17. I(3)S141405 is required for embryonic cell death	67
Figure 1-18. I(3)S141405 is required for neuronal development.....	68
Figure 1-19. I(3)s141405 ^{phop} mildly rescues Hid induced killing but does not block developmental cell death in the eye.....	69
Figure 1-20. Tango7 is required for interommatidial cell death.....	70

Figure 2-1. Stress induces abundant and validated unannotated RNAs (unRNAs).	110
Figure 2-2. Many unannotated transcripts are radiation responsive and <i>p53</i> dependent.	111
Figure 2-3. Novel transcript conservation between species varies.	112
Figure 2-4. Deletions of UNTs	113
Figure 2-5. Validation of novel transcript deletion animals.....	114
Figure 2-6. D2 animals lay short eggs.	116
Figure 2-7. D2 animals have low hatch rates.....	117
Figure 2-8. D2 animals have mild developmental defects.....	118
Figure 2-9. Novel transcript mutations have lower eclosion rates after irradiation but are dependent upon background effects.....	119
Figure 2-10. Eclosion rates of trans-heterozygous animals at 0 and 2 krad indicated background effects.	120
Figure 2-11. Pupation rates after irradiation.....	121
Figure 2-12. Novel transcript deletions are not defective in irradiation induced cell death.	122
Figure 2-13. Twin spot analysis.	123
Figure 2-14. Twin spot analysis reveals that H99 out competes wild type tissue but UNT mutations do not.	124
Figure 2-15. Mutants recover fertility after 11kr irradiation.....	125
Figure 3-1. The <i>p53</i> response element maps near validated stress induced pro- apoptotic genes.	151

Figure 3-2. The p53 enhancer regulates stimulus-induced transcription of multiple genes in the reaper region.....	152
Figure 3-3. The p53 enhancer does not regulate <i>grim</i> , an unresponsive cell death gene in the Reaper region.	153
Figure 3-4. The p53 enhancer regulates stimulus-induced transcription of multiple Radiation Induced, p53 dependent (RIPD) genes outside of the reaper region....	154
Figure 3-5. The p53 enhancer loops to multiple genes in the reaper region.....	155
Figure 3-6. 3C looping to the p53RE is validated and specific.....	156
Figure 3-7. The p53 enhancer is necessary for looping.....	157
Figure 3-8. Fine mapping of looping contacts between the p53RE and Hid locus.....	158
Figure 3-9. The p53 enhancer loops to multiple Radiation Induced, p53 dependent (RIPD) genes outside of the Reaper region.....	159
Figure 3-10. Fine mapping of looping contacts between the p53RE and distant loci <i>xrp1</i> and <i>ku80</i>	160
Figure 3-11. p53RE looping is developmentally dynamic.	161
Figure 3-12. Reaper region looping is developmentally dynamic.....	162
Figure 3-13. XRP1 region looping is developmentally dynamic.....	163
Figure 3-14. Ku80 region looping is developmentally dynamic.....	164
Figure 3-15. An exogenous rescue construct restores looping to the Ku80 region in D2 ^{p53RE} mutants.....	165

LIST OF TABLES

Table 1-1. High priority phenocopy hits.....	73
Table 1-2. High priority phenocopy hit phenotypes.....	77
Table 1-3. Low priority phenocopy hits	83
Table 1-4. Low priority phenocopy hit phenotypes.....	91
Table 2-1. Sequences of primers used to identify novel transcripts.....	126
Table 2-2. Novel transcript data.....	128
Table 2-3. Nearest neighbor for select transcripts	129
Table 3-1. Affymetrix array data indicates RIPD genes require the p53RE for regulation	167
Table 3-2. Primer sequences used in RT-PCR reactions	168
Table 3-3. BACs used to verify 3C primer pairs.....	169
Table 3-4. Primer sequences used in 3C reactions	172

LIST OF ABBREVIATIONS

3C- Chromosome conformation capture

4C-Chromosome conformation capture on chip

BAC- Bacterial artificial chromosome

BH3 – Bcl-2 homology 3

Bcl- B-cell lymphoma

Caspase – CysteinyI aspartate-specific protease

Ced – Cell death defective

CNS-central nervous system

Dark – Drosophila apaf-1 related killer

DIAP- Drosophila inhibitor of apoptosis protein

Dp53 – Drosophila melanogaster p53

Dp53RE- Drosophila melanogaster p53 response element

Dronc – Drosophila nedd2-like caspase

dsRNA- double stranded RNA

ENCODE- Encyclopedia of DNA elements

FLP-Flippase

FRT- FLP recognition target

GFP – Green fluorescence protein

Hid – Head involution defective

HIPK- Homeodomain interacting protein kinase

Hs- heat shock

IAP – Inhibitor of apoptosis protein

IR – ionizing radiation

Kb-kilobases

Krad- kilorads

Mb-megabases

modENCODE- model organism encyclopedia of DNA elements

ncRNA- noncoding RNA

PCD- programmed cell death

RFP- Red fluorescent protein

RIPD – Radiation induced p53 dependent

RNAi – RNA interference

Rpr – Reaper

Skl – Sickle

TM1- Tropomyosin 1

TUNEL- Terminal deoxynucleotidyl transferase dUTP nick end labeling

UAS- Upstream activating sequence

UV – ultra-violet

UNT- Unannotated transcripts

Vg- Vestigial

Forward

Upon joining the lab, I became heavily involved in a screen for novel cell death mutations. We used the wing as a model to identify genes required for cell death. As we characterized cell death in the wing, we found that these cells underwent an unappreciated form of cell death we coined “communal cell death.” Understanding the mechanism of communal cell death in the wing could perhaps illuminate mechanisms involved in such processes as mammary or uterine involution, where enlarged tissues undergo several steps, including epithelial cell death, to return to its normal state. Mutants identified from this screen could provide insights into communal cell death, and currently, work is ongoing to identify what stimulates this novel process.

At the same time, the scientific community was beginning to understand that much more of the genome is transcribed than previously thought. I joined the lab at the beginning of a provocative project aimed to map and characterize noncanonical transcription using a genetic model. We generated a saturation tilling array with the Garner lab and explored novel RNA labeling technology to try to identify the best way to map unannotated transcription. We quickly found that technology at the time was not ideal, but eventually we were able to map unannotated RNAs and begin our aim to identify function, if any, of these novel RNAs.

During my work to characterize these noncanonical transcripts, I generated several deletions for loss of function analysis. One of these mutations also removed a very well characterized p53 transcription factor binding site. Upon closer examination of this mutant, we discovered phenotypes suggesting that a single p53 binding site might

be able to control transcription of genes throughout the genome. If these findings are conserved, enhancer-promoter transcriptional control might be complicated by long-range cross-chromosomal control. This extremely exciting and fast moving project concludes my thesis work. My dissertation aims are presented below.

Dissertation objectives

The aim of my thesis study is divided into three main themes: 1) to characterize communal cell death while using this model to identify novel apoptotic proteins, and 2) explore stimulus and p53 dependent noncanonical transcription and 3) map p53 transcriptional regulation of multiple genes through a single enhancer. The following specific aims will be presented in subsequent chapters.

Characterization of communal cell death

We discovered a novel form of communal cell death in the wing where an entire epithelium is eliminated within minutes. Characterization of communal cell death is presented in Chapter One.

Identification of novel cell death defective mutations

Using the wing, we queried lethal mutations for defects in communal cell death. Our efforts are intended to provide insights in both coordination of communal cell death and control of the canonical cell death pathway. Results from this project are presented in Chapter One.

Exploration of noncanonical transcriptional activity in the Reaper region

We used saturation tiling arrays to map all transcriptional activity in a well-characterized region of the *Drosophila* genome. We found a vast amount of unannotated transcription throughout the region, and using sophisticated genetic tools, we assessed a select number of these unannotated transcripts for function. Results from this aim are presented in Chapter Two.

Map multigenic regulation through a single p53 enhancer that acts in cis and in trans

Using loss-of-function genetic analysis, we examined stimulus dependent activity at a single p53 enhancer and found this enhancer coordinates induction of multiple genes throughout the genome. We describe how this enhancer controls expression of multiple targets in Chapter Three.

Characterization of communal cell death and identification of novel programmed cell death mutations in *Drosophila melanogaster*

SUMMARY

Apoptosis is essential for the development of metazoans. The key component that functions in apoptosis, the apoptosome, is a molecular machine that initiates caspase activation and is conserved throughout the animal kingdom. *Drosophila* strains that are mutated for genes encoding the apoptosome show pronounced defects in programmed cell death (PCD).

We applied a live imaging RFP reporter system to examine programmed elimination of the wing epithelium in newly eclosed flies. In this context, we found a novel type of cell death, which occurs communally, in the form of rapid, collective 'suicide waves' without a final engulfment step. We further showed that like apoptotic death in earlier developmental stages, this collective form of cell death is controlled through the apoptosome proteins, together with the IAP antagonists. Lesions in these pathways caused epithelial cells to persist, prompting a characteristic late-onset phenotype. We validated this unique abnormality as a powerful indicator for PCD defects and leveraged these observations to identify new cell death genes. Our screening rationale recovers mutants that phenocopy tissues lacking apoptogenic effectors. Relevant genes discovered from this analysis will be discussed.

INTRODUCTION

Apoptosis

Apoptosis, or programmed cell death (PCD), describes the deliberate removal of cells in development, normal aging, and disease. This form of cell death is driven by conversion of inactive enzymes called caspases to their activated state. Elimination of cells by programmed cell death (PCD) is a universal feature of development and aging (Jacobson et al., 1997; Vaux and Korsmeyer, 1999). In both vertebrates and invertebrates, dying cells often progress through a stereotyped set of transformations referred to as apoptosis. In this form of PCD, the nucleus condenses, and the collapsing cell corpse fragments into “apoptotic bodies” that are engulfed by specialized phagocytes or neighboring cells (Kerr and Harmon, 1991; Kerr et al., 1972; Wyllie et al., 1980). Apoptosis requires autonomous genetic functions within the dying cell, and extrinsic cues that elicit apoptosis have been investigated in numerous experimental models (Danial and Korsmeyer, 2004; Salvesen and Abrams, 2004).

Other forms of death are also thought to contribute during development and differ from apoptosis with respect to cellular morphology, mechanism, or mode of activation. These may include necrosis, characterized by swelling of the plasma membrane, or autophagic cell death, which is linked to extensive vacuolization in the cytoplasm (Kroemer and Martin, 2005). These forms of cell death can be caspase dependent or independent and may or may not be under deliberate genetic control (Kroemer and Martin, 2005).

The apoptosome

Apoptosis functions through the highly conserved set of proteins that are collectively known as the apoptosome (Figure 1-1). In mammals, Apaf-1 and Caspase 9 oligomerize to form the apoptosome. Once activated, Caspase 9 subsequently activates downstream caspases (Adams and Cory, 2002). In the nematode, CED-4, an Apaf-1 homolog, directly activates CED-3, the counterpart of Caspase 3. The fly apoptosome consists of Dark, an Apaf-1 homolog, and Dronc, the Caspase 9 homolog. This complex forms when Dark oligomerizes and binds to Dronc. Dronc becomes activated and in turn activates downstream caspases to initiate PCD (Abrams, 1999). These fundamental steps in apoptosis activation are conserved throughout evolution.

Studies in the mouse show that components of the apoptosome are essential for proper PCD in the nervous system. For example, *apaf-1* knockouts exhibit a marked decrease in apoptosis in portions of the hindbrain and midbrain (Yoshida et al., 1998). These knockout mice also show severe defects in the forehead and face due to overproliferation in the forebrain, thalamus, or hypothalamus. Similar studies with mutants of *caspase 9* and *caspase 3* confirm apoptotic defects in the nervous system. *caspase 9* knockouts have enlarged brains due to decreased apoptosis while many other tissues appear normal (Kuida et al., 1998). *caspase 3* mutants show the same protruding defects in the brain as *apaf-1* mutants (Kuida et al., 1996), demonstrating that the components of the apoptosome and their downstream effectors are necessary for correct nervous system development.

In *Drosophila*, mutants in *dark* and *dronc* show similar neuronal phenotypes. *dark* mutants show an enlarged central nervous system compared to wild type animals and have defects in PCD observed most dramatically in the nervous system (Rodriguez et al., 1999). If we rescue a lethal mutation of *dark* specifically in the nervous system, but not in other areas of the animal, we can rescue lethality (Akdemir et al., 2006), demonstrating that apoptotic function is essential in the nervous system. *dronc* mutants possess extra neuronal cells and an enlarged CNS (Chew et al., 2004). Furthermore, animals mosaic for mutant alleles of both *dark* and *dronc* also show a progressive dark blemish phenotype in the wing (Chew et al., 2004; Rodriguez et al., 1999). That is, when the fly first ecloses (emerges), the wings are normal. However, as the fly ages, blemishes appear and worsen with age (See figure 1-2). This unique phenotype is highly characteristic for cell death defective mutants. Even more striking, when mutations for *dark* and *dronc* are combined in the same animal, the progressive phenotype becomes drastically more severe. Likewise, mutants in *Drosophila p53*, (a tumor suppressor known to transmit stress signals to downstream effectors to promote apoptosis) also qualify as enhancers of this phenotype. These genetic interactions indicate that *dark*, *dronc* and *p53* function in a genetic pathway that fundamentally regulates PCD in this model system.

Activation of cell death

As demonstrated from the above studies, the function of the apoptosome is highly conserved, and mutants of the apoptosome show similar characteristics. However, activation of the apoptosome varies in different model systems. In *C.*

elegans, a Bcl-2 family like protein, CED-9, directly interacts with CED-4, the Apaf-1 homolog, to inhibit apoptosis (See figure 1-1)(Hengartner et al., 1992; Yuan and Horvitz, 1992). EGL-1, a pro-apoptotic Bcl-2 protein, directly interacts with CED-9 to release inhibition on CED-4(del Peso et al., 2000) which is then free to activate CED-3, stimulating apoptosis.

Mammalian regulation of PCD is evidently different than the worm and is thought to function through Cytochrome c. Upon stimulation by pro-apoptotic Bcl-2 family members, mitochondria release Cytochrome c, which binds to and oligomerizes with Apaf-1 to form the apoptosome with Caspase 9(Li et al., 1997; Yu et al., 2005). In fibroblast and other mammalian cell types, injection of Cytochrome c is sufficient to induce apoptosis. However, in wild type neuronal cells, injection of Cytochrome c does not induce PCD(Potts et al., 2003), suggesting that, even when comparing different cell types in the same species, distinct pathways regulate the apoptosome. The role of Cytochrome c has been difficult to study *in vivo* because of its additional essential function in electron transport. Recently, Hao *et al.* generated a knock-in *cytochrome c* mouse that could still function in electron transport, but not in the activation of the apoptosome. These knock-in mice have clear apoptotic deficiencies with some defects similar to *apaf-1* knockouts. More intriguing, though, was that in these mice, considerable Apaf-1 dependent, caspase dependent cell deaths still occurred, even in the absence of active Cytochrome c(Hao et al., 2005).

Similar studies suggest Cytochrome c is not an essential element of the apoptosome during PCD in *Drosophila* (Dorstyn et al., 2004; Dorstyn et al., 2002). In

flies, Cytochrome c does not drive the formation of the apoptosome nor is it present within the apoptosome once the complex is formed(Yu et al., 2006). However, it is evident from studies by Yu *et al.* that the structure of the *Drosophila* apoptosome resembles the mammalian apoptosome(Yu et al., 2006).

Together, these findings indicate that 1) additional regulators of the apoptosome may exist and 2) *Drosophila* is a useful model to discover these novel regulators and investigate their functions in the nervous system. The sophisticated experimental tools and genetic manipulations possible in this animal afford us with rigorous approaches to study conserved pathways of cell death.

MATERIALS AND METHODS

Generation of mutant wing clones

The *l(3)Sxxxxxx* (Bellotto et al., 2002) and *l(2)SHxxxx* (Oh et al., 2003) FRT stocks were obtained from Szeged Stock Center. *vg-Gal4, UAS-FLP; FRT79, FRT82* and *vg-Gal4, UAS-FLP, FRT40, FRT42* were provided by K. Basler (University of Zürich, Zürich, Switzerland). *MS1096-Gal4, UAS-FLP* flies are from J. Jiang (UT Southwestern Medical Center, Dallas, TX). *FRT-Df(H99)* stocks were provided by A. Gould (National Institute for Medical Research, London, UK) and J. O'Tousa (University of Notre Dame, Notre Dame, IN). To generate wing clones, 4 males of the genotype *l(3)Sxxxxxx-FRT82/TM3(6)* were crossed to 3 females of *vg-Gal4, UAS-FLP; FRT79, FRT82*. F1 flies were examined at eclosion and at 1 and 2 wk of age for appearance of “melanized blemishes” on the wing. *l(3)Sxxxxxx-FRT80/TM3(6)* and *l(2)SHxxxx-FRT40/Cyo* flies were similarly screened by crossing to *vg-Gal4:UAS-FLP; FRT80* and *vg-Gal4:UAS-FLP, FRT40, FRT42* flies, respectively. *MS1096-Gal4:UAS-FLP; FRT42B* was used for mutations on 2R. Adult wings were removed at different ages and fixed in paraformaldehyde for standard histology. Electron micrographs were generated using an electron microscope (TEMP2 1200 EX II; JEOL).

Detection of persisting wing epithelium

The FLP/FRT system was used to generate mutant wing clones, and persisting cells were visualized using DsRed. *UAS-RedStinger/Cyo; dronc51-FRT79/TM6* was

crossed to *vg-Gal4:UAS-FLP; FRT79, FRT82*. After eclosion, adults were aged from 1 to 14 days. Wings were removed, mounted on glass slides, and visualized using a fluorescent DLM (Axioplan; Carl Zeiss MicroImaging, Inc.) and a monochrome digital camera (Hamamatsu). *Df(H99)-FRT80*, *dark82-FRT42D*, or *HIPKD1-FRT79* lines with or without UAS-RedStinger were also crossed to their respective FLP/FRT lines and imaged as stated above. Epithelial cell death was recorded in time-lapse experiments using the previous crosses to image *w1118; UAS-RedStinger/vg-Gal4, UAS-FLP; TM3(6)/FRT79* adults at 1–2 h after eclosion using a stereomicroscope (SteREO Discovery V.12; Carl Zeiss MicroImaging, Inc.) with Pentafluor S. Adults were glued on their dorsal surface to glass slides and imaged while alive. UAS-RedStinger lines were from Bloomington Stock Center.

Dual color clonal analysis was generated by crossing *ms1096-Gal4, UAS-FLP; FRT42D-GFP* animals to *dark82 FRT42D; UAS-DsRed*. Newly eclosed adults were isolated and immobilized with super glue on glass slides and imaged with SteREO Discovery V.12; Carl Zeiss MicroImaging, Inc.

Inverse PCR

P-element insertion sites were mapped by inverse PCR according to protocols from BDGP (<http://www.fruitfly.org/about/methods/inverse.pcr.html>). Genomic DNA of insertion lines containing the PlacW insertion element was extracted using Wizard Genomic DNA Extraction kit (Promega) and digested with HhaI, HpaII, and MboI restriction enzymes for 2.5 h at 37°C. Resulting digestions were diluted into 400 µl T4

DNA ligase (Roche) reactions and incubated overnight at 4°C. DNA was ethanol precipitated and used in Expand Long Template (Roche) PCR reactions with primers specific to the PlacW insertion. Unique PCR products were gel purified and sequenced, and insertion locations were confirmed using genomic PCR with primer sets specific to PlacW and surrounding genomic sequences.

HIPK deletion strains

Deletions were generated using the Exelixis collection of P elements as described previously (Parks et al., 2004; Thibault et al., 2004). To delete the HIPK locus, insertions f03158 and d10792 were placed in trans together with hs-FLP and heat-shocked to generate a FRT-mediated deletion. PCR primers directed to the remaining P elements and the surrounding genomic locus were used to identify deletion alleles (5'-TACTATTCCTTTCA-CTCGCACTTATTG-3' and 5'-TAGATGAGGAAGTTCTGCGTGCAAGA-3', 5'-CCTCGATATACAGACCGATAAAAC-3' and 5'-CGACCTTCACCGACT-GATCCTGGAT-3'). Two additional primer pairs, one producing a novel PCR product spanning the deleted HIPK locus (5'-GTGTCACTCGAAATT-CGCCAGTGACT-3' and 5'-GACGACTGACTCGGTAGCCTACTTCG-3') while another specific to the deleted locus producing a negative result (5'-CGCTACTATCGTGCTCCCGAAATCAT-3' and 5'-CGGATGCCTTGAC-ATTGTTGCAGT-3'), were used to confirm deletions.

Germline clones

Germline clones were generated using the dominant female sterile technique described previously (Chou and Perrimon, 1996).

Whole eye clones

HIPKD1-FRT79/TM6 animals were crossed to *ey-FLP/Cyo; FRT79 gmr-Hid/TM6y+*, and pupated animals were removed and aged for 48–55 h. After aging, pupal eyes were dissected and fixed in 4% formaldehyde in PBS. Aged matched siblings carrying *TM6y+* were used as controls.

gmr-hid; L(3)S141405^{hop}-FRT82 animals were crossed to *ey-FLP/Cyo; FRT79 gmr-Hid/TM6y+*.

Cell death staining

Embryos were collected and dechorionated in 50% bleach, washed, and transferred to a mixture of 0.05µg/ml acridine orange in PBS and heptane. Vials were shaken for 3 minutes and embryos were transferred to glass slides with halocarbon oil for imaging.

TUNEL stained tissues were fixed in 4% formaldehyde in phosphate buffer and stained as described using Chemicon's ApopTag in situ cell death detection kit with Roche's TdT enzyme. Fluorescein secondary antibodies were used, and tissues were mounted in Vectashield.

Immunohistochemistry

Immunohistochemistry was performed as described in (Chew et al., 2004). Guinea pig α -Kruppel was used 1:600 (Kosman et al., 1998), rabbit α -dHb9 was used 1:500 (Brohier and Skeath, 2002), and α -Dlg was used 1:500 (Developmental Studies Hybridoma Bank) at 4°C overnight. Secondary antibodies used were labeled with Texas red or Fluorecein from Vector Laboratories (1:250) or Alexa 568 from Invitrogen (1:500). Genotyping was done using anti-GFP (1:1,000) from Invitrogen recognizing GFP-labeled balancers. Confocal z-series were taken using a confocal microscope (TCS SP5; Leica) and used for counting. Z-series were stacked for presented images.

Microscopy

Adult wings were dry mounted, and images were acquired using a microscope (Stemi V6; Carl Zeiss MicroImaging, Inc.) equipped with a 1.0X lens using a digital camera (Coolpix5000; Nikon) or a stereomicroscope (SteREO Discovery V.12; Carl Zeiss MicroImaging) with PentafluorS using 0.63X or 1.5X PlanApoS lenses and an MRm or MRc5 digital camera (Axiocam) and Axiovision Release 4.6 software. Additional fluorescent wing images were acquired with a microscope (Axioplan 2E; Carl Zeiss MicroImaging, Inc.) and a monochrome digital camera (Hamamatsu) using Plan Neofluar 10X/0.30, Plan Apochromat 20X/0.60, and Plan Neofluar 40X/0.75 objectives and OpenLab software. Confocal images of tissues stained with Fluorescein and Alexa 568 were mounted in Vectashield (Vector Laboratories), and images were acquired on a confocal microscope (TCS SP5; Leica) with Leica LAS AF software. The following lenses were used: HC PL APO 20X/0.70, HCX PL APO 40X/1.25-0.75 oil, and HCX PL

APO 63X/1.40-0.60 oil objectives. All images were taken at room temperature and were processed in ImageJ or Photoshop. Occasionally, images were linearly rescaled to optimize brightness and contrast uniformly without altering, masking, or eliminating data.

RESULTS

Proper maintenance of the adult wing requires apoptogenic gene action

Previous work established that wings mosaic for *dronc*⁻ tissue exhibit normal morphology at eclosion but develop progressive, melanized blemishes with age (Chew et al., 2004). We applied similar methods to determine whether lesions in other apoptogenic genes present a similar phenotype. After eclosion, wings mosaic for *Df(H99)*, a deletion removing the apoptotic activators *reaper* (*rpr*), *grim* and *hid* (Abrams, 1999) were morphologically normal at eclosion, but over the course of 3-7 days, melanized blemishes appeared at random positions throughout the wing (Figure 1-2 C). Likewise, newly eclosed homozygous *drice*^{Δ1} adult ‘escapers’ deficient for the effector caspase Drice (Muro et al., 2006), also presented normal wings at eclosion but developed identical blemishes with age (Figure 1-2 D). We next examined wings mosaic for *dark*⁸², a null allele of *dark* (Akdemir et al., 2006). These were indistinguishable from wild type at eclosion (Figure 1-2 A), but within days, all mosaic animals developed blemish phenotypes. These late-onset blemishes became markedly more severe as animals aged (Figure 1-2 B). Similar, yet less severe, wing blemishes occurred in adults homozygous for *dark*^{CD4}, a hypomorphic allele of *dark* (Chew et al., 2004). Together, these observations establish that late-onset progressive blemishing in mosaic wings is a characteristic phenotype shared among mutants in canonical PCD pathways.

Live cell imaging reveals collective elimination of the wing epithelium

To directly examine the death of these cells *in vivo*, we adapted a transgenic source of nuclear DsRed driven by *vestigial-Gal4* (Barolo et al., 2004; Vegh and Basler, 2003), designated *vg:DsRed*, to follow the fate of wing epithelial cells soon after eclosion. Observations with this pan-epithelial marker in the wing confirmed earlier studies from Kimura et al. who applied a different fluorescent transgene, *en:GFP*, to label cells in the posterior compartment (Kimura et al., 2004; Xu et al., 2005). Figure 1-3A shows that within one hour of eclosion, intact epithelial cells are clearly present and regularly patterned throughout the wing. However, 1-2 hours later (2-3 hours post-eclosion), virtually the entire epithelial layer disappears, manifested here by the abrupt loss of nuclear DsRed throughout the wing blade (Figure 1-3B). Live, real time imaging of the wing in newly eclosed adults revealed unique and unexpected features associated with the elimination of the intervein epithelium (Figure 1-4 and 1-5). Briefly, epithelial cells, indicated by nuclear fluorescence, were arranged in a regular, predictable pattern throughout the wing. Then, consistent with nuclear breakdown, fluorescence became redistributed throughout the cell followed by the appearance of fragmenting cells, an indication of blebbing (Figure 1-4). Occasionally, weak fluorescence enclosed in cell corpses condensed to bright punctate bodies. This series of apoptogenic changes spread extremely rapidly throughout the epithelium, appearing as a collective wave initiating from the peripheral edge and moving across the wing blade (Figure 1-5, top panels). Within just four minutes, virtually all nuclei (~450 cells) within a space of about 114mm^2 converted from viable to apoptotic morphology (Figure

1-5, top panel). Moreover, the process involved tight coordination at the group level since the likelihood of a single cell apoptosing was clearly linked to similar behaviors by nearest neighboring cells over short time frames. Unlike virtually all conventional examples of PCD in development, we found no indication that overt engulfment of apoptotic corpses occurred at the site of death. Instead, DsRed labeled cell remnants were passively swept *en masse* toward nearest wing vein (Figure 1-5, bottom panels) where, apparently under hydrostatic pressure, cell debris streamed proximally toward the body along the wing vein (Figure 1-5, bottom panels). Together, these observations describe a communal form of PCD that rapidly eliminates the wing epithelium through coordinated group behavior.

Cells mutated for genes in the cell death pathway persist in the wing epithelium

We used the *vg:DsRed* reporter to follow the fate of mosaic wing epithelia where mutant clones were induced. In sharp contrast to wild-type wings, abnormally persisting cells could be readily detected as patches of DsRed in the nuclei of epithelial cells in mosaic tissues. For example, wings mosaic for *dronc*⁻ clones retained extensive patches of persisting DsRed labelled cells (Figure 1-3C). Here, cells and nuclei were readily detected 4 days after eclosion (Figure 1-3C), and even at 11 days post-eclosion, extensive evidence of cell debris was seen (not shown). Using the same methodology, we found that wings mosaic for the *H99* deletion gave identical results with patches of persisting cells or cell remnants evident at 24 hours post eclosion (Figure 1-3D). Likewise, adults mutated for *dark* also exhibited persisting cells throughout the wing

blade. Consistent with this, rare *drice*^{Δ1} escapers also showed evidence of persisting cells 24 hours post-eclosion (Muro et al., 2006). These observations link failures in PCD to progressive melanized wing blemishes, raising the possibility that other PCD genes might confer the same characteristic phenotype.

Communal cell death signals

The entire wing epithelium dies within a few short hours suggesting that these communally dying cells are linked to their neighbors. We have shown that within 30 minutes, over 450 cells die within a given area and are removed from the wing (Figure 1-5). To coordinate this behavior, it is possible that a signal is propagated throughout the epithelium from one cell to another or through hemolymph that washes out the wing. To test a signal propagation model, we designed a unique dual color live cell imaging experiment. First, we labeled all cells with nuclear DsRed and generated clones of *dark* tissue in the wing, creating small patches of mutant tissue surrounded by wild type tissue. We labeled the wild type tissue with GFP, and after the two signals are overlaid, the resulting wing consists of red mutant patches with yellow wild type tissue (figure 1-6A). This dual color analysis allows a direct examination of events at the borders of clonal tissue, providing a platform to dissect if and how signals are passed from cell to cell. There are three possible outcomes to this experiment: 1) communal cell death is completely cell autonomous (mutant cells survive while wild type cells die), 2) cells that should be eliminated fail to die, indicating that a death signal is blocked by mutant tissue at the clone interface, or 3) cells programmed to survive are eliminated by death signals passed from wild type tissue into mutant tissue (Figure 1-6B). We generated time-lapse

images of newly eclosed flies with the above conformation and found that cells lacking the apoptosome (*dark*) always persist, suggesting that signals from wild type cells cannot influence mutant tissue (Figure 1-7). However, additional imaging experiments are required to determine if mutant tissue can block the death of wild type tissue by preventing communal death signals from moving throughout the epithelium.

During metamorphosis, the steroid hormone ecdysone is known to mediate gene expression changes to stimulate the removal of larval tissue by cell death (reviewed by(Yin and Thummel, 2005)). However, the signal for post-eclosion cell death remains unclear. Previous work from Kimura *et al.* suggested that a hormone, possibly Bursicon, is the signal that stimulates post-eclosion cell death in the wing by activating Rickets (DLGR2), a G-protein coupled hormone receptor(Kimura et al., 2004). Downstream signaling is thought to occur through production of cAMP and activation of Protein Kinase A (PKA). To test whether Rickets plays a role in communal cell death in the wing, we acquired *rickets* mutants, generated clones in the wing, and looked for persisting cells after eclosion. We saw no persisting cells in *rickets* mutants, suggesting that *rickets* is not essential for post-eclosion communal cell death. However, we did not perform an exhaustive time course after eclosion, and if a mutation in *rickets* delays rather than prevents cell death, we might not have visualized this event.

Communal cell death appears to be tightly regulated, suggesting that a signal might be propagated from cell to cell. Gap junctions directly connect the cytoplasm between two cells and allow molecules to freely pass between cells. In this manner, a death signal such as the small pro-apoptotic Reaper protein could plausibly be passed

throughout the epithelium quickly and stimulate communal cell death. To determine if gap junctions play a role in coordinating communal cell death, I acquired several mutations affecting gap junctions, generated wing clones, and looked for defects in communal cell death. We did not find any defects in communal cell death but because these do not encompass all components of gap junctions, we cannot rule out the possibility that connections between cells play a role.

A phenocopy screen recovers new cell death defective mutations

Unlike many previously described wing defects that are congenital and evident at the time of eclosion (Lawrence, 1992; Lindsley and Zimm, 1992), the age-dependent phenotype described here is characteristic of mutations in genes that function in canonical PCD pathways. Moreover, when the dosage of *dronc* was reduced by half in *dark^{CD4}* adults (Chew et al., 2004) or if wild-type Dmp53 was removed from these animals, melanized blemishes became far more severe (not shown). These genetic interactions are specific since numerous other mutants showed no such effects in combination with a *dark* hypomorph. Additionally, wing defects were never observed in Dmp53⁻ homozygous flies or in *dronc⁵¹* heterozygous flies (P.C and J.M.A, unpublished observations). We reasoned that additional regulators and effectors in PCD pathways should phenocopy wings mosaic for *dark⁻* or *dronc⁻* tissue if genetically eliminated. Based on this rationale, we screened a large collection of pre-existing transposon mutants to recover insertions that exhibit normal wings at eclosion but develop melanized blemishes with age. Our strategy exploits the FLP/FRT system together with wing-specific drivers (see methods and figure 1-8) to interrogate animals bearing wing

genotypes mosaic for clones of P element derived lethal mutations. Progeny with mosaic wings were examined for the distinctive late-onset wing blemishing phenotype at 7 and 14 days post-eclosion. In this way, we screened over 1000 lethal insertions, representing 356 second chromosome mutations and 707 third chromosome mutations.

The vast majority insertions (87%) produced no visible defects as wing mosaics. 13% of insertions tested (total 139) produced abnormalities, and these were scored for the phenotypic categories shown in Figure 1-9. Congenital defects including notched, blistered, or wrinkled wings occurred alone or occasionally as compound phenotypes (Figure 1-9, A-D). The candidate strains that developed wing blemishing were further subdivided based on the phenotype severity. Insertions in class A developed obvious, dark blemishes within a week of eclosion (as in Figure 1-9E), whereas those in class B developed relatively light-colored patches between 1 to 2 weeks after eclosion (as in Figure 1-9F). Mutant lines exhibiting the apoptogenic blemish phenotype comparable to Figure 1-9E were rare (about 2%). All members of this class lacked blemishes at eclosion and displayed progressive blemishing with age (Figure 1-9E). New alleles of *dark* (I(2)SH0173) and *DIAP1* (I(3)S048915) were recovered in this class (Table I-I, 1-2), providing reassuring validation for our screening strategy. Some members of both classes had congenital notches or blisters and were noted. Congenital examples, where blemishes appeared upon eclosion, were not found.

We applied inverse PCR to map or confirm insertion sites of many class A and B strains that phenocopied blemishes seen in canonical apoptotic mutants. These strains and corresponding loci are listed in Tables I-I, 1-2, 1-3, and 1-4. In addition to new

alleles of canonical cell death genes *dark* and *thread* (*DIAP1*), we isolated several mutations associated with genes previously implicated in PCD. For example, I(2)SH2275 contains an insertion 2 kb upstream of *mir-14*, a microRNA capable of modulating Reaper-induced cell death (Xu et al., 2003). Hence, aberrant expression of this microRNA could explain the cell death defective phenotypes recovered in this strain. Likewise, I(3)S055409 maps near *misshapen*, a kinase upstream of Jun N-terminal kinase (JNK, *Drosophila basket*) (Su et al., 1998) implicated in cell killing triggered by Reaper or Eiger, the drosophila ortholog of TNF (Igaki et al., 2002; Kuranaga et al., 2002). Several insertions map in or near transcriptional or translational regulators that might alter the expression of cell death genes. For example, *grunge* (I(3)S146907), an Atrophin-like protein (Erkner et al., 2002) functions as a transcriptional repressor (Zhang et al., 2002), while *belle* (I(3)S097074) belongs to the DEAD-box family of proteins (Johnstone et al., 2005) often implicated in translational regulation and in RNA processing.

A portion of the class A and B hits were also directly examined for defective PCD by applying the *vg:DsRed* reporter in mosaic wings. Of the 29 strains tested, 14 showed obvious evidence for persisting cells in the wing epithelium (Table I-2, 1-4). One strain, I(2)SH0173, was mapped to the *dark* locus. This new dark allele exhibits both progressive blemishing and ‘undead’ epithelial tissue as shown in Figure 1-9G and H.

Homeodomain interacting protein kinase (HIPK) is essential for normal PCD of the wing epithelium

One unmapped strain, I(3)134313, exhibited severe late-onset blemishing (Figure 1-11D) and a persisting cell phenotype (Figure 1-11F). We mapped this insertion to the first intron of the *homeodomain interacting protein kinase (HIPK)* gene, suggesting that disruptions at this gene were responsible for progressive wing blemishing and persisting epithelial cells. To definitively assign these defects to the loss of HIPK, we independently produced null alleles at this locus by a customized deletion strategy illustrated in Figure 1-10. Two FRT containing P element insertions flanking the coding region of *HIPK* (Figure 1-10A) were used to generate a novel deletion depicted in Figure 1-10C (see methods). PCR was used to verify recombination between P elements, and a total of 8 deletion strains were recovered (see Figure 1-10B). These validated alleles eliminated exons 4 -12, removing over 92% of the residues in the predicted *HIPK* open reading frame. Deletions at the *HIPK* locus were uniformly lethal prior to the 3rd instar stage. However, zygotic HIPK is evidently not essential to complete embryogenesis since about 70% of *HIPK* homozygote embryos hatch to 1st instar larvae. However, when cuticle preparations were performed on *HIPK*^{D1} animals, severe developmental defects were obvious in the form of abnormal or missing denticle bands (Figure 1-12). *HIPK*^{D1} was recombined on the FRT79 chromosome in order to generate adult wings mosaic for the *HIPK* genotype. We found that adult wings mosaic for HIPK function developed significant progressive blemishes (Figure 1-11E) and a persisting cell phenotype (Figure 1-11G) more severe than the original P insertion allele, suggesting

that I(3)134313 represents a hypomorphic *HIPK* allele. Together, these findings establish that the action of HIPK is essential for post-eclosion PCD of the wing epithelium.

Using general stains (acridine orange) or TUNEL methods, embryonic PCD was not overtly disturbed in HIPK mutants (figure 1-13). To investigate the possibility of more subtle or specific phenotypes, we examined the nervous system using antibodies that label specific populations of neurons affected by the H99 deletion (White et al., 1994). Using α -Kruppel antibody (Kosman et al., 1998), we confirmed that stage 14–15 WT embryos contained 9–12 Kruppel-positive cells in the Bolwig's Organ (Fig. 1-14, A and C). However, a portion of animals lacking maternal HIPK contained as many as 15 cells per organ (Fig. 1-14, B and C) at a penetrance comparable to H99 animals, which are completely cell death defective (Fig. 1-14 C). We also examined neurons expressing dHb9, a homeodomain protein marking a subset of cells that persist in cell death-defective H99 embryos (Rogulja-Ortmann et al., 2007). In germline clones, distinct classes of dHb9 staining patterns emerged. A subset of animals exhibited extreme patterning defects. Other animals displayed a striking increase in dHb9-positive cell numbers (Fig. 1-14, E–G) when compared with WT embryos of the parental strain (Fig. 1-14 D). These data establish that HIPK fundamentally regulates cell numbers in the nervous system, and because the same subpopulation of cells is affected by the H99 mutation, they implicate HIPK as a more general regulator of PCD.

Previous reports implicate the mammalian HIPK family of proteins to play a role in p53-mediated, stress-induced cell death. HIPK has been shown to bind and

phosphorylate p53 after DNA damage (D'Orazi et al., 2002; Hofmann et al., 2002; Zhang et al., 2003). This promotes activation of p53 and induction of downstream targets to promote cell death. Therefore, we examined whether *Drosophila* HIPK is required for stress-induced cell death. We generated animals with clones lacking HIPK, irradiated L3 larvae to induced DNA damage, and performed TUNEL on dissected wing discs to assay for stress-induced cell death. We found that HIPK mutant tissue had comparable levels of TUNEL positive labeling when compared to its wild type counterpart (figure 1-15), suggesting that HIPK is not required for DNA damage induced cell death in *Drosophila*.

Analysis of 141405, a novel cell death gene required for embryonic cell death

In our screen for cell death defective mutations, we isolated a mutation that produced mosaic wing defects indistinguishable from tissue lacking the apoptosome (e.g. *dronc* or *dark*) (Figure 1-16). Furthermore, I also linked this same strain to profound PCD defects in the embryo. For example, in embryos, apoptosis was absent in segments posterior to the head (Figure 1-17), and likewise, a dramatic increase in cell numbers was seen in the nervous system (1-18). Together, these observations indicate that l(3)S141405 animals are cell death defective in diverse tissue contexts.

To determine the gene responsible for cell death defects, I originally mapped the insertion to *CG31522*, is a member of a broadly conserved ELO family of proteins not previously linked to cell death. However, after much work generating novel mutations and subsequent phenotypic analysis, I found that *CG31522* was not responsible for cell death defects found in l(3)S141405. Another insertion in l(3)S141405 was mapped to

Tropomyosin 1 (TM1), an Actin binding protein. We acquired several alleles of TM1 and tested these alleles for cell death defects as homozygotes and in *trans* to each other and I(3)S141405 but did not find any cell death defective phenotypes. Therefore, we generated a revertant of TM1 in which we precisely excised the P element insertion in TM1, leaving the genetic locus intact which was verified by sequencing. In this strain, noted as I(3)S141405^{phop}, wing cell death defects were eliminated but the provocative embryonic cell death defects remained. These data suggest that another mutation on the same chromosome is responsible for embryonic phenotypes, while an interaction between TM1 and this second mutation may lead to wing phenotypes observed in the original line, I(3)S141405.

To determine whether the gene mutated in I(3)S141405^{phop} was a general regulator of programmed cell death or specific to embryonic cell death, I assayed for apoptosis defects in a variety of settings: DNA damage induced cell death in the wing disc, an *ex vivo* hemocyte model of cell death, and developmental cell death in the pupal eye all showed no defects in cell death. To determine whether I(3)S141405^{phop} had abnormal neuronal cell numbers indicating a cell death defect, I stained with antibodies that label specific populations of neurons affected by the H99 deletion and found that the morphology of I(3)S141405^{phop} animals was severely irregular, indicating that the embryonic cell death defects may be a result of failed or atypical embryonic development. One final experiment using forced overexpression of Hid, a proapoptotic killer, in the eye while in the background of I(3)S141405^{phop} indicated that the gene mutated in this strain mildly rescues Hid killing in the eye (Figure 1-19). This data

places *l(3)S141405^{phop}* downstream of *Hid*. To map the mutation, I crossed *l(3)S141405^{phop}* to the third chromosome deficiency kit, but found no region to which the lethality in *l(3)S141405^{phop}* maps. Recombination mapping to identify a cell death gene that presents cell death defects in the embryo only when germline clones are generated is not feasible. However, I performed a small scale recombination mapping to identify lethality in *l(3)S141405^{phop}* but the gene mutated in *l(3)S141405^{phop}* remains unknown.

Tango7, a novel gene required for cell death

Using genome-wide double stranded (ds) RNA library, members of the lab isolated genes that, when silenced, block apoptosis induced by Smac mimetic, a small molecule that binds to and inhibits the IAPs. From this screen, *Tango7* was identified as required for Smac induced killing *in vitro*. To verify its role in apoptosis *in vivo*, I utilized an *in vivo* dsRNA construct to knock down *Tango7* in the developing pupal eye and assay for cell death defects in these cells. I found that animals lacking *Tango7* (Figure 1-20e) had many more interommatidial cells than animals with an irrelevant dsRNA targeted to the same location (Figure 1-20d). The number of interommatidial cells from an irrelevant dsRNA (5881) along with two different insertion lines of *Tango7* (8309R1 and R3) are displayed in (1-20f). At least 30% of eyes silenced for *Tango7* also displayed a progressive blackening of the eye, indicative of tissue degeneration.

DISCUSSION

Elimination of the wing epithelium in newly eclosed adults is predictable, easily visualized, and experimentally tractable. The major histomorphologic events involve cell death, delamination, and clearance of corpses and cell remnants. Insightful studies from Kimura and colleagues recently established that post-eclosion PCD is clearly under hormonal control (possibly via the tanning hormone, bursicon) and involves the cAMP/PKA pathway (Kimura et al., 2004). While dying cells in the adult wing present apoptotic features (e.g. sensitivity to p35 and TUNEL positive), elimination of the epithelium here is also distinct from classical apoptosis in several important respects. First, unlike most *in vivo* models, overt engulfment of cell corpses does not occur at the site of death (Ashkenas et al., 1996; Johnson and Milner, 1987). Instead, dead or dying cells and their remnants are washed into the thoracic cavity via streaming of material along and through wing veins (see Figure 2, supplemental movies, and (Kimura et al., 2004)). Second, extensive vacuolization is seen in ultrastructural analyses, which could indicate elevated autophagic activity (see (Johnson and Milner, 1987; Kimura et al., 2004) and Figure 1 I, J, K). Third, the widespread and near synchronous death that occurs in this context defines an abrupt group behavior. The process affects dramatic change at the tissue level, causing wholesale loss of intervein cells and coordinated elimination of an entire layer of epithelium within minutes. Rather than die independently, these cells die communally, as if responding to coordinated signals propagated throughout the entire epithelium, perhaps via intercellular gap junctions.

This group behavior starkly contrasts with canonical *in vivo* models where a single cell, surrounded by viable neighbors, sporadically initiates apoptosis.

The progressive blemish phenotype is a highly characteristic indicator of PCD failure, and as established here, is also reliably produced by lesions in canonical pathway elements such as apoptosomal genes (*dark/dronc*), IAP antagonists (*rpr*, *grim* and *hid*) and the effector caspase, *drice*. The screen described here sampled nearly one fourth of all lethal genes and nearly 10% of all genes in the fly genome. Though not saturating, the fact that we recovered new alleles of *dark* (I(2)SH0173) and *DIAP1* (I(3)S048915) provides reassuring validation for the design of our strategy. We note that animals displaying this rare characteristic phenotype were detected if - and only if - the outcome of wing development and wing expansion are both normal in mosaic tissue. By enhancing selectivity toward functions acting after the wing is formed, these prerequisites serve as a useful filter against misspecification defects potentially impacting unrelated processes.

Among those surveyed using *vg:DsRed*, nearly half of the mutants (48%) that produced melanized wing blemishing also displayed a cell death defective phenotype. The precise link between these defects is unclear, but a likely explanation suggests that as the surrounding cuticle fuses, persisting cells, now deprived for nutrients and oxygen, become necrotic and may, in the process, initiate melanization. Mutants in this class could arrest at upstream steps, involving the specification or execution of PCD, or alternatively, they might affect proper clearance of cell corpses from the epithelium.

Previous studies have suggested that an epithelial to mesenchymal transition (EMT) accounts for the removal of epithelial cells after eclosion (Kiger et al., 2007). While our results do not exclude EMT associated changes in the newly eclosed wing epithelium, work here and elsewhere (Kimura et al., 2004) offer several lines of compelling evidence establishing that elimination of the wing epithelium occurs by PCD *in situ* after eclosion and before cells are removed from the wing. First, prior to elimination, wing epithelial cells label prominently with TUNEL. Second, every mutation in canonical PCD genes so far tested failed to effectively eliminate the wing epithelium, and at least two of these were recovered in the screen described here. Third, elimination of the wing epithelium was effectively reversed by induction of p35, a broad-spectrum caspase inhibitor (Kimura et al., 2004). Fourth, using time-lapse microscopy, we clearly detected condensing or pycnotic nuclei, followed by the rapid removal of all cell debris in time frames (minutes) not consistent with active migration. Instead, removal of cell remnants occurred by a passive streaming process, involving perhaps hydrostatic pressure from hemolymph to remove these cell corpses quickly.

Though first identified as an NK homeodomain binding partner (Kim et al., 1998), we find that HIPK is required for post-eclosion PCD. Of the four mammalian *HIPK* genes, *HIPK2*, the predicted ortholog of *Drosophila HIPK*, has been placed in the *p53* stress-response apoptotic pathway (D'Orazi et al., 2002; Di Stefano et al., 2004; Di Stefano et al., 2005; Hofmann et al., 2002), but whether HIPKs exert more global roles as PCD determinants is still unknown.

Additionally, we isolated a potential cell death defective mutation in I(3)S141405. However, we found that the chromosome contains more than one mutation. Wing defects for which the strain was originally isolated are most likely due to compound effects from two or more mutations contained on the same chromosome. One mutation mapped to TM1, but TM1 alone has no cell death defects. In addition, a precise excision of TM1 loses cell death defects in the wing but retains some defects in the embryo. While the embryonic phenotypes are tempting, we did not identify any additional cell death defects. Therefore, we have assigned the apoptotic defects in the wing to compound effects of multiple mutations, and without wing phenotypes, I(3)S141405 is not worth pursuing.

PERSPECTIVES AND FUTURE DIRECTIONS

We described a novel form of programmed cell death that occurs in the wing of *Drosophila*. This form of cell death could potentially illuminate how cells are coordinated for immediate death in other known processes such as involution. Using clonal analysis, we plan to dissect this pathway to determine what initiates death. First, clonal analysis of apoptosome proteins may illuminate whether communal cell death is cell autonomous. Second, mutations we isolated from our screen can provide insights into the control of communal cell death. By generating clones of these mutants, we can directly look at the cell death using live cell imaging, and based on the morphology of cells that fail to die, dissect this event. Several mutations on our high priority list and most mutations on our low priority list remain to be assayed using live cell imaging, but now that this process is streamlined, live cell imaging can be applied to all remaining mutations.

Currently, there are 26 high priority hits and 77 low priority hits. Our efforts have not identified any mutations that strike us as essential cell death genes, but because many remain unanalyzed, we cannot exclude this possibility. Future work includes placing these mutations in the reporter background, and using live cell imaging to visualize the communal cell death event. Any mutations that appear to mimic apoptosome mutants will be analyzed in other tissues for cell death defects.

One hypothesis proposes that a small molecule moves from cell to cell to stimulate communal cell death. In order for this to happen, a molecule must either move directly from cell to cell through a connection (perhaps a gap junction) or be

released in the hemolymph for travel through the wing. If the former case is true, genetically removing the channel in which a signal travels would inhibit transmission of communal cell death, resulting in persisting cells. Additionally, the signal would have an initiation site and spread systematically throughout the wing. A more complete mutant analysis of junctions between cells may help clarify if this is true. However, if the latter is true, the death signal would travel randomly in the hemolymph once released resulting in no clear pattern of death.

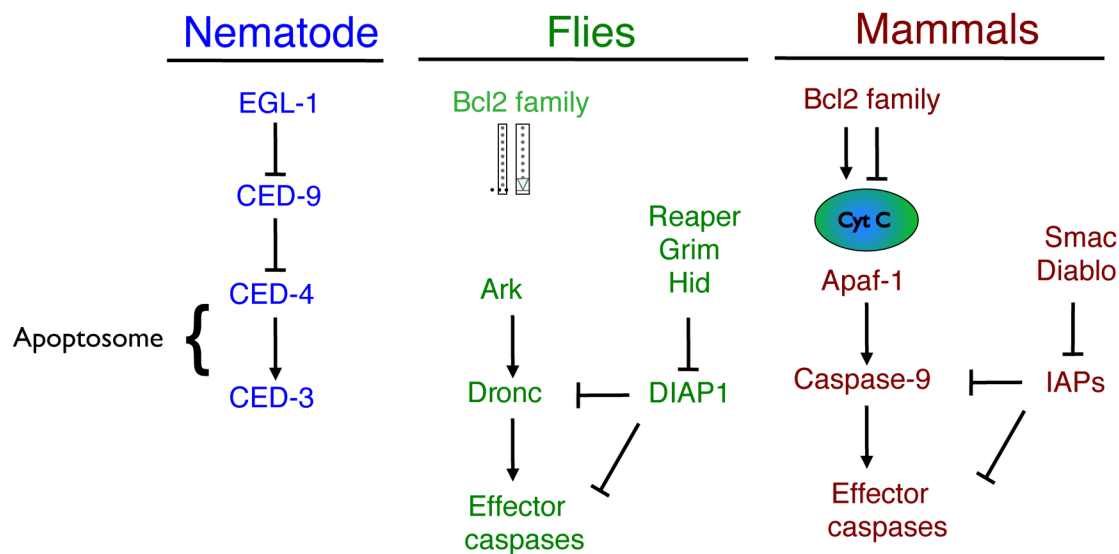


Figure 1-1. Apoptosis is conserved throughout evolution.

The genetic control of apoptosis was first studied in the nematode when the global cell death defective mutants, *ced-3*, *ced-4*, and *ced-9*, were discovered. CED-3 encodes an apical caspase homologous to Dronc and Caspase-9, and CED-4 has homology to mammalian Apaf-1 and *Drosophila* Dark. CED-9, an inhibitor of apoptosis, shows homology to the mammalian Bcl-2 family of proteins that regulate apoptosis. The inhibitors of apoptosis proteins (IAPs) negatively regulate this pathway.

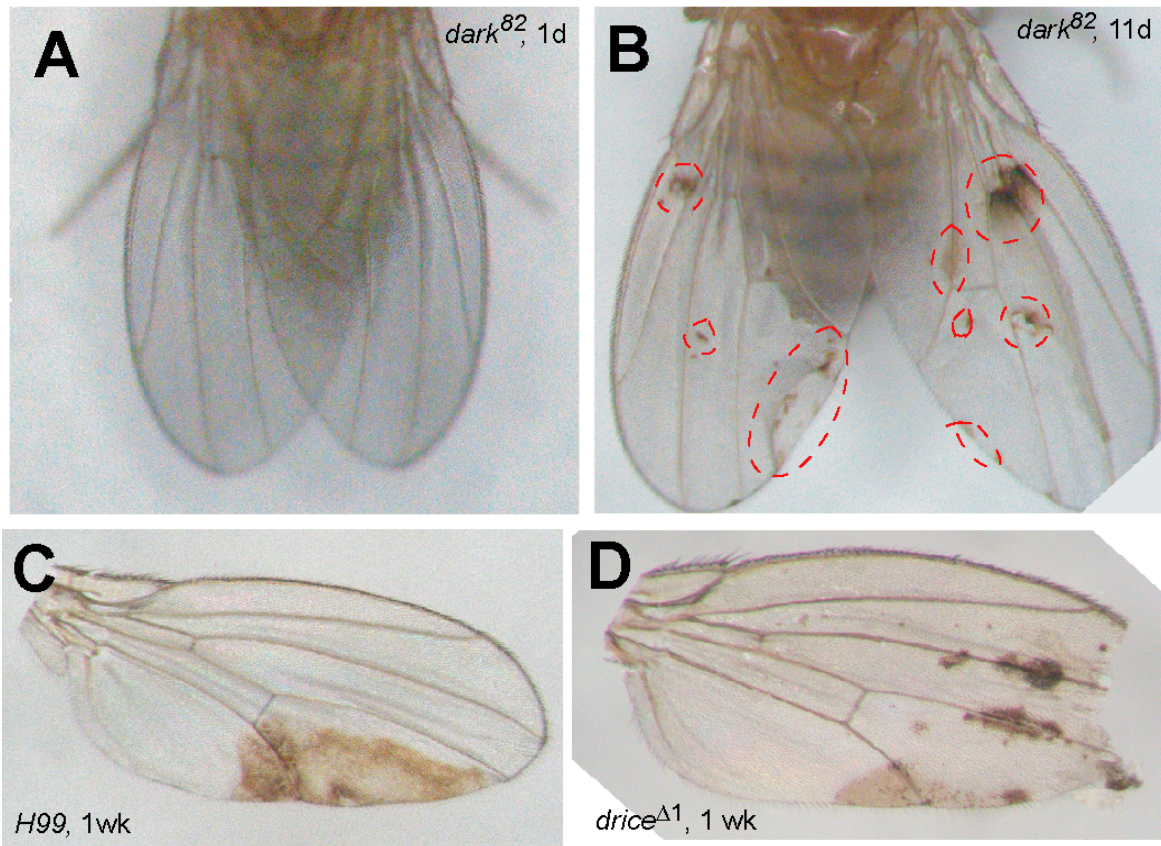


Figure 1-2. Canonical cell death mutations display a progressive blemish phenotype.

(A) Mosaic wings of animals bearing *dark⁸²* clones have normal morphology 1 day (d) after eclosion. (B) The same adult as in panel A developed melanized blemishes (dotted circles) 11 days after eclosion. (C) Wings mosaic for H99 and (D) *drice^{Δ1}* 7 days after eclosion.

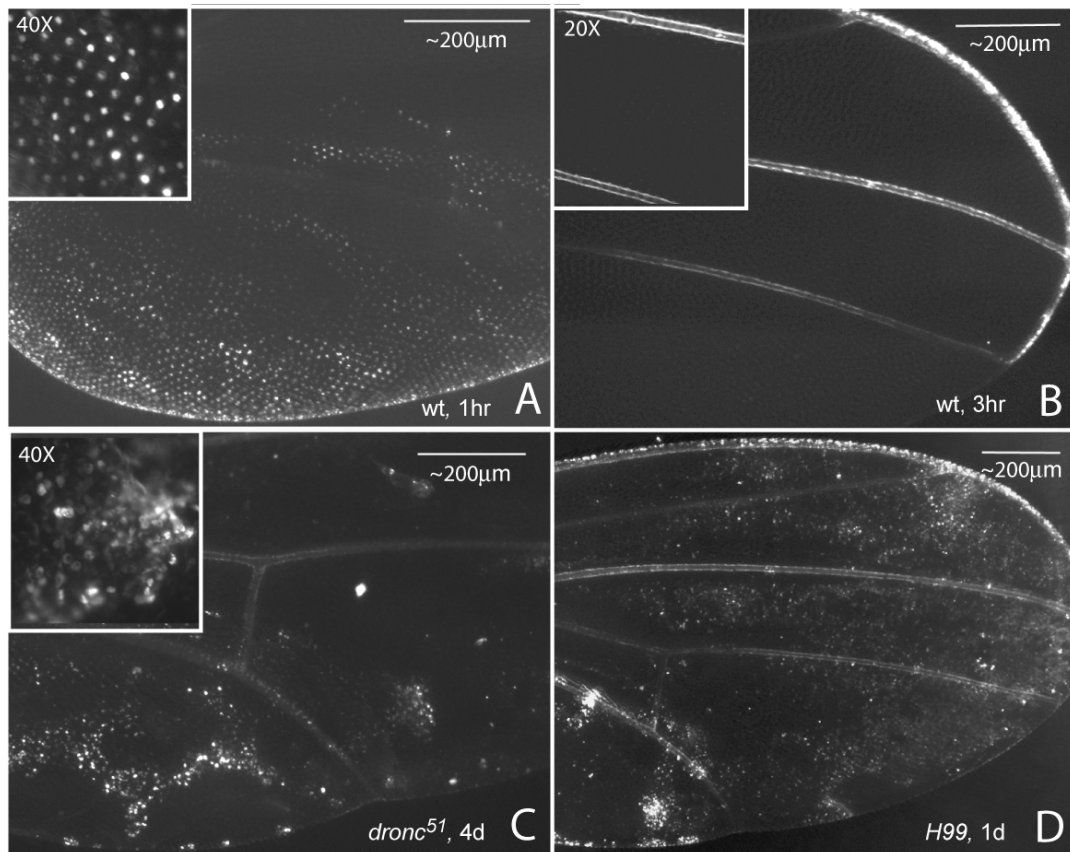


Figure 1-3. Apoptosis in the wing requires the canonical cell death pathway.

Wild type wing epithelium is visualized with *vg:DsRed* within 1 hr of eclosion (A). By 2-3 hrs post-eclosion, these cells completely disappeared (B). Wings that are mosaic for *dronc*⁻ (C) or *H99* (D) retain persisting wing epithelial cells, shown here 4 days, 24 hrs, and at least 6 hrs after eclosion.

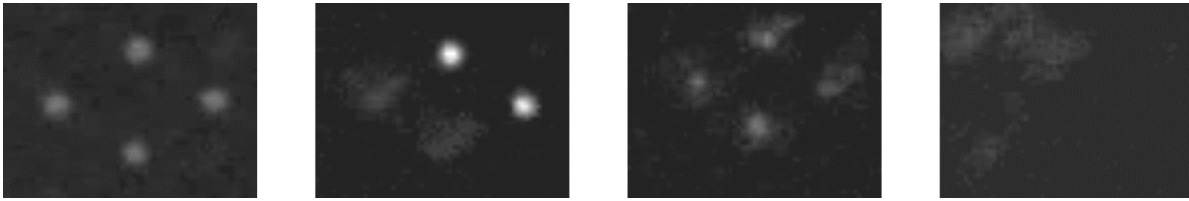


Figure 1-4. Epithelial wing cells are removed by apoptosis.

Time-lapse imaging of the adult wing shortly after eclosion using a nuclear RFP marker shows the process of apoptosis as epithelial cells are removed from the wing. The first panel shows intact cells with RFP localized to the nucleus. Panel 2 shows the beginning of apoptosis as nuclear signal is lost from two cells on the left but still retained on the right. In panel 3, all cells have lost nuclear signal indicating nuclear break down, and dying cells are starting to condense, a hallmark of apoptosis. Panel 4 shows dying cells as they are washed from the wing.

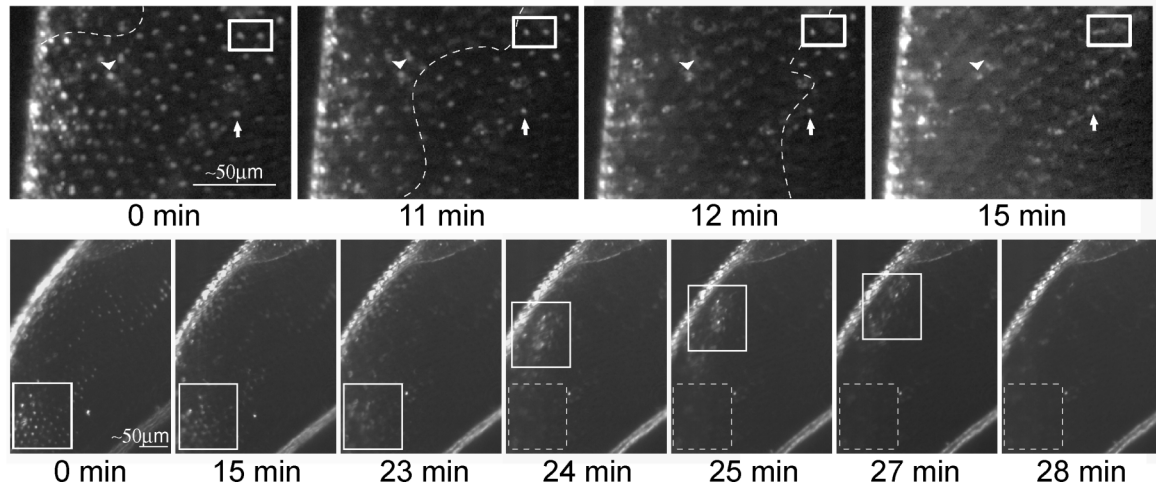


Figure 1-5. Collective cell death eliminates the wing epithelium

Time-lapse micrographs of *vg:DsRed* marked wings of newly eclosed adults depict communal cell death. In the top panel, at 0 min, cells are intact. At 11 min, several cells lose nuclear localized fluorescent signal as fluorescence distributes throughout the cell consistent with nuclear breakdown and blebbing (arrowheads). 1 minute later (12 min), apoptosis has occurred further away from the wing margin, and by 15 min, all cells have undergone PCD. The dotted line in 0, 11, 12 min marks the progression of an “apoptotic wave” through the epithelium, while the box and arrows represent the same cells in each panel. At 11 min, both cells in the box are intact. However, at 12 min, the right cell has clearly undergone PCD while the left cell remains intact. Finally, at 15 min, both cells have lost their nuclear signal and have undergone PCD. The lower panels depict intact cells at 0 min (box), but by 15 min, cells have apoptosed and have begun movement toward the wing vein at 24 min. All cells are eliminated by 28 min. In these frames, the solid box follows the group of cells as they move while the dotted box marks the original location of the cells.

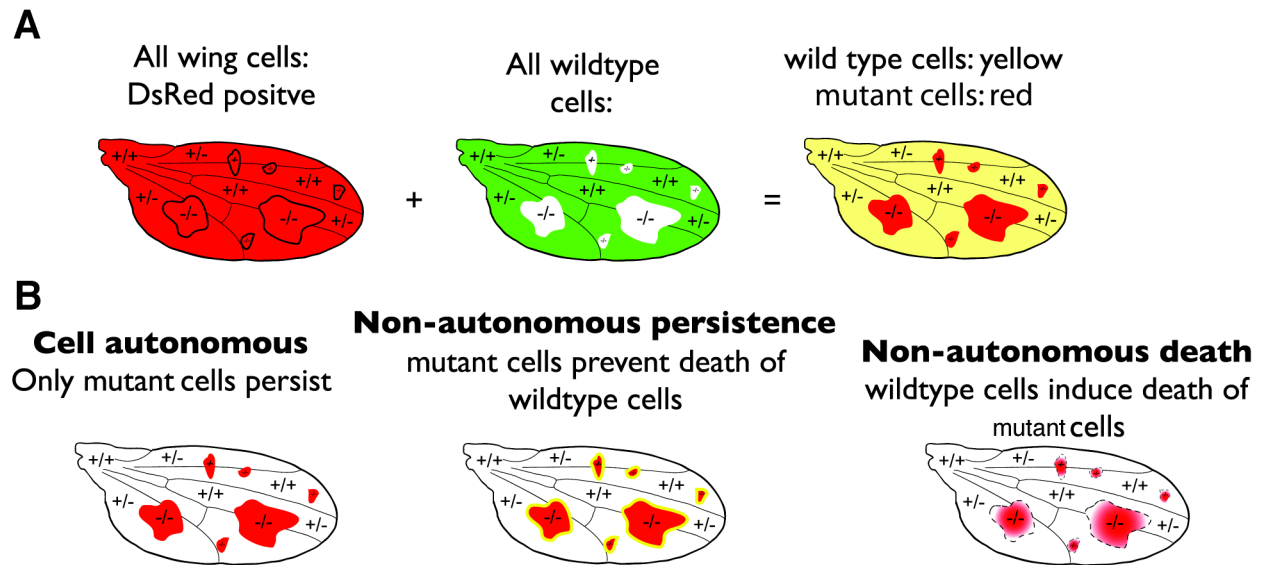


Figure 1-6. Rationale for clonal analysis of communal cell death in the wing

To determine if a signal is passed from one cell to another, wing clones of *dark*⁸² are generated in a wild type background (see methods). (A) All wing cells are labeled with nuclear DsRed while wild type cells are labeled with GFP, and when channels are merged, wild type cells appear yellow while mutant cells, in this case *dark*⁸², appear red. Predicted outcomes and interpretations are listed in B.

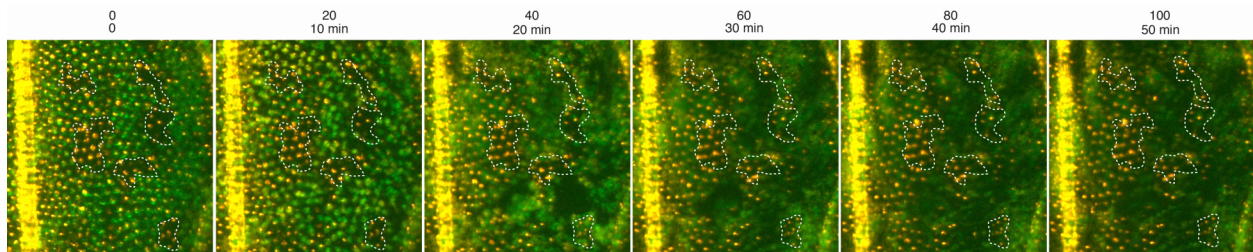


Figure 1-7. Communal cell death is cell autonomous.

Time-lapse images of clonal wing analysis. All cells are marked as shown in figure 1-6. Clones of *dark*⁸² are outlined in white. As time passes, wild type cells die while mutant cells persist. Analyses thus far indicate cell autonomous signals stimulate communal cell death. However, I also observed indications of wild type cells that persisted when they otherwise should have died, indicating that cells that fail to die can influence their neighbors. These data were not analyzed here as additional time-lapse images are necessary.

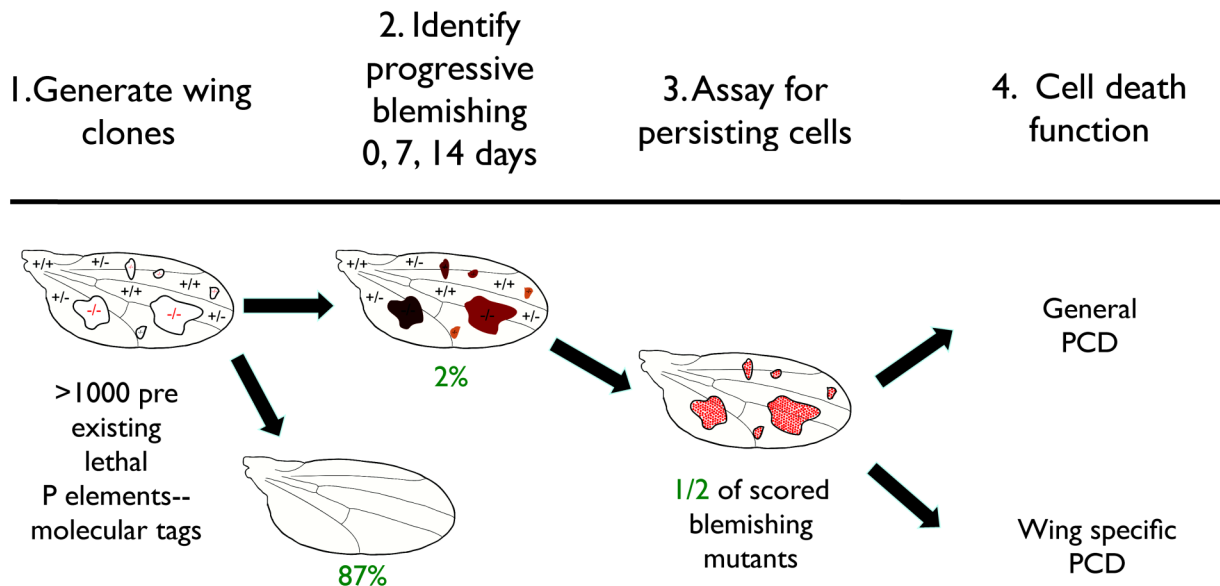


Figure 1-8. Screen for cell death defective mutations.

A preexisting collection of lethal P element transposon insertions on the second and third chromosomes (Szeged *Drosophila* stock center) recombined onto a FRT chromosome were used to generate mitotic clones in the wing. Adult flies were collected as they first eclosed, and wings were visualized at 0, 7, and 14 days after eclosion for melanized patches. Strains with phenotypes indistinguishable from *dark* and *dronc* (normal wings at day 0 but developed blemishes by day 7 or 14) were considered 'hits'. 2% of screened mutations were considered high priority candidates with blemishes similar to apoptosome mutants. These mutations were then assayed for persisting cells in the wing.

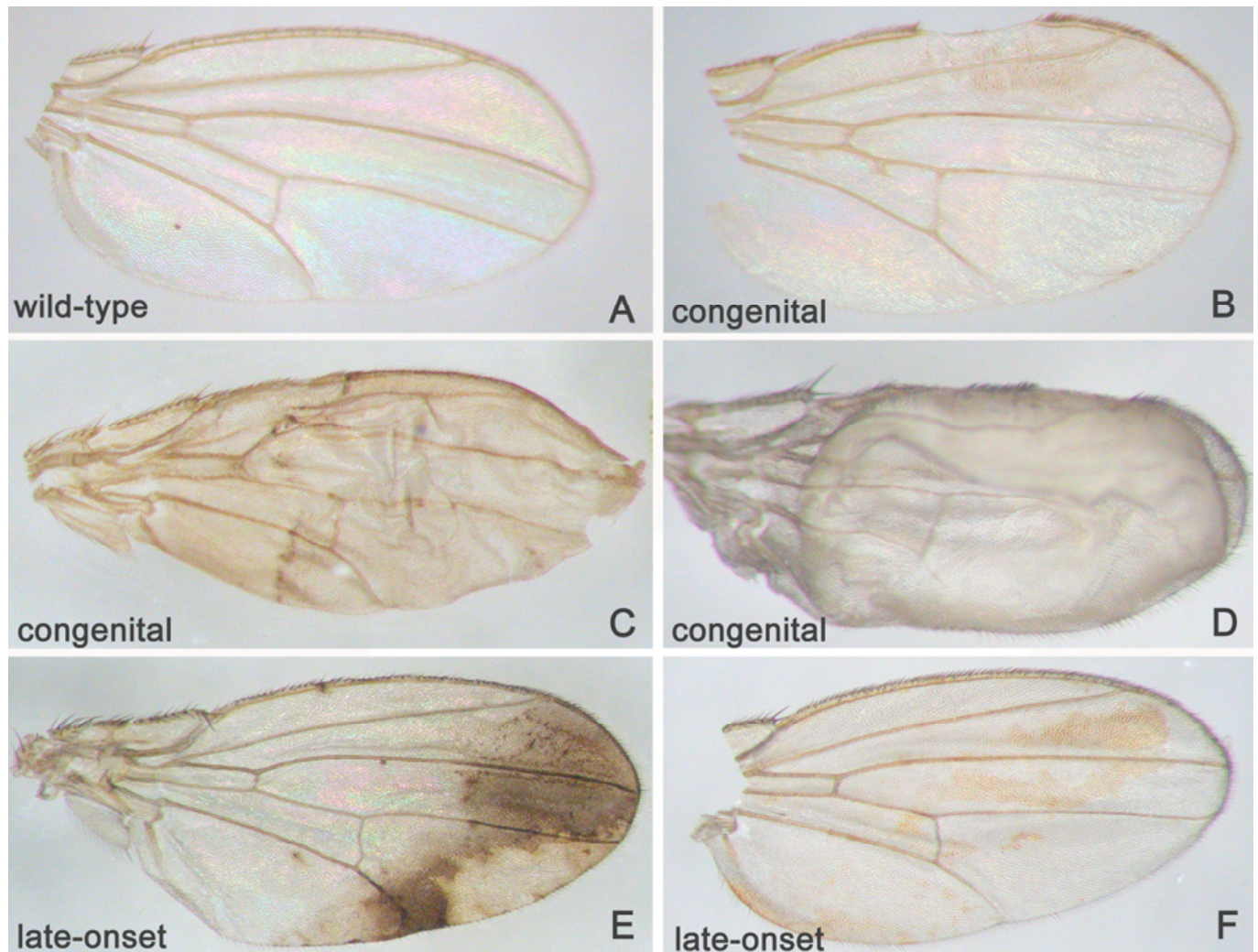


Figure 1-9. Classification of wing phenotypes.

Wings mosaic for homozygous P insertion were scored as normal (A) or positive for one of the phenotypic categories defined here. Congenital defects included notches (B), wrinkles (C), and blisters (D). Late-onset defects were normal at eclosion, progressing to severe (E) or mild (F) blemishes when scored at 7 days or older. One or more phenotypic category could be assigned to a given strain. No instances of congenital wing blemishes were seen.

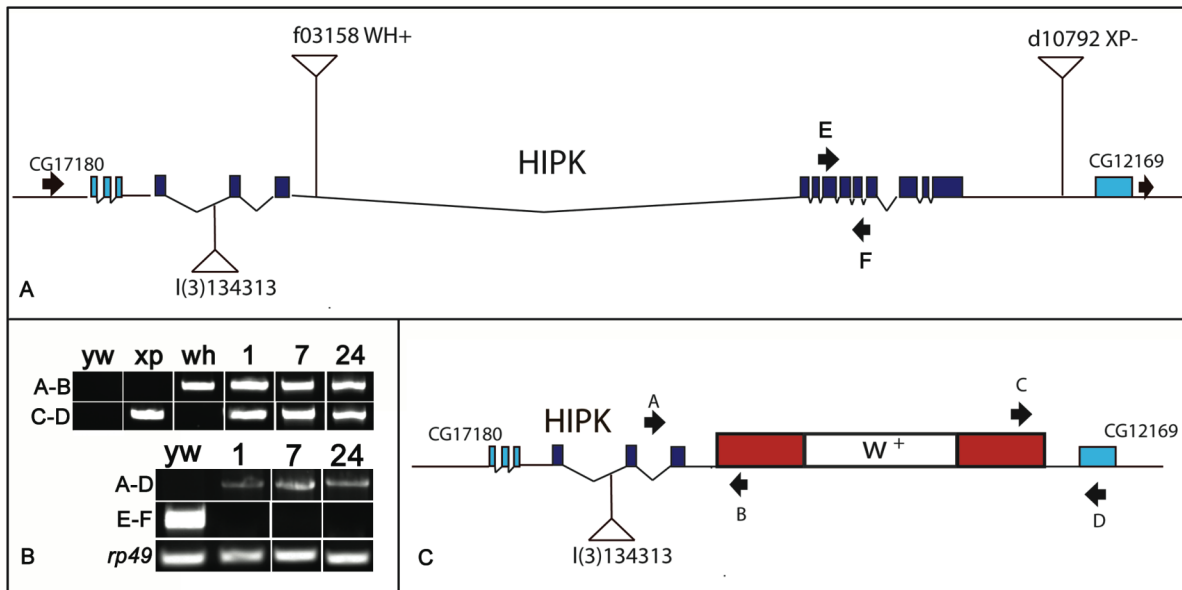


Figure 1-10. Generation of a null mutation in *homeodomain interacting protein kinase*.

The genetic locus of *hipk* is shown in (A) with known p element insertions. L(3)134313 is the original insertion isolated from the apoptosome phenocopy screen. F03158 and d10792 are exelaxis insertions used to generate the null *hipk* allele (C) which removes most of the protein coding sequence. Primers labeled in (C) were used for PCR validation shown in (B)

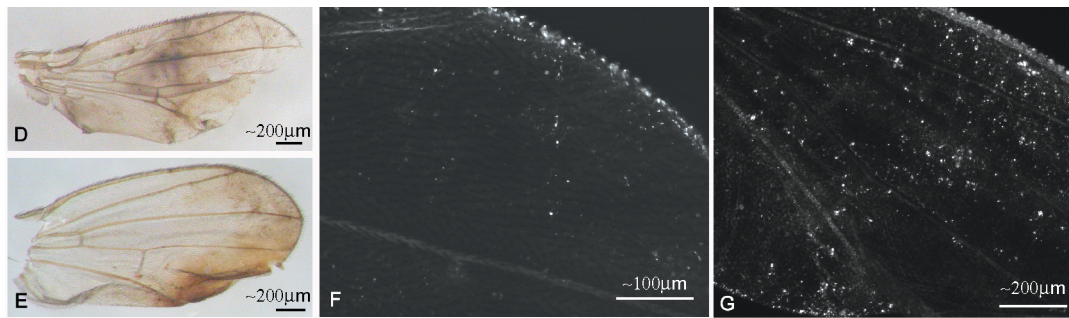


Figure 1-11. HIPK is required for communal cell death in the wing

Wings mosaic for both HIPK^{l(3)S134313} (D and F) and HIPK^{D1} (E and G) were normal at eclosion, but upon aging showed severe blemishing and persisting cell phenotypes (D–G), with HIPK^{D1} wings exhibiting additional persisting DsRed cells (G). Note that the progressive blemishing phenotypes were not seen in parental strains, including those used to produce FRT recombinants.

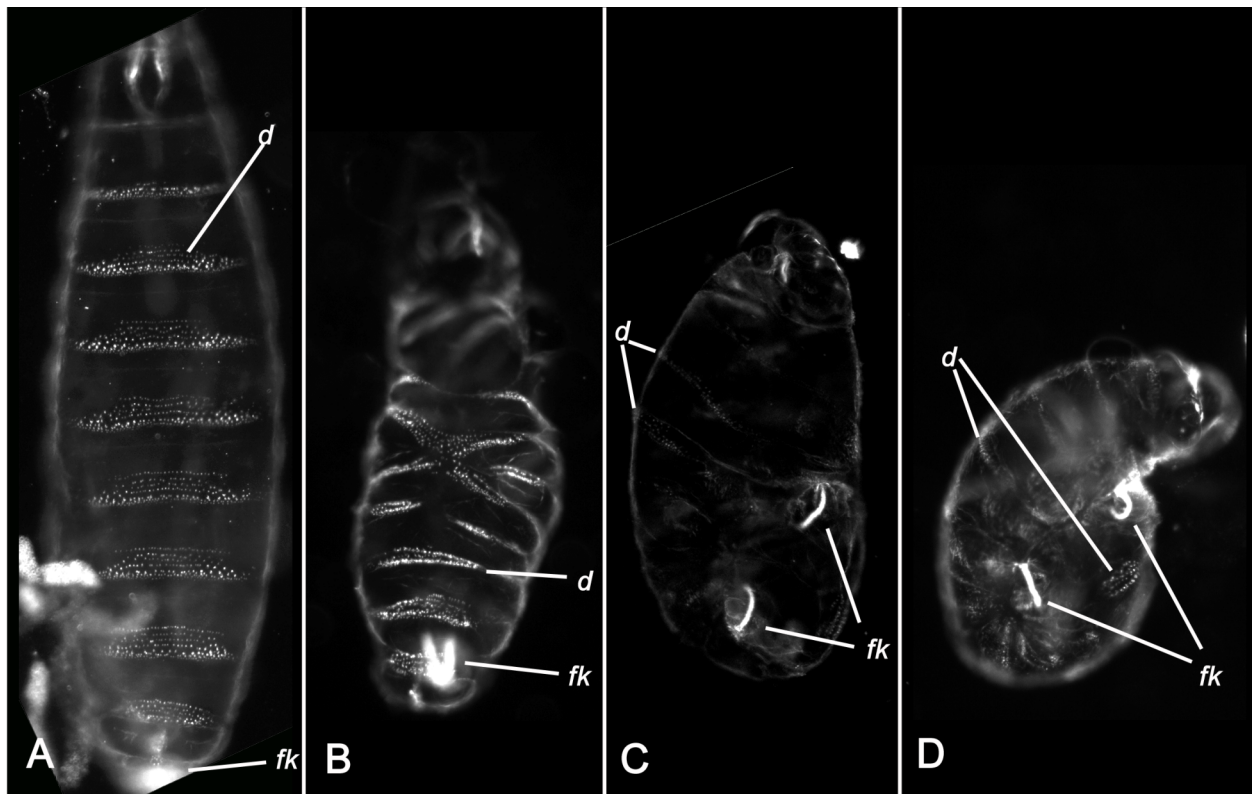


Figure 1-12. *hipk* null mutants display developmental defects.

Shown here as cuticle preps of wild type and zygotic null *hipk* larvae. Denticles (d) have a distinct pattern in a wild type animal (A) while HIPK animals display varying degrees of cuticle defects (B, C, D). Additionally, the filzkörper (fk) appear abnormally fused (B) or separated (C, D).

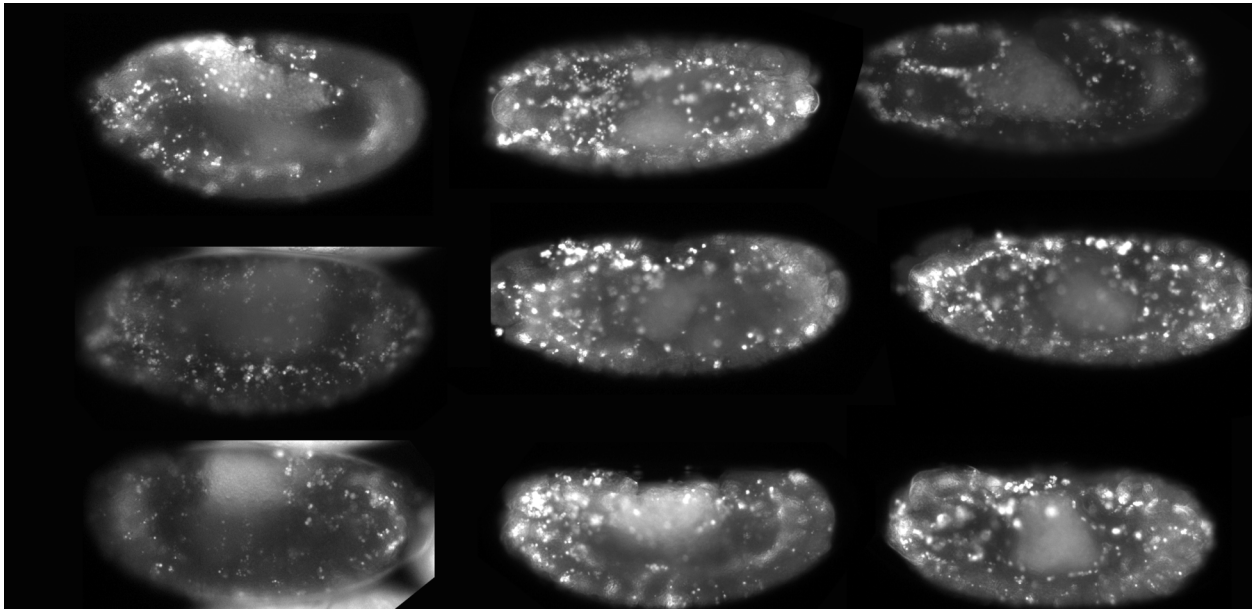


Figure 1-13. HIPK displays normal developmental cell death in the embryo

Germline clone of *hipk^{d1}* animals were stained with acridine orange to mark developmental apoptosis. Bright punctate dots represent dead or dying cells. *Hipk* mutant animals show no defect in embryonic developmental apoptosis. All animals pictured here are *HIPK* mutants. For wild type acridine staining, see figure 1-17.

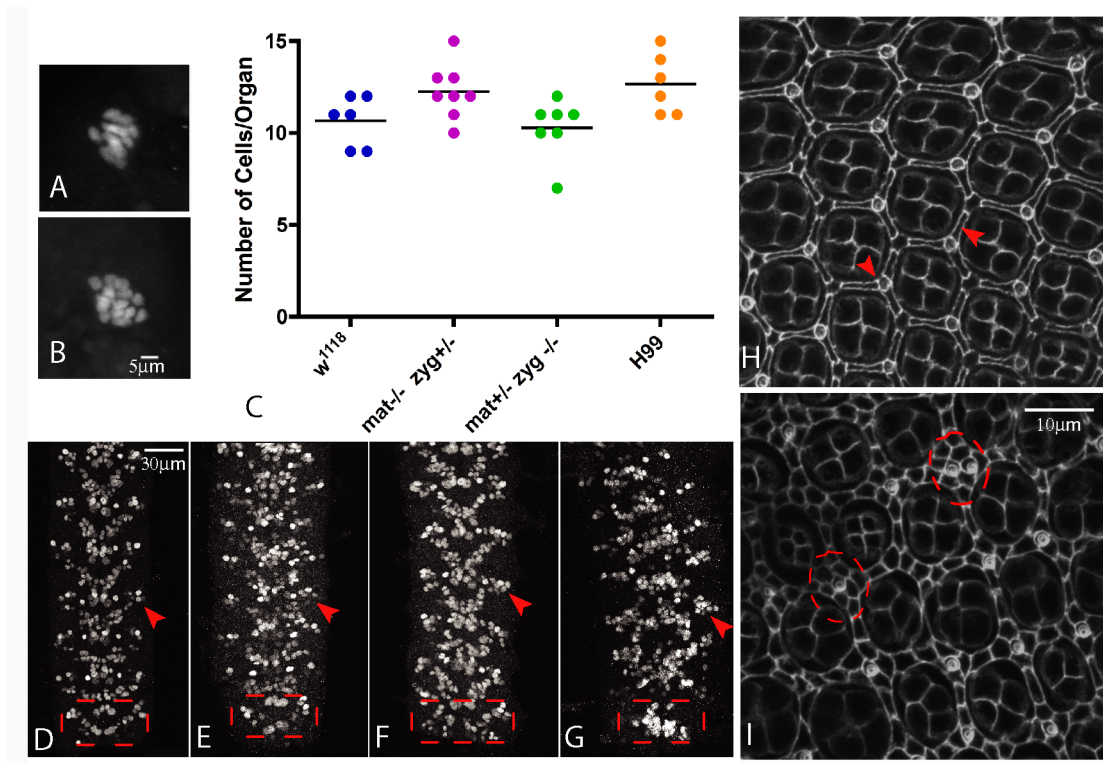


Figure 1-14. Without HIPK, excessive neurons and cells are retained.

α -Kr Ab staining of Bolwig's organ precursors in WT (w1118) (A) and HIPK (B) mutants. The number of cells per organ is plotted in C. Note that zygotic HIPK⁻ animals possess cell numbers equivalent to WT, but maternal HIPK⁻ embryos have supernumerary cells comparable to levels seen in H99 mutants. α -dHb9 Ab staining in w1118 embryonic CNS filets shows the normal pattern of dHb9-positive cells in the ventral nerve cord at stage 16–17 (D). HIPK mutants at this same embryonic stage (E–G) show extra dHb9-positive cells and altered CNS patterning. Arrows and boxes indicate extra cells. The WT pattern of pupal eyes stained with α -Dlg is displayed in H with arrows illustrating interommatidial cells. HIPK mutant pupal eyes (I) exhibit more interommatidial cells (dotted lines), indicative of a defect in cell death. Distorted patterning of ommatidia and abnormal numbers of primary pigment cells were also seen in a subset of animals (not depicted).

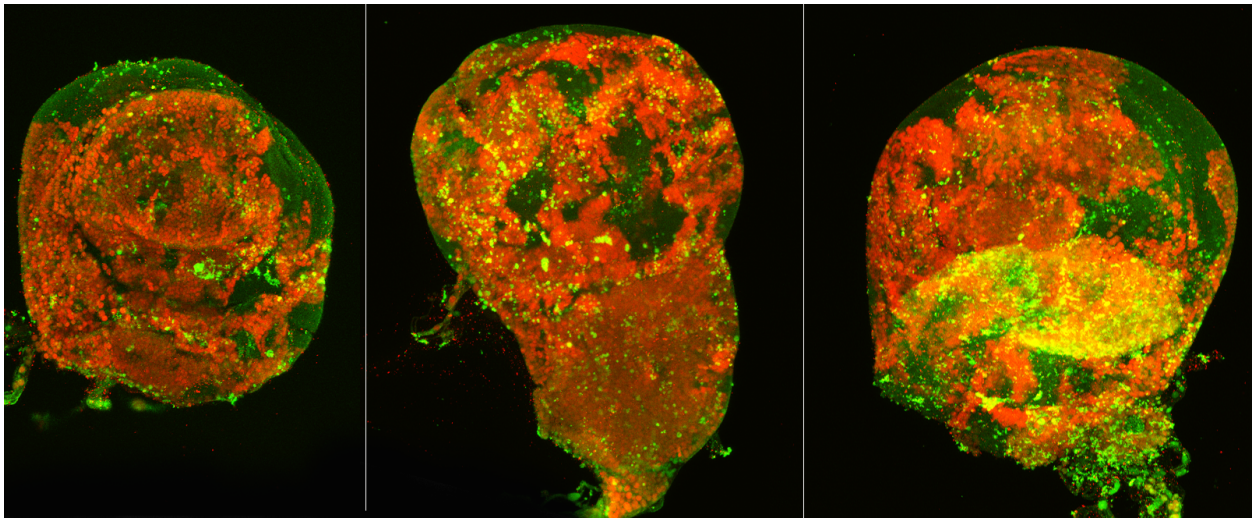


Figure 1-15. HIPK displays normal stress-induced cell death

Wing discs containing mitotic *hipk* null clones were marked by the absence of red signal (antibody staining against GFP which marks wild type tissue) and stained with TUNEL (green punctate structures) to mark apoptosing cells. *Hipk* mutant tissues have similar TUNEL staining to their wild type counterparts and show no defects in stress-induced cell death.

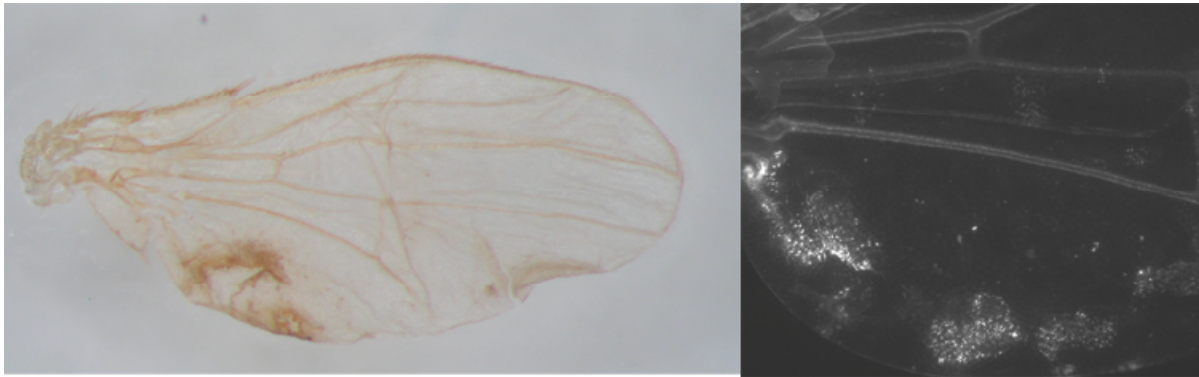


Figure 1-16. I(3)S141405 displays cell death defects in the wing

A strong phencopy screen hit, I(3)S141405 displays a strong blemish phenotype (left panel) and has a persisting cell phenotype (right) indistinguishable from mutants in canonical cell death genes.

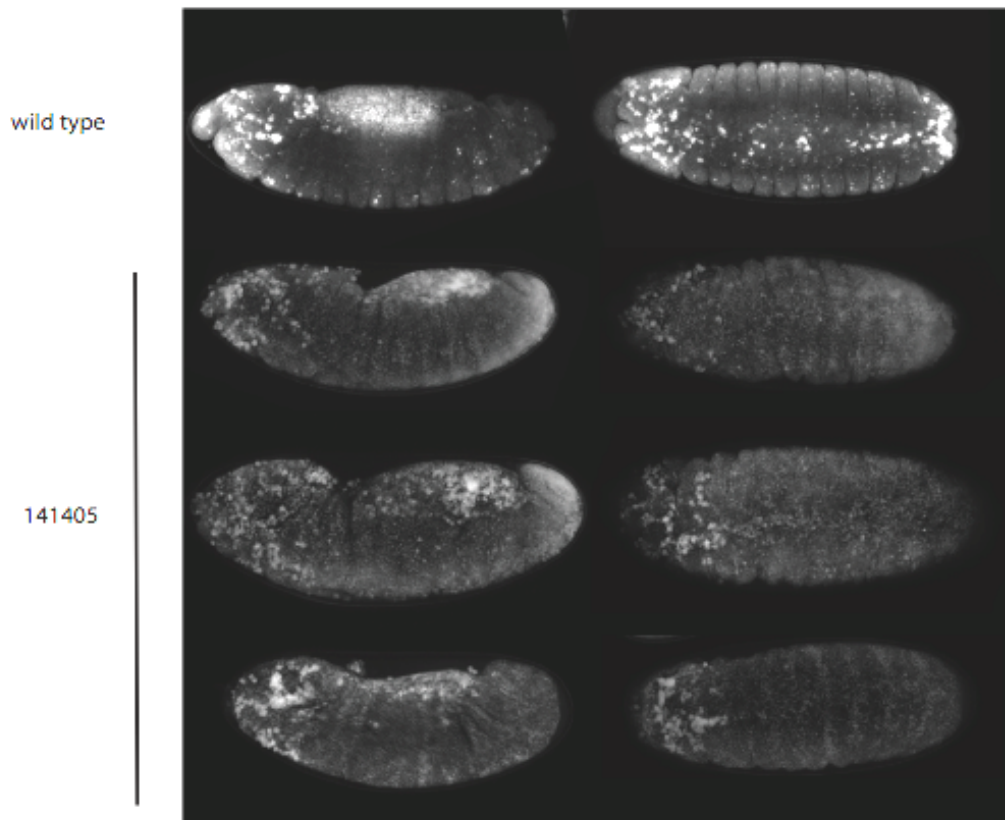


Figure 1-17. *l(3)S141405* is required for embryonic cell death

Wild type animals stained with acridine orange display normal developmental cell death while germline clones of *l(3)S141405* stained with acridine orange to mark dying cells display normal cell death in the head region but show no cell deaths in more posterior segments and throughout the ventral nerve cord.

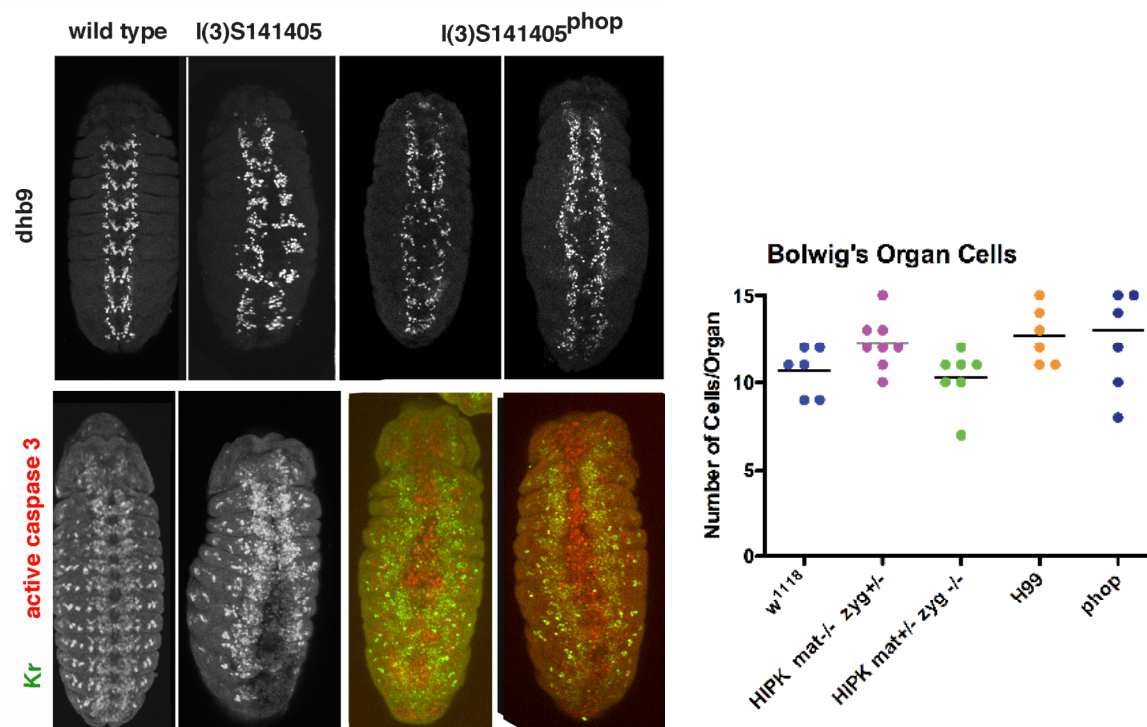


Figure 1-18. I(3)S141405 is required for neuronal development

Germline clones of I(3)S141405 display abnormal neuronal development as displayed by dHb9 and Kr staining. The original insertion of I(3)S141405 was precisely removed to produce I(3)S141405^{phop} and germline clones were generated. Staining patterns of dHb9 and Kr show abnormal neuronal phenotypes in I(3)S141405^{phop} similar to the original insertion line, I(3)S141405, suggesting that an additional mutation is responsible for neuronal defects. Bolwig's organ cells were counted in Kr stained I(3)S141405^{phop} animals and displayed on the right. I(3)S141405^{phop} animals appear to have varying numbers of cells, but some animals contain as many as H99 animals which are completely cell death defective.

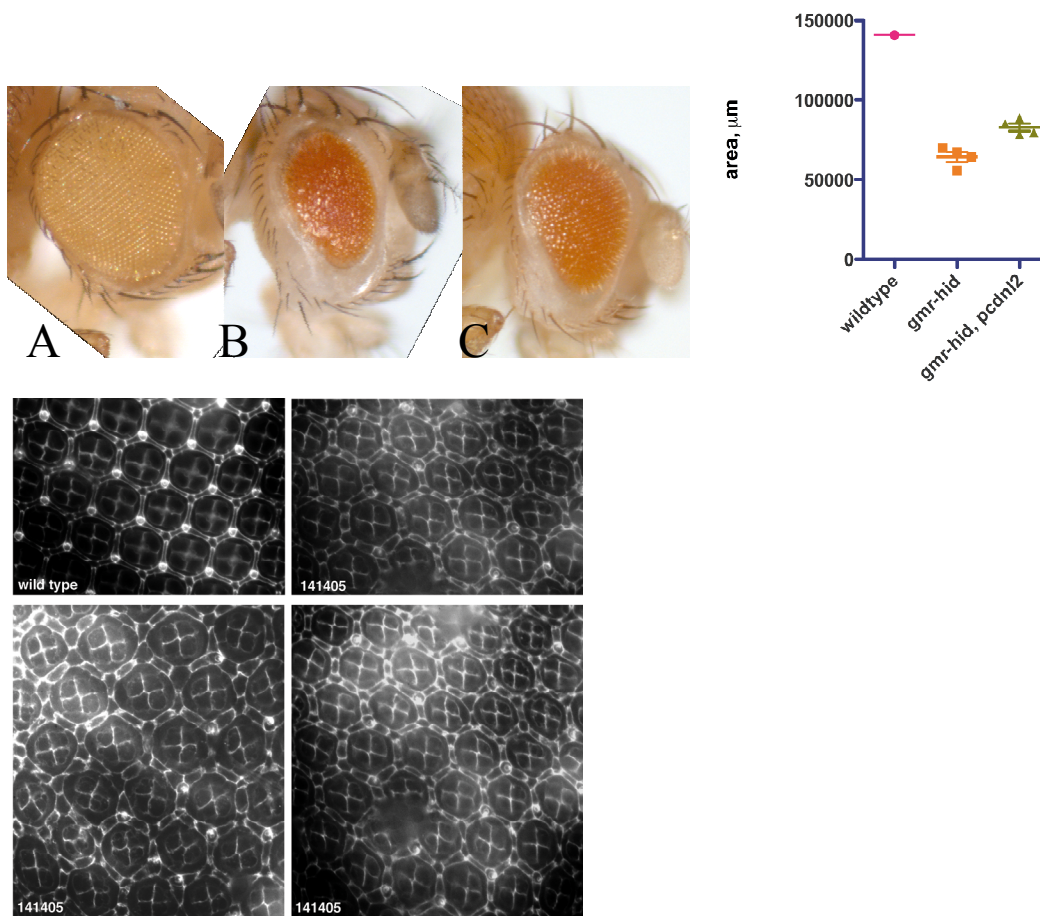


Figure 1-19. *I(3)s141405^{phop}* mildly rescues *Hid* induced killing but does not block developmental cell death in the eye

Epistatic relationships were tested using whole eye clones of *I(3)S141405^{phop}* generated in the background of *hid* overexpression. (A) displays heterozygous *I(3)S141405^{phop}* animals as controls. (B) is overexpression of *hid* using *gmr-Gal4* to drive *UAS-hid*. (C) is whole eye clones of *I(3)S141405^{phop}* while using *gmr-Gal4* to drive *UAS-hid*. Note that in (B), eyes are small and rough compared to wild type (A) due to ectopic killing by *Hid*. However, if placed in the *I(3)S141405^{phop}* background, the eye is less rough and larger than *hid* overexpression alone, suggesting that *I(3)S141405^{phop}* partially rescues ectopic killing by *Hid* and places *I(3)S141405^{phop}* downstream of *Hid*. The graph displays size measurements of each animal in microns.

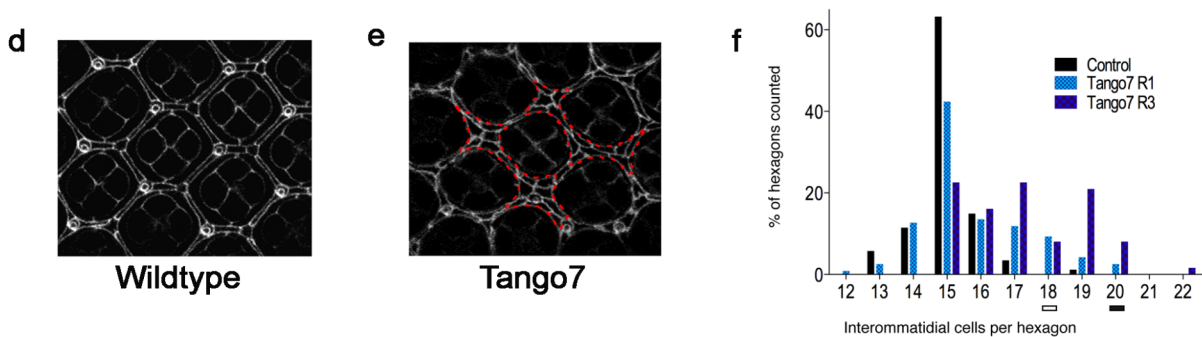


Figure 1-20. Tango7 is required for interommatidial cell death.

Transgenic dsRNAs that silence Tango7 (8309R1) and an irrelevant gene (5887R1) were targeted to the eye and caspase-dependent death of interommatidial cells in the pupal retina was examined after staining with α -DLG to outline cell borders (see (Muro et al., 2006; Xu et al., 2005) and methods for complete genotypes). Counts of hexagonal ommatidial assemblies were adapted from ((Wolff and Ready, 1991)). In control retinas, the majority (63%) of hexagonal assemblies were populated by the stereotypical number interommatidial cells (15) with fewer than 5% showing 17 or more cells per hexagon (N=87). In contrast, eyes silenced for Tango7 produced 28% of hexagonal assemblies with 17 or more cells per ommatidia (N=118) and only 40% of hexagonal assemblies showed the stereotypical number interommatidial cells. Insets show wild type (control) and Tango7 patterns of extra interommatidial cells, outlined in red.

High priority apoptosome phenocopy hit descriptions

Strain	Gene	Location	Nucleotide Insertion	PCR confirmed	Onset day	Severity	Persisting cells	Penetrance
I(3)S018222- FRT82	CG7187, Ssdp	90F6-7				+++		incomplete
I(3)S005115- FRT82	taranis,	89B		yes	33,4	+++	weak (alex)	57%
I(3)S045831- FRT82	tara, last intron	89B8--9	12075150	yes		++		incomplete
I(3)S133610- FRT82	tara, last intron	89B	12075351	yes		+++		
I(3)S059813- FRT82	tara	89B		yes		+++		
I(3)S142204- FRT82	homothorax	86C		previously mapped		+++		
I(3)S132307- FRT82	homothorax	86C		previously mapped		+++		
I(3)S070701- FRT82	CG31132(WD-40 domain), 4th intron	95F12-- 13	20146062	yes,		+++(+)	weak	
I(3)S145211- FRT82					2	+++		incomplete
I(3)S110106- FRT82								
I(3)SH017- FRT82								
I(3)SH023- FRT82								
I(3)SH116- FRT82								
I(3)S134313- 80	CG17090(HIPK2), 1st intron	61C3--5	527728	yes		+++	few	


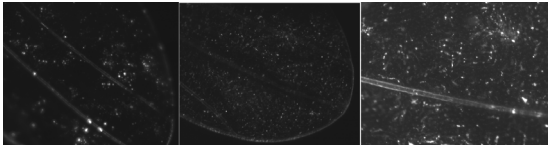



I(3)S048915-80	th	72C-D	16011180	previously mapped		++	yes in blister	
I(3)S55409-80	msn	62E	2569755	yes		+++	no(a few remnants) alex..some	
I(3)S11505-80	CG8177(bicarbonate transporter), 1st exon	67C	9737695	yes		+++	very weak to none	
I(3)S126608-80	furry	67C	9649518	yes				
I(3)S115915-80	CG11563 (100D) confirmed by pcr-- not on right side						yes (alex)	
I(3)S012815-80	NOT CKIIa—that's FRT						no. (wj alex)	
L(3)S024409A-FRT80								
L(3)S146907-FRT80	grunge	66C						
L(3)S145006-FRT80	mir-279 (99A) confirmed by pcr...not on right side							
SH0142-FRT40	CG17646 (ABC transporter complex?)	22A4--B1						
SH1181-FRT40	bsf (bicoid mRNA stability factor, 3'-UTR)	36F5						
I(2)SH0173-FRT 42	dark							

--	--	--	--	--	--	--	--	--


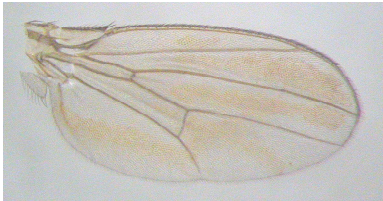
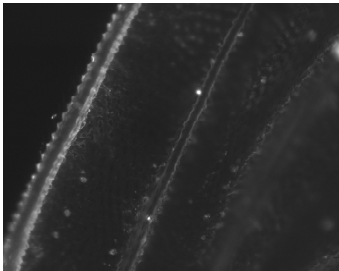


Table 1-1. High priority phenocopy hits

High priority hits from the phenocopy screen with strain number, insertion location using genome release 3 and descriptions of phenotypic data.

High priority apoptosome phenocopy wing phenotypes

Strain	Gene	Severity	Persisting cells
I(3)S018222- FRT82	CG7187, Ssdp	+++	
I(3)S005115- FRT82	taranis,	+++ 	weak (alex) 
I(3)S045831- FRT82	tara, last intron	++	
I(3)S133610- FRT82	tara, last intron	+++ 	
I(3)S059813- FRT82	tara	+++ 	
I(3)S142204- FRT82	homothorax	+++ 	

I(3)S132307-FRT82	homothorax	+++ 	
I(3)S070701-FRT82	CG31132(WD-40 domain), 4th intron	+++(+) 	weak 
I(3)S145211-FRT82		+++ 	
I(3)S110106-FRT82			
I(3)SH017-FRT82			
I(3)SH023-FRT82			
I(3)SH116-FRT82			
I(3)S134313-80	CG17090(HIPK2), 1st intron	+++ 	few

I(3)S048915-80	th	++ 	yes in blister
I(3)S55409-80	msn	+++	no(a few remnants) alex..some
I(3)S11505-80	CG8177(bicarbonate transporter), 1st exon	+++ 	very weak to none 
I(3)S126608-80	furry		
I(3)S115915-80	CG11563 (100D) confirmed by pcr-- not on right side		yes (alex)
I(3)S012815-80	NOT CKIIa—that's FRT		no. (wj alex)
L(3)S024409A-FRT80			
L(3)S146907-FRT80	grunge		


L(3)S145006- FRT80	mir-279 (99A) confirmed by pcr...not on right side		
SH0142- FRT40	CG17646 (ABC transporter complex?)		
SH1181- FRT40	bsf (bicoid mRNA stability factor, 3'- UTR)		
I(2)SH0173- FRT 42	dark		

Table 1-2. High priority phenocopy hit phenotypes

High priority hits and pictures of their wing phenotypes.

Low priority apoptosome phenocopy hit descriptions

Strain	Gene	Location	Insertion location (Rel 3)	PCR confirmed	Onset day	Severity	Persisting cells	Penetrance
I(3)S073214 -FRT82	CG10272 gpp (grappa)(trith orax group), 1st exon/5'upstre am	83E6--7	2232379	yes	2,3	+	No	30-50%, 67
I(3)S086909 -FRT82	CG9924(Traf- like domain), 7th intron	88A3--4	9802015	yes	1,5	+		incomplete
I(3)S060015 A-FRT82	tara		12068517	yes	3,4	+/-		75
I(3)S126209 B-FRT82	osa	90C1--2	278963	yes	8	+, ++	in progress	4
I(3)S141405 -FRT82					1	+, 1	yes strong	
I(3)S023802 -FRT82					4,5	+, ++		incomplete,55
I(3)S023713 -FRT82	CG31522	88E12--13	278965	yes	6	+	in progress	57
I(3)S047903 B-82					>14	-		5
I(3)S097074 -FRT82	how				1	++		100
I(3)S053606 -FRT82	how, 1st intron	94A1	?17868472	yes, two inserts		++		
I(3)S090417 -FRT82	how, 2nd intron	94A1	17878295	yes		++	some with wrinkles	

I(3)S074407 -FRT82	bel, 1st intron	85A5	4484608	yes		++		
I(3)S119515 -FRT82	cg5919, 1st exon	93D2	17096238 (+/- 50)	yes		+		incomplete
I(3)S057310 -FRT82	gammaCOP	100C6			1,4	+ (++)	no	
I(3)S058617 A-82	bnl	92B2--3			1,4	++ (-)	no	88
I(3)S009102 -FRT82						+		incomplete
I(3)S100604 -FRT82								
I(3)S115806 -82								
I(3)S072703 -82								
I(3)S069805 -82								
I(3)S126908 -82	CG17625							
I(3)S024836 -82	CG31132							crumbled wings, darken w/ age
I(3)S051311 -82							no	
I(3)S047110 -82	CG5919					+	weak	
I(3)S122009 -82								
I(3)S130405 -82								blister, curved, how, patchy

								outside blister
L(3)S11791 1-FRT82								
L(3)SH146- FRT82								
I(3)SH007- FRT82								
I(3)S115307 -FRT82								
I(3)S139114 -FRT82								
I(3)SH157- FRT82								
I(3)S111704 -FRT82								
I(3)S059706 -FRT80								
L(3)S14620 5-FRT80								
L(3)S14740 3-FRT80								
L(3)S14506 9-FRT80								
L(3)S14851 3-FRT80								
L(3)S14111 0-FRT80								
L(3)S14591 1-FRT80								
L(3)S14641 1-FRT80								

L(3)S14740 4-FRT80								
L(3)S14570 9-FRT80								
L(3)S14571 0-FRT80								
L(3)S13571 0-FRT80								
L(3)S14741 2-FRT80								
L(3)S12400 3-FRT80								
L(3)S14561 0-FRT80								
L(3)S14791 5-FRT80								
L(3)S05730 6B-FRT80								
L(3)S14600 4-FRT80								
L(3)S01113 0-FRT80								
L(3)S02301 3-FRT80								
L(3)S02761 2-FRT80								
L(3)S05970 6-FRT80								
I(2)SH2106- FRT42							yes	
I(2)SH2275- FRT42	mir- 14/CG1888						yes	



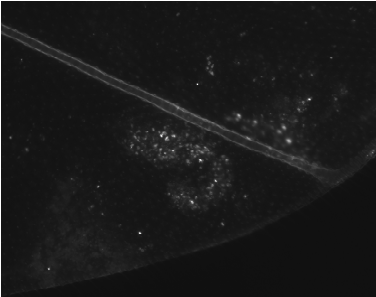

I(2)SH2342 -frt42	prosa6						yes	
I(2)SH0070 FRT42	CG2765		20471915	yes			yes	
I(2)SH0201- FRT 42	vps32						yes	
I(2)SH0123- FRT 42								
I(2)SH0240- FRT 42								
I(2)SH0473- FRT 42								
I(2)SH0497- FRT 42								
I(2)SH0636- FRT 42								
I(2)SH0676- FRT 42								
I(2)SH0912- FRT 42								
I(2)SH0941- FRT 42								
I(2)SH0956- FRT 42								
I(2)SH1016- FRT 42								
I(2)SH1170- FRT 42								
I(2)SH1261- FRT 42								
I(2)SH1453 FRT 42								






I(2)SH2214- FRT42								
I(2)SH0270- FRT42								
I(2)SH0742- FRT42								



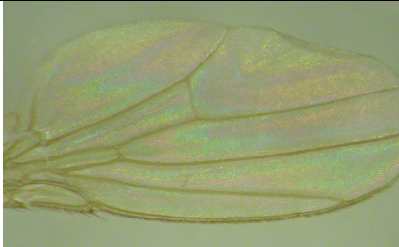

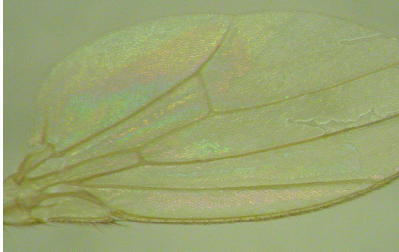
Table 1-3. Low priority phenocopy hits





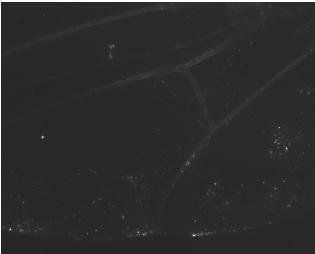
Low priority hits from the phenocopy screen with strain number, insertion location using genome release 3 and descriptions of phenotypic data.

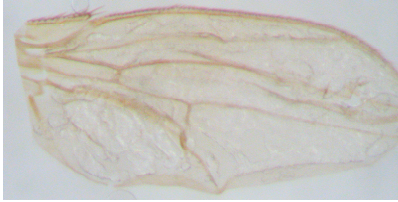
Low priority apoptosome phenocopy hit phenotypes

Strain	Gene	Severity	Persisting cells
I(3)S073214-FRT82	CG10272 gpp (grappa)(trithorax group), 1st exon/5'upstream	 +	no
I(3)S086909-FRT82	CG9924(Traf-like domain), 7th intron	+	
I(3)S060015A-FRT82	tara	+/-	
I(3)S126209B-FRT82	osa	+, ++	in progress
I(3)S141405-FRT82		 +, 1	yes strong 
I(3)S023802-FRT82		 +, ++	
I(3)S023713-FRT82		+	in progress

			
I(3)S047903B-82		 -	
I(3)S097074-FRT82	how	 ++	
I(3)S053606-FRT82	how, 1st intron	 ++	
I(3)S090417-FRT82	how, 2nd intron	++	some with wrinkles
I(3)S074407-FRT82	bel, 1st intron	 ++	

I(3)S119515-FRT82	cg5919, 1st exon	 +	
I(3)S057310-FRT82	gammaCOP	 + (++)	no
I(3)S058617A-82	bnl	 ++ (-)	no
I(3)S009102-FRT82		 +	
I(3)S100604-FRT82			
I(3)S115806-82			
I(3)072703-82			

I(3)S069805-82			
I(3)S126908-82	CG17625		
I(3)S024836-82	CG31132		
I(3)S051311-82			no
I(3)S047110-82	CG5919	 +	weak 
I(3)S122009-82			
I(3)S130405-82			
L(3)S117911- FRT82			
L(3)SH146- FRT82			
I(3)SH007- FRT82			

I(3)S115307- FRT82			
I(3)S139114- FRT82			
I(3)SH157- FRT82			
I(3)S111704- FRT82			
I(3)S059706- FRT80			
L(3)S146205- FRT80			
L(3)S147403- FRT80			
L(3)S145069- FRT80			
L(3)S148513- FRT80			
L(3)S141110- FRT80			
L(3)S145911- FRT80			
L(3)S146411- FRT80			
L(3)S147404- FRT80			
L(3)S145709- FRT80			

L(3)S145710- FRT80			
L(3)S135710- FRT80			
L(3)S147412- FRT80			
L(3)S124003- FRT80			
L(3)S145610- FRT80			
L(3)S147915- FRT80			
L(3)S057306B- FRT80			
L(3)S146004- FRT80			
L(3)S011130- FRT80			
L(3)S023013- FRT80			
L(3)S027612- FRT80			
L(3)S059706- FRT80			
I(2)SH2106- FRT42			yes
I(2)SH2275- FRT42	mir-14/CG1888		yes
I(2)SH2342 - frt42	prosa6		yes
I(2)SH0070 FRT42	CG2765		yes

I(2)SH0201- FRT 42	vps32		yes
I(2)SH0123- FRT 42			
I(2)SH0240- FRT 42			
I(2)SH0473- FRT 42			
I(2)SH0497- FRT 42			
I(2)SH0636- FRT 42			
I(2)SH0676- FRT 42			
I(2)SH0912- FRT 42			
I(2)SH0941- FRT 42			
I(2)SH0956- FRT 42			
I(2)SH1016- FRT 42			
I(2)SH1170- FRT 42			
I(2)SH1261- FRT 42			
I(2)SH1453- FRT 42			
I(2)SH2214- FRT 42			
I(2)SH0270- FRT 42			

I(2)SH0742- FRT42			
----------------------	--	--	--

Table 1-4. Low priority phenocopy hit phenotypes

Materials from Chapter One were originally published in the following:

1. Link N, Chen P, Lu WJ, Pogue K, Chuong A, Mata M, Checketts J, and J. M. Abrams. (2007) A collective form of cell death requires homeodomain interacting protein kinase. ***Journal of Cell Biology*** 178: 567-574.
2. Chew SK, Chen P, Link N, Galindo K A, Pogue K, and J.M. Abrams. (2009) Genome-wide silencing in Drosophila captures conserved apoptotic effectors. ***Nature*** 460: 123-127.

Stimulus-responsive noncanonical transcription in

Drosophila melanogaster

SUMMARY

We produced 'saturation tile' arrays by digital optical chemistry for an unbiased sampling of transcriptional activity in the *Drosophila* genome. Complete coverage, without gaps, through a 335kb interval was achieved in the form of 25bp matched and mismatched features. Validated profiling of samples prepared from control and irradiated animals produced three salient observations. First, the scope of unannotated transcriptional activity is extensive and widespread. Second, a dominant population of noncanonical transcripts was acutely stress-responsive. Third, stimulus-dependent induction of unannotated RNAs required p53, a master regulator of conventional stress-responsive target genes in vertebrates and invertebrates.

INTRODUCTION

Recent studies have described a vast amount of unannotated transcription throughout eukaryotic genomes. Several groups are taking a genome-wide approach to map all transcriptional activity in various model organisms, and collectively, data suggest that more of the genome is transcribed than annotations predict. The ENCODE (Encyclopedia of DNA Elements) project is an international consortium working to annotate not only all transcription in the human genome (Birney et al., 2007), but also potential functional elements including transcription factor binding sites, histone marks, and chromatin accessibility to name a few (Raney et al.). Groups such as the modENCODE are extending this research to both *C. elegans* and *D. melanogaster* genomes (Celniker et al., 2009; Roy et al., 2010).

With recent advances in genomics and ability to map transcription genome-wide, we still do not understand the function of the extensive non-canonical transcription throughout many genomes. Reports from *D. melanogaster* have shown that non-coding transcription is regulated throughout development (Manak et al., 2006a). However what these transcripts are doing remains unclear.

Few studies have advanced our understanding of the function of non-coding transcripts. For example, many non-coding RNAs are involved in X chromosome inactivation (Chureau et al., 2010; Shin et al., 2010). Long non-coding RNAs have been shown to regulate gene expression (Huarte et al., 2010; Petruk et al., 2006; Rinn et al., 2007) and perhaps even act as enhancers (Orom et al., 2010).

The complete extent of unannotated transcription is not accurately known and the functional content of this unannotated transcription is virtually unknown. However, the significant and vast levels of unconventional activity raise important questions that challenge conventional concepts of meaningful genetic code versus “junk DNA”. Therefore, an important task is to determine whether unpredicted or noncanonical RNAs actually encode meaningful content. In principal, this goal can be achieved through comprehensive mapping of transcriptional activity at high resolution combined with functional testing available in sophisticated genetic models. Toward this end, we devised an unbiased method for comprehensive profiling of transcriptional activity, without gaps, through a large, well-defined interval of the *Drosophila* genome. We applied a ‘saturation tile’ oligonucleotide array in hybridization experiments, together with rt-PCR validations to derive three salient observations. First, the scope of unannotated transcription is widespread. Second, much of this noncanonical activity was stress-responsive (defined here as induced by radiation). Third, stimulus-dependent transcription of unannotated RNAs was clearly impacted by p53, a master regulator of conventional stress-responsive target genes (Lu and Abrams, 2006; Vousden and Lu, 2002; Vousden and Prives, 2005).

MATERIALS AND METHODS

Darkstar Array Design

Arrays were kindly generated in the Garner lab using digital optical chemistry (DOC) as described in (Luebke et al., 2002). Contiguous 25 base pair probes were printed through 335kb of *D. melanogaster* chromosome 3L starting at base pair 18123001 (genome release 4.0) to . Each 'tiled' sequence was represented with three probes for each strand: wildtype, one-mismatch at base 13, and two-mismatches at bases 13 and 14. Mutations were designed as purine–pyrimidine shifts (complementary base pairs). Controls outside the tiled region include sequences for *actin 42a*, *rp49*, and *grim*, the radio-responsive genes *mnrs*, *reaper*, *sickle*, *CG17836* (Akdemir et al., 2007) and *D. melanogaster* microRNAs including *mir-3*, *mir-4*, *mir-5*, *mir-7*, *mir-9*, *mir-11*, *mir14*, *mir-317*, and *bantam*. Additional control microRNAs included *Homo sapien mir-150*, *mir-152*, *mir-27a*, *mir-34c*, *mir-93*, *Mus musculus mir-191*, *mir-200c*, *mir-292*, *mir-324*, *mir-325*, *Rattus norvegicus mir-101b*, *mir-15*, *mir-34c*, *mir-16*, *Caenorhabditis elegans mir-244*, *mir-246*, and *mir-40*. Other controls sequences were printed corresponding to portions encoding the 18S and 28S ribosomal RNAs. Internal controls for print uniformity and specificity were from portions of the HIV viral genome (Garner, ; Luebke et al., 2002). Among the wild type sequence features on the darkstar array, less than 2% are not unique to the contig. The resulting prototype, designated 'darkstar', was custom produced by the Garner lab.

Embryo Collection

Embryos from w^{1118} (wildtype) and $p53^-$ mutants were collected for 2.5 hours, aged for 2.5 hours, and either mock treated or irradiated at 4000 rads followed by a 1.5 hour recovery. Embryos were dechorionated with 50% bleach for 2-3 minutes and rinsed with water. Embryos were snapped frozen using liquid nitrogen and stored at -80°C until needed. To verify irradiation effects, a small portion of embryos were stained with acridine orange, a marker of apoptosis to visualize stress-induced cell death.

RNA isolation

Embryos were removed from -80°C and immediately ground in lysis buffer using chilled glass homogenizers. Total RNA was isolated using Ambion's mirVana miRNA Isolation Kit following the total RNA isolation protocol. Resulting samples were run on agarose gels to assess RNA degradation. Polyadenylated RNA was isolated using Oligo dT cellulose (Ambion) or Qiagen's Oligotex mRNA isolation kit. Samples were concentrated using a Millipore Microcon YM-30.

Labeling and Hybridization

Cy3 or Cy5 was incorporated into mock-treated and irradiated RNA samples using Amersham's CyScribe First-Strand cDNA Labeling kit in oligo(dT) and random nonamer reverse transcription reactions. Labeled cDNA was purified using Millipore Microcon YM-30 and simultaneously hybridized to the same Darkstar array after heat

denaturation in hybridization solution containing 2XSSC and 2X Denhardt's solution. Hybridizations were carried out in a humidified chamber at 37°C overnight in the dark. Arrays were washed with 2XSSC at 37°C (2X) and at room temp (6X). Dried arrays were scanned using the Genepix Personal 4100A (Axon Instruments), and data were harvested using DOCUMENTOR, a custom built program generated by the Garner Lab for the DOC microarray synthesizer. Probe expression was defined as 3 standard deviations away from background.

Identification of novel transcript regions

Primers to validate novel transcription regions were designed to regions of contiguous expression (two or more probes adjacent to each other on the array that have expression three standard deviations away from background) on the array that were a significant distance from known annotations. Regions with increased signal intensity or an increased number of probes with positive signal after irradiation challenge were higher priority. Primers were designed to flank novel transcript regions covering 250bp-1kb of genomic sequence.

Reverse Transcription Polymerase Chain Reactions

0.2µg of total RNA from wildtype and *p53*⁻ mutant animals was used in Invitrogen SuperScript™ III One-Step RT-PCR System with Platinum® *Taq* DNA Polymerase in 50µl reactions with primers specific to Darkstar novel transcript regions. 10µl of each reaction mixture was analyzed using 1% agarose gel electrophoresis.

Deletion Strains

Deletions were generated using the Exelixis collection of P elements as described in (Parks et al., 2004)

Egg Hatching

Animals were placed in collection vials, embryos were collected for short intervals, and the amount of embryos hatching to larvae was counted 36 hours later. To measure egg length, pictures were taken on SteREO Discovery V.12 and embryo length was measured using Zeiss software.

Pupation and eclosion assays

Wandering third instar larvae were collected in vials and subjected to various amounts of irradiation. Time after irradiation was monitored by counting the number of prepupa at hourly intervals. Eclosion rates were monitored by counting the number of viable adult animals.

Twin spot analysis

Animals of the genotype *hs:flp*; *FRT-80 GFP* were crossed to *H99-FRT80*, *D2-FRT80*, or *FRT-80*. First and second instar larvae were heat shocked at 37C for up to 4 hours. If stressed, wandering third instar larvae were collected and irradiated at 2-4 krad. Resulting adults were imaged on the SteREO Discovery V.12 and eye clone size was measured using Zeiss software.

RESULTS

Saturation tiled microarray

We sought to investigate transcriptional activity at the highest possible resolution in a well-curated, genetically accessible genome. For this purpose, we designed a microarray representing ‘saturation’ tiled coverage of a contig spanning ~335kb in region 75C of the *Drosophila* genome. Over 85,000 features were printed as 25bp tiles that contiguously span both strands of this entire genomic interval without gaps. Each tile on this array (designated *darkstar*) includes one perfect probe and two mismatched probes, permitting assignment of confidence values for signals generated by each tile. Also printed on this array are technical controls for specificity, print uniformity, and numerous ‘surveillance controls’ (see methods), including portions of the 18s and 28S rRNAs, constitutive genes (e.g. actin, rp49 and ribonucleotide reductase), known miRNAs and selected stimulus-responsive genes. The genomic region sampled on this array presents several advantages. First, it is genetically well characterized (Abbott and Lengyel, 1991) and the entire interval is represented in the form of a phage DNA walk (White et al., 1994). Second, the region includes few repeat sequences and over 98% of the tiles are unique to the contig. Third, the contig spans vast stretches of DNA for which no or few transcripts are reported. Finally, stimulus-responsive genes (*rpr*, *hid*, *skl*) with known functions map to the region (Brodsky et al., 2004; Christich et al., 2002; Sogame et al., 2003). We reasoned that unannotated and/or non-canonical transcripts induced by a stressful stimulus would be plausible candidates for

investigating potential adaptive functions when challenged. The ‘stimulus’ chosen for these studies exploits standard protocols of radiation stress that prompt acute and well-studied biologic responses in *Drosophila* embryos (Brodsky et al., 2000; Jaklevic and Su, 2004; Nordstrom et al., 1996; Peters et al., 2002; Sogame et al., 2003; Xu et al., 2001).

Quality control hybridizations to the *darkstar* array were initially conducted using labeled genomic DNA. These tests demonstrated a robust dynamic range, spanning more than two orders of magnitude when test probes were compared to negative probes (from the HIV genome). For assurance of stimulus-dependent measurements, positive controls were applied at two stages in these studies. Prior to sample labeling, robust induction of cell death was confirmed using acridine orange staining of irradiated embryos prior to RNA isolation, and after hybridization, we verified induced signals from two known radioresponsive genes (*reaper* and *Xrp1* (Akdemir et al., 2007; Brodsky et al., 2004)).

Figure 2-1 is a panoramic view of transcripts detected on the darkstar array using mRNAs isolated from early *Drosophila* embryos that were either mock treated (green signal) or radiation-challenged (red signal) as in (Brodsky et al., 2000; Nordstrom et al., 1996; Sogame et al., 2003). Note that, for practical reasons, ‘present’ symbols are disproportionately over-sized, thereby over-representing signal densities and under-representing the true distance between positive tiles. At a global level, two significant findings emerge from these data. First, significant populations of unannotated transcripts (hereafter designated UNTs) were found. These were sporadically

distributed throughout the genomic interval sampled and a considerable fraction mapped to large intergenic regions. This outcome is consistent with significant intergenic transcription in the fly genome reported previously (Manak et al., 2006b; Stolc et al., 2004) and similar findings from tiling studies on the genomes of mice and humans (Bertone et al., 2004; Carninci et al., 2005; Cheng et al., 2005; Kapranov et al., 2002; Katayama et al., 2005; Rinn et al., 2003; Shoemaker et al., 2001). More striking, however, a dominant population of UNTs appeared only after stress challenge, exposing a widespread dimension of stimulus-conditional UNTs that was wholly unexpected.

UNT validation

rt-PCR strategies were used to authenticate a subset of UNTs detected on the darkstar array (Figure 2-2). Clustered signals were chosen for validation based on the following criteria. First, we required that contiguous or tightly clustered tiles produce present calls, with more than 3 fold signal to noise ratios. Second, each cluster chosen for validation spanned at least three 'nearest neighbor' tiles (for a distance of ~75 bp or greater). Third, each candidate mapped to an overtly nongenic region (in so-called 'gene deserts', see Table 2-3), thereby minimizing the chance that a given UNT simply represents an undiscovered exon of an already annotated gene.

From a total of 22 loci sampled, 11 UNTs were rt-PCR validated (purple signal Figure 2-1, table 2-1, table 2-2). Of these, radio-responsive behavior was confirmed in four cases, with transcript levels elevated post-irradiation challenge. In flies, as in mammalian systems, conventional responses to radiation are often mediated by p53, a

transcriptional regulator that coordinates global responses to genotoxic stressors (Brodsky et al., 2000; Brodsky et al., 2004; Jin et al., 2000; Lee et al., 2003; Ollmann et al., 2000; Sogame et al., 2003). Therefore, we also examined each confirmed UNT in animals lacking wild type p53. We found that overtly radio-responsive UNTs were profoundly impacted in p53⁻ animals (Figure 2-2). In three cases (#s10030, 10160, 10871) constitutive as well as stimulus-induced expression was abolished and in one case (#8521) radio-responsive induction failed but constitutive expression was unaffected (designated Group I). A second group of UNTs (Group II) were not overtly responsive to stress, but clearly required wild type p53 for basal expression.

We hypothesized that more highly conserved UNTs might be more likely to be transcribed in the animal. Therefore, we compared percent sequence similarity between *D. melanogaster* and *D. persimilis* of transcribed and non-validated (regions with signal on array but no signal from rt-PCR) UNTs. Using two different algorithms, ClustalW and Align, we found a wide range of conservation in both the transcribed and non-validated UNTs (Figure 2-3), suggesting increasing conservation does not map to active transcription. When average conservation was compared between transcribed and non-validated UNTs, transcribed UNTs percent similarity was marginally higher, but not near as high as protein coding genes (Figure 2-3). These results suggest that some, but not all, UNT regions may be highly conserved.

UNT functional analysis

To determine whether these validated UNT's function in the animal, we generated defined deletions uncovering four UNT's (4299, 10030, 10160, and 10871)

(Figure 2-4). Deletions were generated using FRT mediated homologous recombination and PCR validations are shown in Figure 2-5. Deletions uncovering UNT 10871 (D3) appeared normal, while deletions spanning 10030 and 10160 (D2) exhibit reduced viability and shortened egg length (Figure 2-6 and 2-7). However, these phenotypes disappeared when placed over a larger deficiency. Occasionally animals displayed minor defects including abnormal bristle and abdominal segment patterning and rotated terminalia (Figure 2-8). Deletions covering 4299 (D4) were female sterile, however we observed female sterility in the parental line, suggesting that 4299 does not contribute to this phenotype. As stated above, these UNT regions are stress responsive or p53 dependent. Therefore, we hypothesized that these RNAs may function in response to stress. To test this hypothesis, we first assayed these deletions for interactions with known regulators of stress responses in the animal. We combined our UNT deletions with mutants for the global transcriptional regulator *p53* and its upstream kinase *chk2* and found no obvious phenotypes. We also assayed p53 function using an *in vivo* p53 reporter system (Lu et al., 2010) and found no defect in p53 action. Similarly, cell death that occurs after ionizing radiation, which is dependent upon p53, in the developing larval imaginal wing disc was normal, further suggesting that the p53 pathway is unaffected in these mutants (Figure 2-12).

Next, we assayed animal sensitivity to stress during development. We hypothesized that if these UNT transcripts had a function after stress, UNT deletions would display a radiosensitive or radioresistant phenotype after ionizing radiation. To test this hypothesis, we examined wandering third instar larvae for sensitivity after

stress. We treated animals with increasing doses of ionizing radiation and tested for time to pupation and eclosion (hatching) rates. We found that D3 animals showed no difference from control genotypes for time to pupation (Figure 2-11). However, D2 and D4 placed in trans to a larger deletion showed faster pupation rates after 4 krad irradiation compared to wild type. Alas, when compared to a single copy of the larger deletion alone, there was no significant difference, suggesting that D2 and D4 do not contribute to faster pupation. We also looked at eclosion rates of all deletions with increasing doses of irradiation (Figure 2-9). Wild type animals (w^{1118}) LD₅₀ for survival was 3 krads irradiation while p53 LD₅₀ was near 2.5 krads. For all UNTs, the LD₅₀ was shifted lower to between 1 and 1.5 krads (Figure 2-9). To determine whether this sensitivity to irradiation was due to a background effect, we generated trans-heterozygous lines for all deletions, trans-heterozygous lines of deletions over larger deficiencies and trans-heterozygous parental lines and tested for irradiation sensitivity. Unfortunately, the larger deficiencies masked D2, D3, and D4 increased sensitivity (Figure 2-9), and most trans-heterozygous lines had a similar increase in irradiation sensitivity as deletions alone (Figure 2-10), suggesting background mutations of D2, D3, and D4 are responsible for radiation sensitivity phenotypes. We tested cell lethality rates after stress in the adult eye using ionizing radiation of twin spots (Figure 2-13), and found no difference in size between mutant and wild type animals (2-14). The above results suggest that these selected UNTs do not exert dramatic functions globally after stress tests used here. However, minor phenotypes might be missed.

Finally, we tested UNT deletions in a model of regeneration after stress. Wild type and trans-heterozygous animals were irradiated at 11krad ionizing radiation and fertility was assessed each day after irradiation. Wild type animals lose fertility 3-5 days after irradiation, but regain fertility as they recover from irradiation. p53 animals lose fertility but never regain the ability to produce viable animals. All three UNT deletions lose fertility and recover as wild type strains (Figure 2-15) indicating they do not play a role in germline stem cell regeneration after stress.

DISCUSSION

We have produced a high resolution tiling array using digital optical chemistry. Using this technology, we were able to develop and produce the darkstar array onsite. While this gave us the freedom to determine array content, it also produced obstacles to overcome. While many probes on the array hybridized well, others performed poorly due to their inability to hybridize control DNA. Therefore, some areas in our target region were not effectively queried. We chose to build a saturation tiling array covering the region in its entirety, which eliminated the opportunity to optimize probe sequences resulting in suboptimal binding for some probes. Even so, we discovered a substantial amount of noncanonical transcription throughout the tiling region. The darkstar array illuminated vast regions of unmapped transcripts that may encode novel forms of information in the form of noncoding RNA.

Additionally, darkstar illuminated a considerable amount of radiation responsive unconventional RNA material throughout the H99 region. Interestingly, stresses like irradiation do not repress transcription, but instead, a substantial increase in the amount of novel transcription occurs. This is in contrast to conventional wisdom that suggests irradiation inhibits transcriptional activity (Luchnik et al., 1988). Whether this transcription is a mechanism that promotes survival or adaptation to stress, or whether it is a passive process due to damage is unknown. However, the ability to detect these transcripts presents opportunities to functionally dissect this stress response.

p53 has been widely studied as an important tumor suppressor and transcriptional regulator. However, through the use of our tiling array, we have found

that p53 not only regulates canonical transcripts, but appears important for a vast population of unmapped transcription as well. This suggests that noncanonical transcription may be deliberately regulated by the p53 network, and thus, function in development. Since these noncanonical transcripts appear to be regulated by p53, perhaps they function in the same networks that p53 regulates such as cell death, cell cycle, or DNA repair.

In our studies, we did not identify an observable function for the UNTs we deleted. However, while these four UNTs may be “junk” RNA transcripts, our results do not definitively rule out the possibility that other UNTs in the region serve a function or that these UNTs function redundantly. These transcripts may function in a complex manner that is unobservable in the mutant adult animal or concert with redundant functions, hence making functional analysis difficult. Silencing or activating transcription, regulating promoter regions of DNA, or altering DNA chromatin state are a few of the possible functions for the immense population of stress induced transcripts, and with more sophisticated tools we may eventually be able to identify these functions.

PERSPECTIVES AND FUTURE DIRECTIONS

We described the presence and activation of unannotated transcription throughout the Reaper region after stress. Recent data from the ENCODE and modENCODE project are now available in searchable formats. Comparisons between our data and the modENCODE data may validate these unannotated transcripts and provide additional conditions in which they are expressed. Additionally, the chromatin state and transcription factor binding sites surrounding our novel transcripts may provide clues about additional regulation.

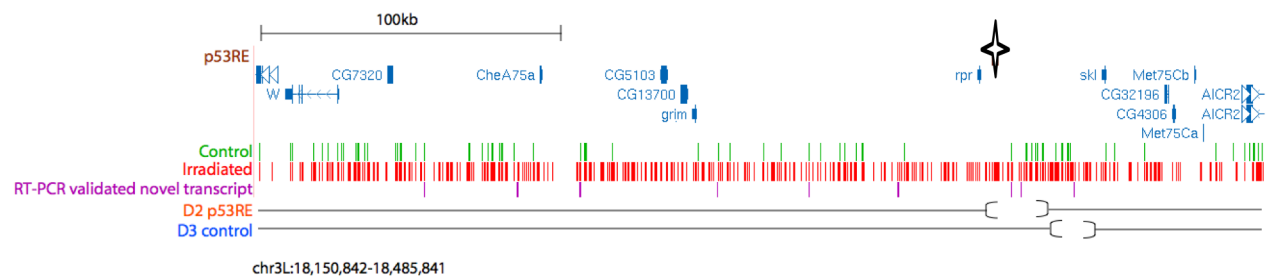


Figure 2-1. Stress induces abundant and validated unannotated RNAs (unRNAs).

Total RNA transcriptional activity was generated using a custom saturation tiling array (see methods) spanning chromosome 3L from coordinates 18,150,842-18,485,841 (*Drosophila melanogaster* assembly release 5). Using the UCSC genome browser, transcription is plotted across the darkstar region. Control (green) plots basal expression while irradiated (red) signal corresponds to transcription after 4000 rads ionizing radiation. Each vertical line represents two consecutive tiles with signal. Note that the abundance of activity post irradiation (red) compared to pre-irradiation (green). RT-PCR confirmed unannotated novel transcripts are noted in purple. Annotated protein coding genes are labeled in blue. The p53 response element is annotated with (⚡) and is eliminated in the D2 mutation but remains intact in D3.

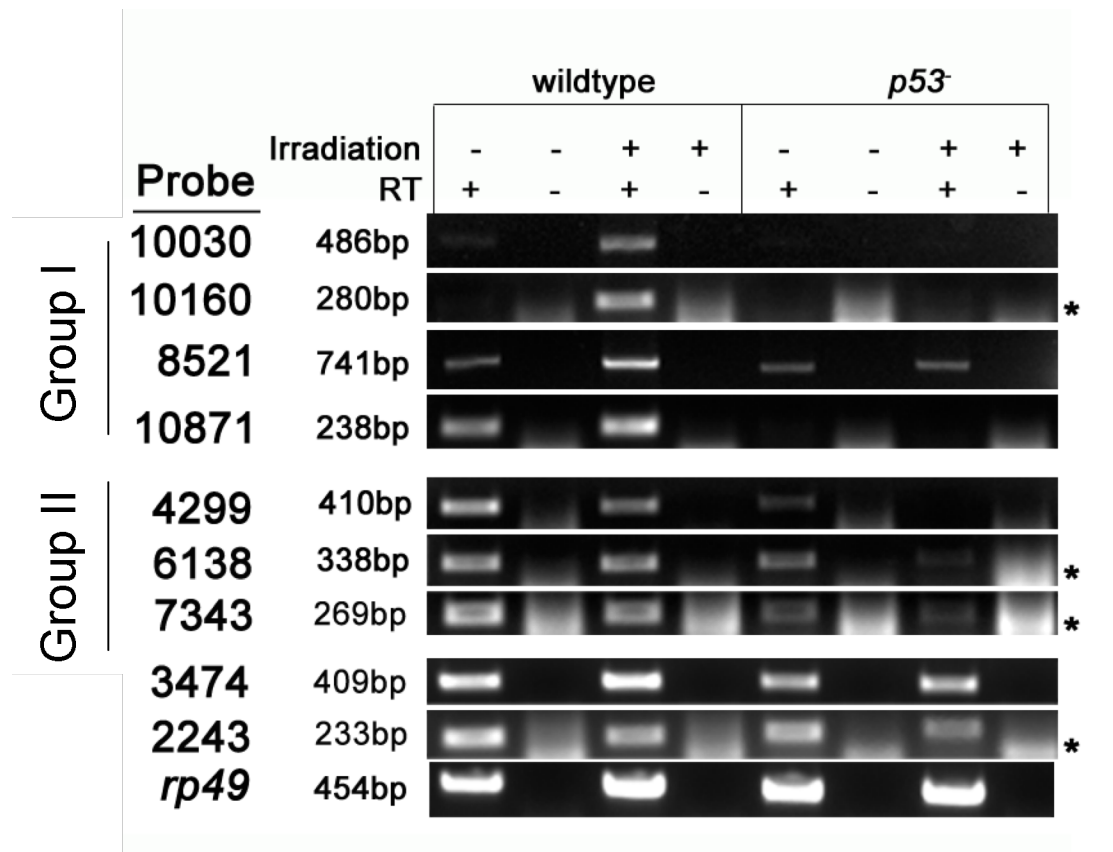


Figure 2-2. Many unannotated transcripts are radiation responsive and *p53* dependent.

Novel transcripts detected by tiling array were validated using reverse transcription-PCR reactions in control and gamma irradiated RNA samples from stage 4-6 wild type (*w1118*) or *p53*⁻ *Drosophila* embryos. Reactions were carried out with (RT+) and without (RT-) reverse transcriptase. Transcripts detected by probes 10030, 10160, 8521, and 10871 increase after radiation and are dependent upon functional *p53*. Transcripts detected by probes 4299, 6138, and 7343 required *p53* for normal expression after stress. 3474 and 2243 are constitutively expressed and *rp49* was used as a control. * denotes nonspecific products.

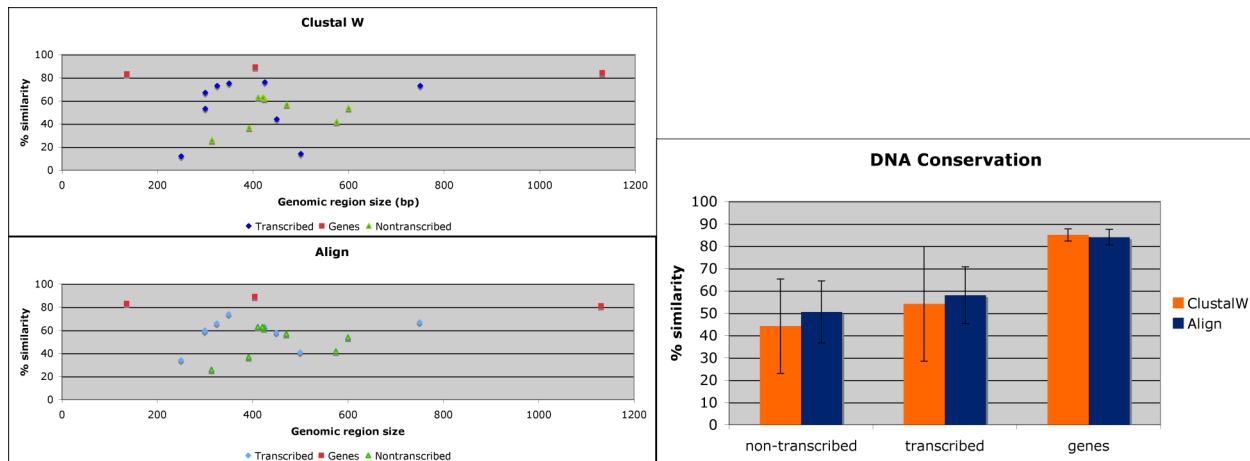


Figure 2-3. Novel transcript conservation between species varies.

Regions encompassing predicted novel transcripts from *Drosophila melanogaster* were compared to *Drosophila persimilis* using two alignment tools, ClustalW and Align. Conservation of each region was plotted in the left two panels, dividing regions into transcribed and unvalidated (no signal from RT-PCR reactions) groups. Three coding genes were used as controls. Some novel transcript regions are highly conserved, but others are not. Average conservation is displayed in the right panel. Transcribed regions are slightly more conserved than unvalidated (no signal from RT-PCR reactions), but conservation is highly variable.

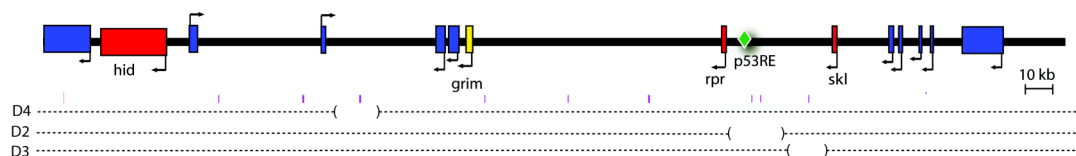


Figure 2-4. Deletions of UNTs

The H99 region is depicted in cartoon above with irradiation responsive cell death genes in red, grim, a non radio-responsive cell death gene, in yellow, and irrelevant genes in blue. PCR validated novel transcripts are noted by the purple vertical lines. Novel transcript deletions are noted by D4, D2, and D3.

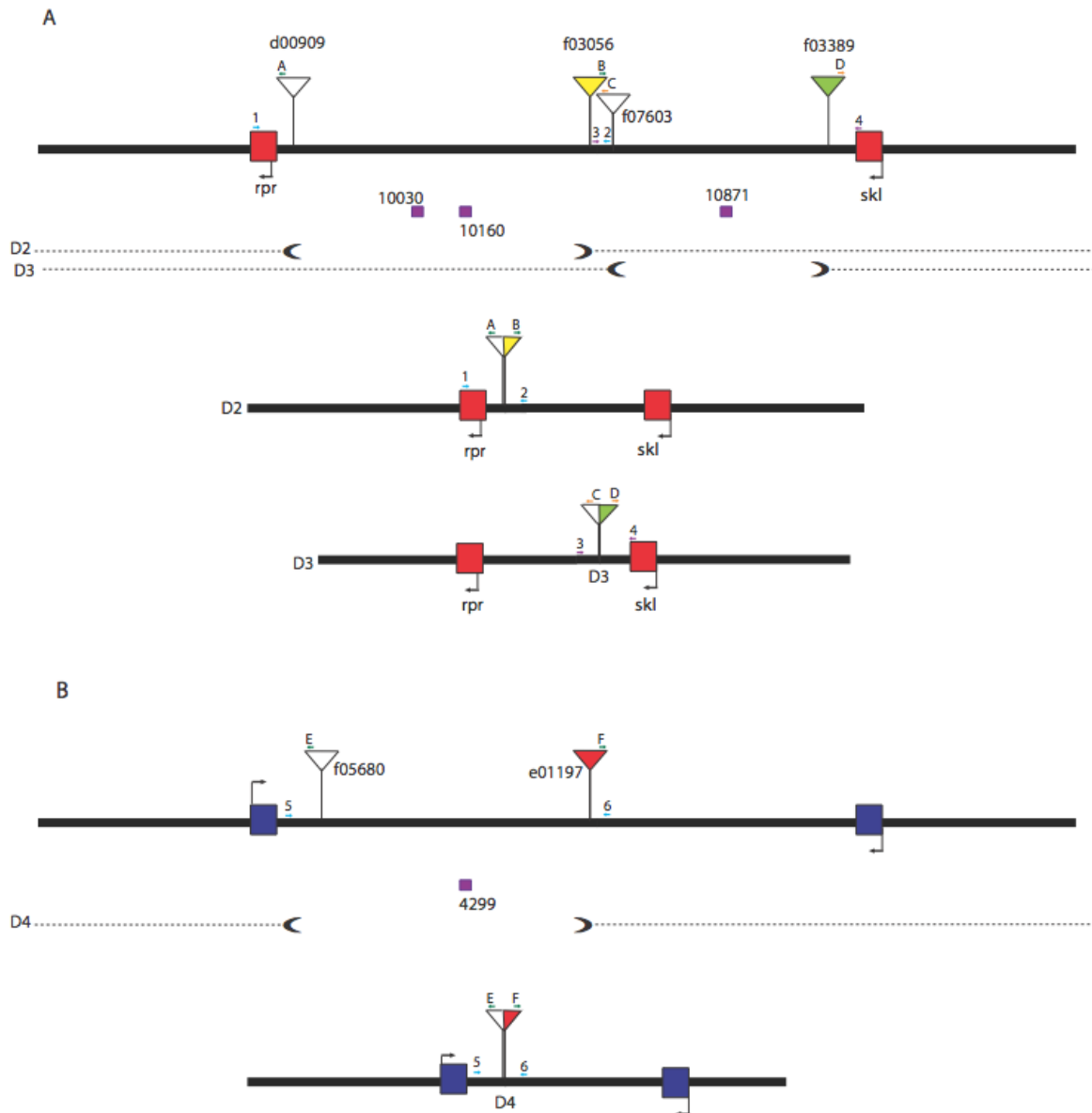


Figure 2-5. Validation of novel transcript deletion animals.

FRT mediated recombination was used to generate customized deletions that eliminate novel transcripts in the Reaper region. Two P elements spanning the region of interest were put in *trans*, together with a source of FLP recombinase to induce recombination, replacing native sequence with P element sequence. Deletions were isolated and verified using the schematics above. (A) displays both D2 and D3 before (top) and after recombination (below). To verify the D2 deletion, primer pairs 1-A, B-2, and 1-2 were used. To verify the D3 deletion, primer pairs 3-C, D-4, and 3-4 were used. (B) displays

D4 before (top) and after recombination (bottom) and primer pairs 5-E, F-6, and 5-6 verified deletions.

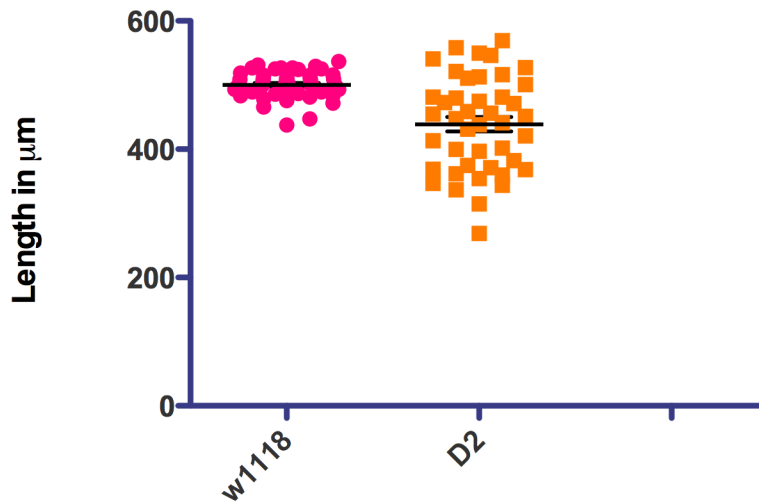


Figure 2-6. D2 animals lay short eggs.

Embryos from w^{1118} and animals homozygous for the D2 deletion were collected and embryo length was measured in microns. Wild type embryo length is 500.5 microns while D2 embryo length varies from 250 microns to near 600 microns, placing the average embryo size at 439 microns. Using a two-tailed t test, means are significantly different with $p < 0.0001$.

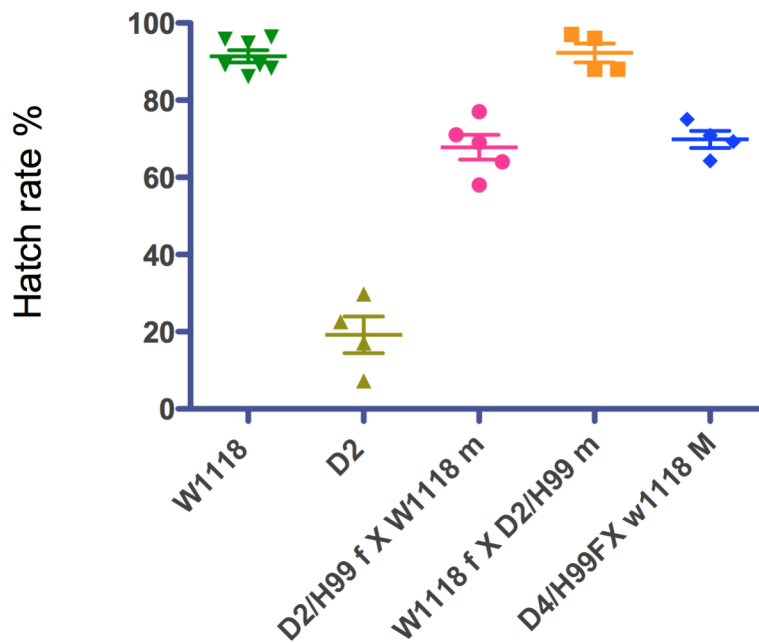


Figure 2-7. D2 animals have low hatch rates.

Embryos from w^{1118} and D2 homozygous animals were collected and scored for hatch rate. Wild type embryos hatched 89.1% of the time while D2 embryos hatched 19.85% of the time. To determine whether low hatch rate was specific to D2 or resulting from a background mutation, D2 was placed in trans to H99 and crossed to wild type animals. Eggs from females transheterozygous for D2 and H99 displayed a 69% hatch rate. Males transheterozygous for D2 and H99 mated to wild type females displayed a 92% hatch rate. These data suggest that low hatch rate is a maternal effect. Finally, females homozygous for the D4 mutation were sterile, and this sterility was mapped to a background mutation as D4/H99 transheterozygous were fertile. However, these females also displayed a low hatch rate (70%). Taken together, these data suggest that haploinsufficiency for H99 results in low hatch rate and the genetic background of D2 and D4 cause fertility defects.

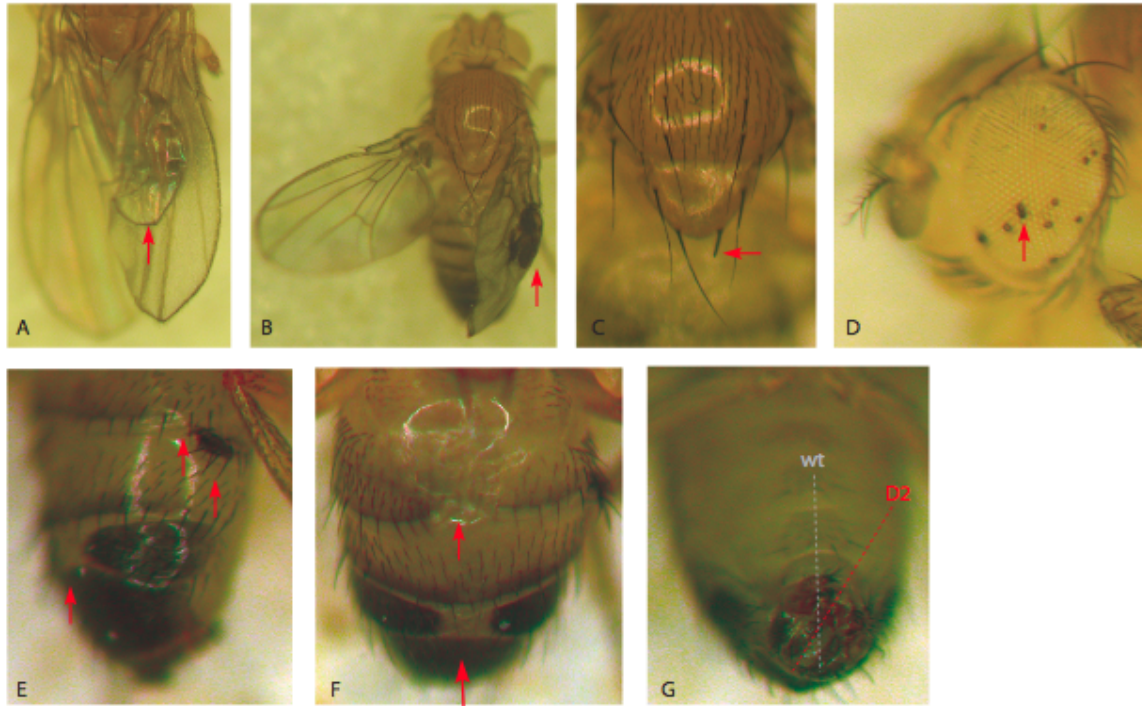


Figure 2-8. D2 animals have mild developmental defects.

D2 homozygous animals have a range of developmental phenotypes from wing defects (A, B), bristle defects (C), black regions in the eye possibly resulting from degeneration (D), body pattern defects (E, F) and rotated genitalia (G).

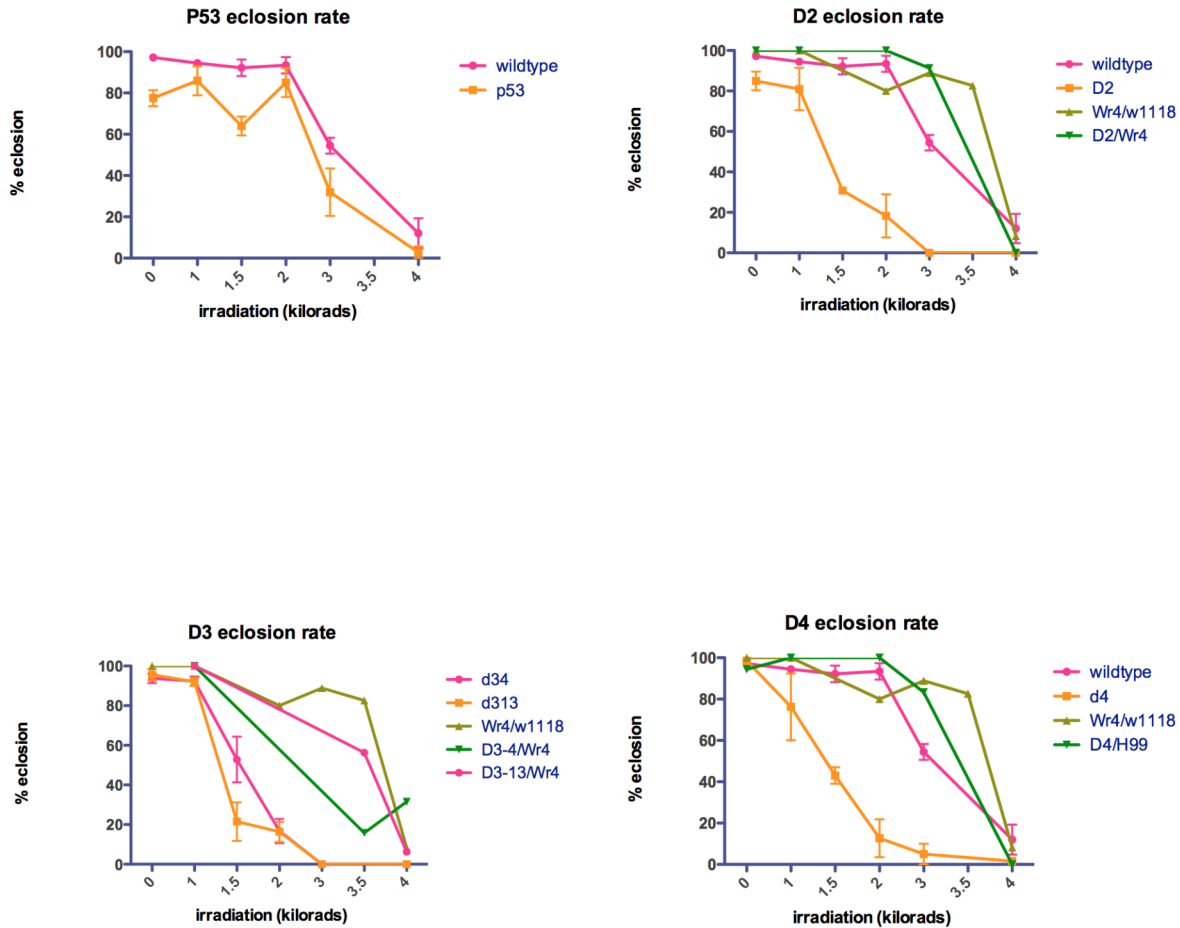


Figure 2-9. Novel transcript mutations have lower eclosion rates after irradiation but are dependent upon background effects.

Animals homozygous for each deletion were isolated at wandering L3 larvae and irradiated at increasing doses from 0-4 kilorads and eclosion rates were monitored. p53 mutant animals were slightly more sensitive than wild type (w^{1118}). All three deletions were much more sensitive and had a lower eclosion rate at each irradiation point tested. To eliminate background effects, each deletion was placed over a larger deletion and tested again for eclosion after irradiation. Animals became less sensitive to irradiation effects when in trans to a larger deletion, suggesting background effects contribute to irradiation sensitivity phenotypes.

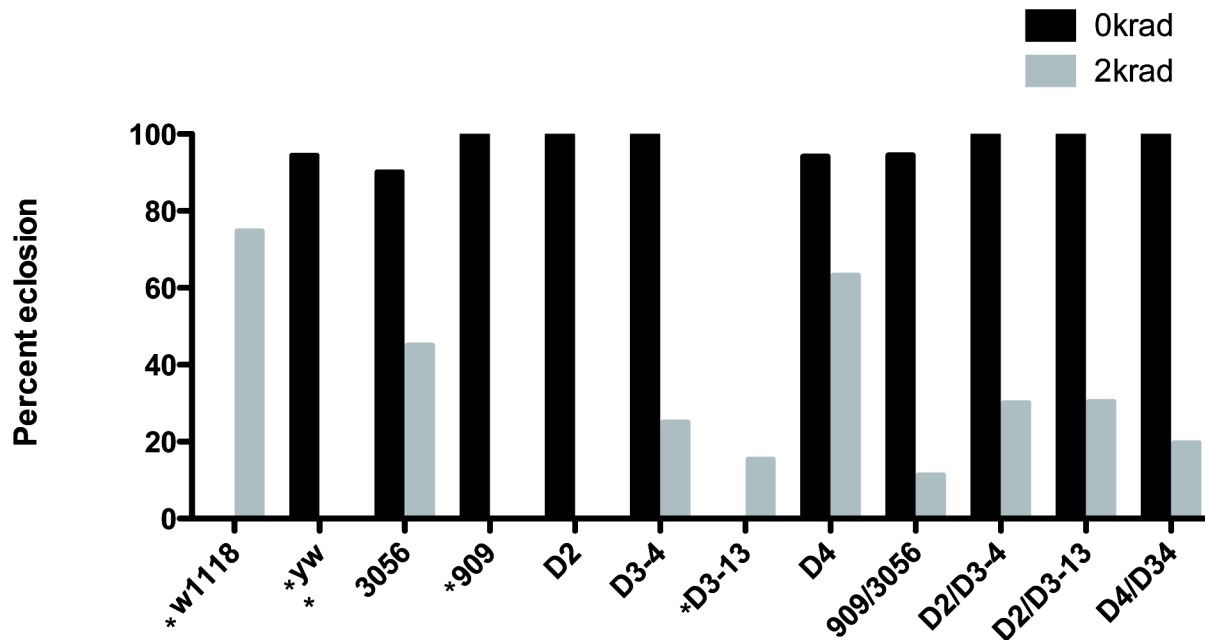


Figure 2-10. Eclosion rates of trans-heterozygous animals at 0 and 2 krad

indicated background effects.

To determine if background effects contribute to eclosion rates after irradiation, each deletion was placed in trans to each other, and eclosion was monitored after 0 and 2 Krad irradiation at the L3 larval stage. Deletions in trans show much lower eclosion rate (10-30%) than wild type animals (75%), suggesting that background mutations affect eclosion rates after irradiation. Stars indicate timepoints not assayed.

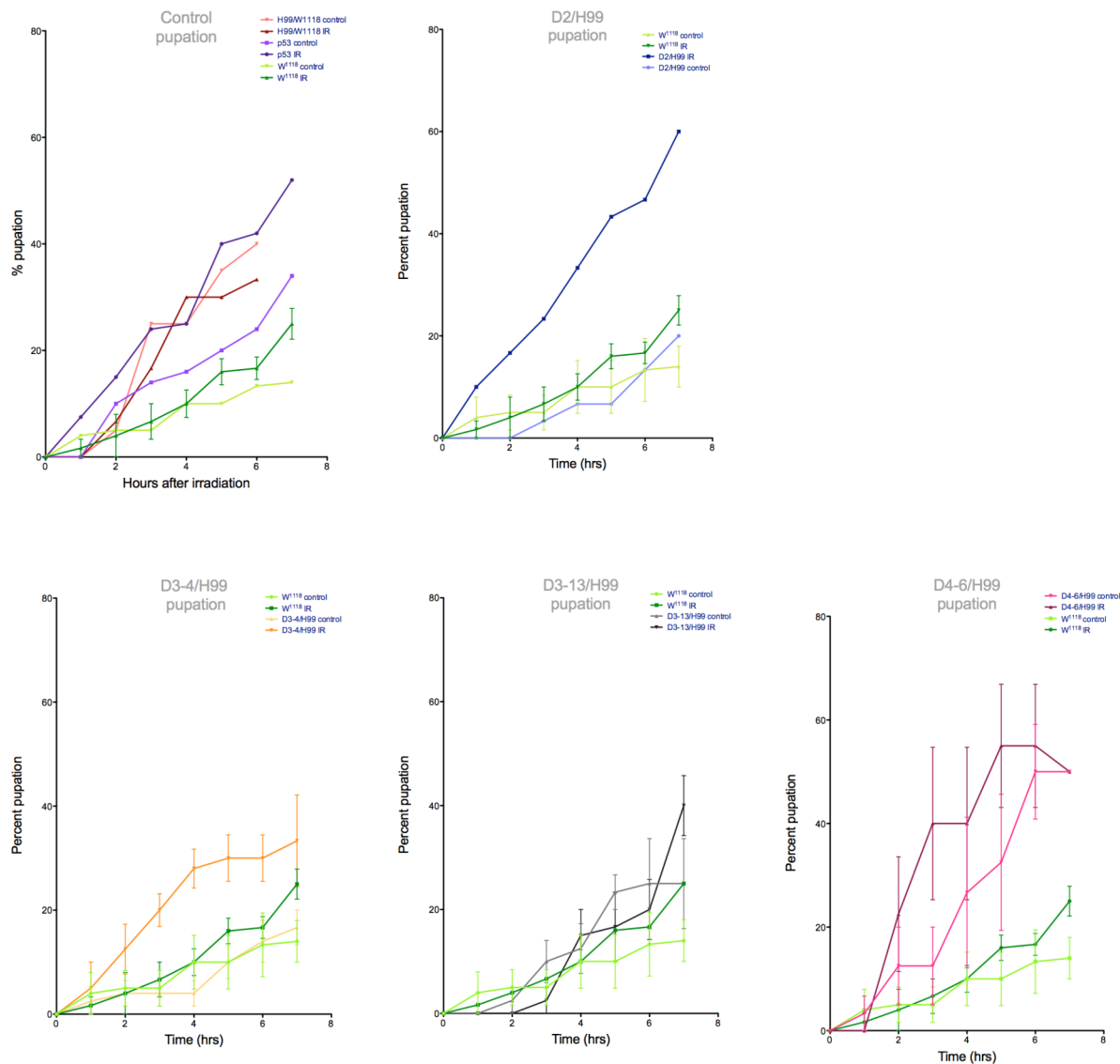


Figure 2-11. Pupation rates after irradiation.

Animals trans-heterozygous for each deletion and a larger deficiency were isolated at wandering L3 larvae and irradiated at 4 kilorads and time to pupation was monitored. Irradiated p53 mutant animals pupated faster than non-irradiated p53 and wild type (w^{1118}) animals. D3 appeared wild type while D2 and D4 appeared to pupate faster. However, animals heterozygous for the larger deficiency alone also pupated faster, suggesting these effects do not map to UNTs. Note that rate to pupation was highly variable.

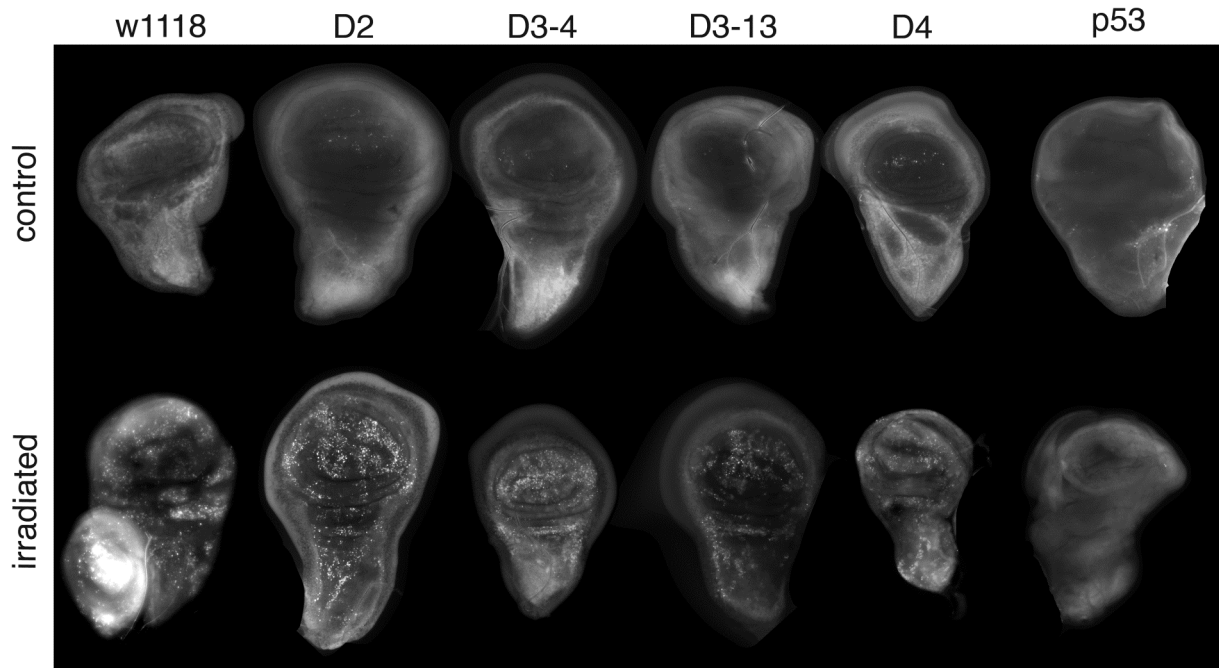


Figure 2-12. Novel transcript deletions are not defective in irradiation induced cell death.

Wandering L3 larvae homozygous for each deletion were irradiated with 4 krad ionizing irradiation. Animals were recovered for 4 hours, wing discs were isolated and stained with acridine orange to label dying cells. p53 animals show no cell death after irradiation while wild type animals (w1118) display large amounts of apoptosis after irradiation. D2, D3, and D4 all display cell death numbers similar to wild type animals.

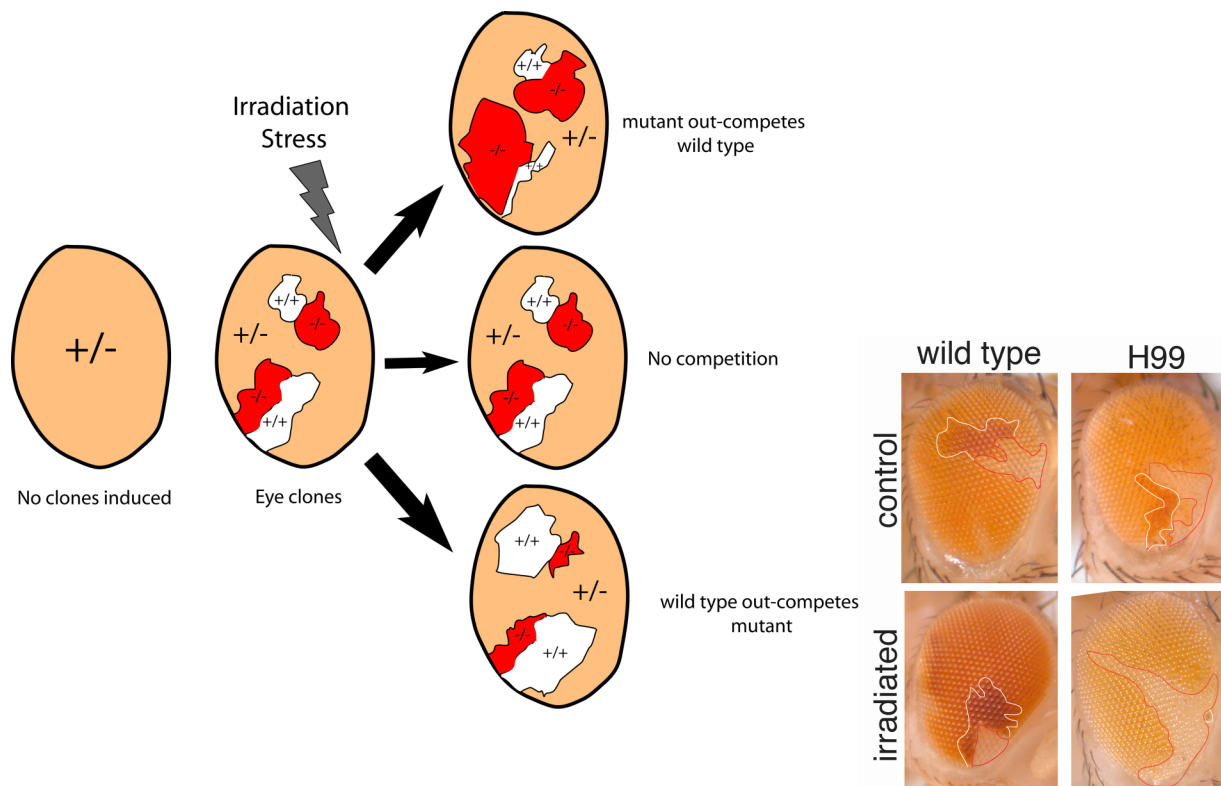


Figure 2-13. Twin spot analysis.

The left panel displays the generation of twin spots. A mutation is placed on an FRT chromosome, clones are generated using heat shock FLP, then the animal is stressed using irradiation. The resulting twin spots have three outcomes: 1) neither the mutant nor the wild type out competes the other leading to similar sized clones, 2) wild type recovers and out competes the mutant generating a larger wild type area, or 3) mutant tissue recovers and out competes the wild type tissue to produce a larger mutant tissue. No irradiation should produce similar sized twin spot tissue. The panel on the right demonstrates that wild type and H99 twin spots are similar in size, but after irradiation, wild type remains similar in size while H99 tissue out competes wild type.

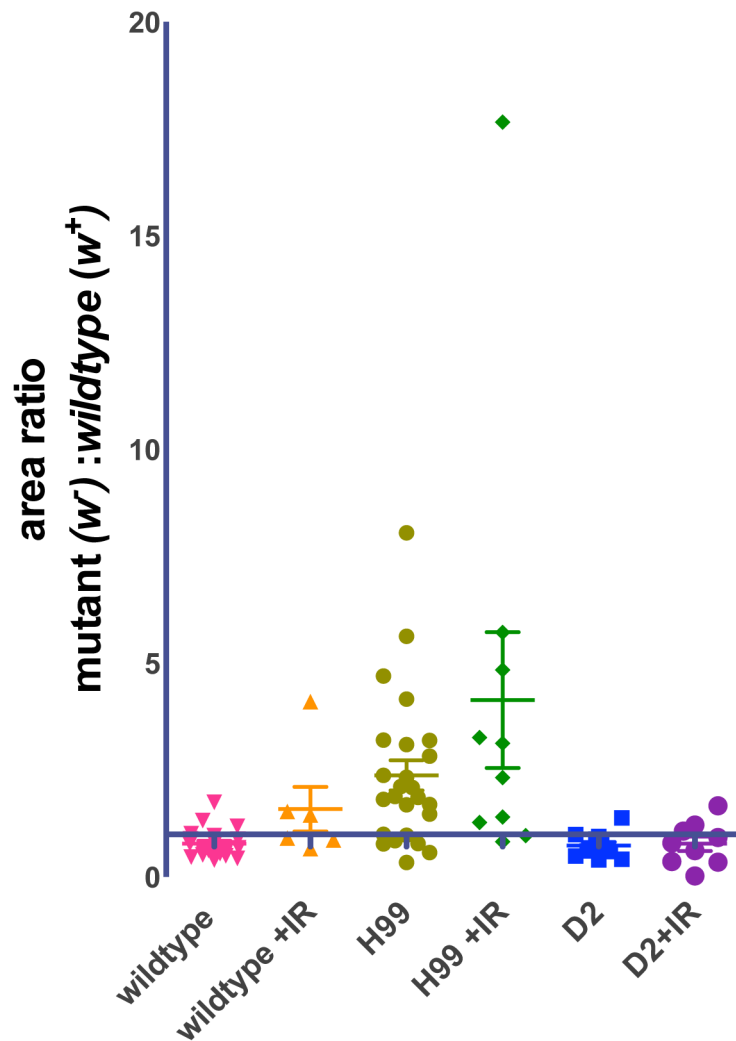


Figure 2-14. Twin spot analysis reveals that H99 out competes wild type tissue but UNT mutations do not.

Twin spots were generated as in Figure 2-13 and tissue size was measured and plotted as a ratio of mutant tissue (w-) to wild type tissue (w+). Wild type shows a nice ratio of 1, and after irradiation, this ratio slightly increases. However, H99 tissue that is defective in cell death clearly occupies a larger area of twin spot tissue without (green) or with irradiation (dark green). D2 tissue occupies the same amount of space as its wild type twin spot with or without radiation stress.

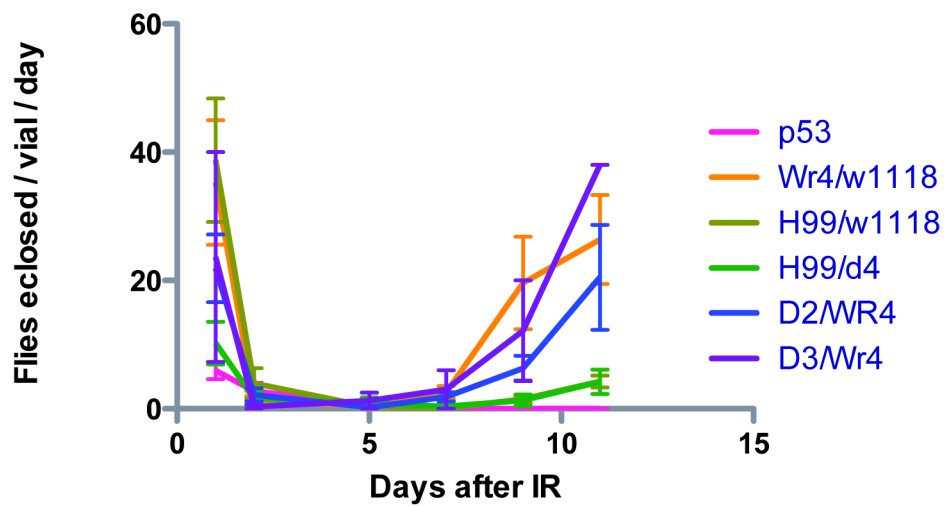


Figure 2-15. Mutants recover fertility after 11kr irradiation.

Transheterozygous flies were mated and irradiated with 11krad irradiation. Females were divided into 10 females per vial. Vials were flipped every two days, and the amount of viable offspring was recorded every day from every vial. Average amount of viable eclosed flies per vial per day is plotted above. Wild type flies become infertile after 11krad irradiation and but recover fertility as they age. p53 animals never recover fertility. Novel transcript mutations behave like wild type animals and recover fertility as they age.

Region	Forward primer	Reverse primer
8053	tctcatgaatgcttacagttggc	gacaaaaggatgaagagaaagtgtgg
1917	tgcaaggagcaaagaatccg	ttgtgtcgttggtcggtcatt
Val4	aagcctcaaaccctgcaagcataat	ttggttgcttggcgggtgtaatg
Val6	ttctgccagcaacaactcaattat	gtccttgatccttactcctgcccaa
Val9	Ctcttagcaactaacaattgagtc	Ctttaatttcctcaattcgctctaa *Doesn't match native sequence
1417	ATGGTCAGAGAGCTGGTGCGTT	GACCAACATAATCGATGATGTGGTGCC
2189	ACAGTCTATTACCCATTGCTTGTCG	CTCCATCCACTCCACTCCAATCCAA
3062	GCGTCTCTTCGTGCGATGTAAGACT	GATTAAGTCCGCCTGAGGGACT
4732	CAACCACGCCAGTACCAGTACCAC	TCAGGTTGCATTGTGGCAAGGTGTT
4867	AATATGACCGCAAACCGACACTCGA	TCCTACTGCCAGCCTGACACAAG
8521	TATCTGGAGACAAAGGACAGTAGCT	CATTCGGATCAAATATCTTGGCTGT
8740	AAGTCCGAATGCCTCGTGGAC	CATATGCAGAAGCTACGGAAACGAA
10030	TCTTAGAATTCAAGTTCCACCGTAA	AATTCGCTCTAAAAGAGCACCCGTA
10160	ACGCCCCATTATTAAGGCTGATTGAC	ATTGTCACACTTTGATTCTGTACAAGA
10622	ATGCAATGTTTGACTGGCAAGGACTTC	CGAACCTGAAGCTATTGATGATCCA
2243	GAAGTGCTACCGTCTTACACAGAT	AACTCGGTCCGTGTATCTTGACA
2544	GCAGAAAGGGAAGTAGAAGAACTACA	ATAAGTGCATACAAGACAAACTGGCGA *Doesn't match native sequence
3474	TACCGTTTATGGCAACCAATGCACT	GCCAGCTTCTCTAATTGCACGGGA
4299	CACGAATCGCTTGTAACAAATCGAC	CCAACGAGCCAAAGATTCAATTCTGCC
6138	TAATGAAGCAATCGAAACGGGACAT	TTAGTCTAGAGGTATATGGGATTGTAC
7343	CCTCTCCGACATCATCTAGCTAC	GGAGCATTACCGAGTTGTCCTTGG
10871	TCCAACCTCCGAAATCGCACCCCTT	GCACTCAACCGTCACTAATCATTTCAATT

Table 2-1. Sequences of primers used to identify novel transcripts

Region	Starting coordinate release 4	Size (bp)	Validated	Irradiation Induced	p53 dependent
8053	18361976	255	No		
1917	18208509	329	Yes	No	
Val4	18334381	524	Yes	No	
Val6	18418106	1750	No transcript		
Val9	18411331	542	No transcript		
1417	18196020	250	No		
2189	18215306	275	No transcript		
3062	18237163	768	No		
4732	18279256	300	No		
4867	18282331	605	No		
8521	18373614	742	Yes	Yes	Yes
8740	18379233	2023	No transcript		
10030	18411381	487	Yes	Yes	Yes
10160	18414602	281	Yes	Yes	Yes
10622	18426218	2520	No transcript		
2243	18216687	232	Yes	No	
2544	18224256	480	No transcript		
3474	18247476	408	Yes	No	
4299	18268186	411	Yes	No	Yes
6138	18314006	339	Yes	No	Yes
7343	18344122	270	Yes	No	Yes

10871	18432368	244	Yes	Yes	Yes
Totals	% of all tested		50%	18%	32%

Table 2-2. Novel transcript data

Nearest Annotated Feature on Same Strand							
		Known Genes		EST		Computed Gene Predictions	
Novel transcript	Strand	5'	3'	5'	3'	5'	3'
1917	minus	86.1kb (CG5103)	20.1kb (hid)	19kb	20kb	86.6 kb	20.5 kb
6952	plus	78.7kb (Che75a)	195kb (off region)	35.7kb	66.1kb	78.8kb	242.3kb
8521	minus	56.8kb (rpr)	66.3kb (grim)	26.7kb	66.3kb	5kb	66.6kb
10030	minus	29.5kb (skl)	10kb (rpr)	9.7kb	10.4kb	27.1kb	10.2kb
10160	minus	26.4kb (skl)	13.4kb (rpr)	6.5kb	13.6kb	23.9kb	10.4kb

Table 2-3. Nearest neighbor for select transcripts

Multigenic regulation through a single p53 enhancer in *cis* and in *trans*

SUMMARY

We examined stimulus dependent activity at a single p53 enhancer, *in vivo*. Through genetic analyses, we showed that this enhancer coordinates stimulus dependent induction of multiple genes spanning over 300kb throughout the Reaper region. Surprisingly, this same enhancer regulated a gene located 20Mb away across the centromere and also controlled at least one gene mapping to a different chromosome. Chromosome conformation capture analyses placed this enhancer in close proximity to these distant targets *in vivo*. Furthermore, these specific DNA looping patterns were markedly influenced by p53 status. A fragment containing this enhancer was able to restore these looping interactions from a different genomic location. Therefore, a single p53 enhancer is necessary and sufficient for long range, multigenic regulation in *cis* and in *trans*.

INTRODUCTION

The tumor suppressor p53 is mutated in a majority of cancers, and most mutations are thought to affect its transcriptional activity (see (Vousden and Prives, 2009)). Functional DNA binding at target response elements containing a consensus binding site (reviewed in (Menendez et al., 2009)) is essential for proper p53 activity, and great deal of literature has refined our knowledge of how p53 exerts transcriptional control of downstream targets through DNA binding.

Like its human counterpart, *Drosophila* p53 responds to genotoxic stress and integrates adaptive responses at the cellular level. A characterized p53 response element (Dp53RE) is a cis-regulatory element (CRE) that lies 4kb upstream of the pro-apoptotic gene *reaper* (*rpr*). As in humans, this enhancer consists of two 10mers, with 18 of 20 base pairs identical to the mammalian p53 consensus sequence. The Dp53RE binds p53 protein and acts as an enhancer for *rpr*, a cell death gene that becomes induced after stress (Brodsky et al., 2000). When tested *in vivo*, the Dp53RE was sufficient for stimulus responsive p53 dependent expression associated with unprogrammed and programmed DNA breaks (Brodsky et al., 2000; Lu et al., 2010).

Genome wide analyses identified additional DNA damage responsive genes that depend on p53 for induction. These include three in the Rpr region (*rpr*, *hid*, and *skl*) along with others throughout the genome (Brodsky et al., 2004) (Akdemir et al., 2007). Presumably, additional p53 enhancers control these genes. Through bioinformatics approaches, other computed p53 binding sites have been mapped in *Drosophila* but whether these elements are functional is not known. Here, we use the *Drosophila*

model to genetically examine a single p53 enhancer *in vivo*. Through loss-of-function analyses, we demonstrate that a single Dp53 enhancer confers long-range *cis* regulation upon multiple linked genes spanning 330 kilobases (kb) in the Rpr region. Surprisingly, this same enhancer exerted regulatory control upon unlinked loci mapping across the centromere and to different chromosomes. Using chromosome conformation capture (3C), we found that the Dp53RE contacts these distant sites via looping interactions that were stabilized by p53 status and influenced by developmental stage. Together, these observations indicate that when bound, a single p53 enhancer exerts long-range multigenic regulation in *cis* and in *trans*, promoting long-range interactions that organize large scale chromatin architecture at large scale.

MATERIALS AND METHODS

Deletion Strains

Deletions were generated using the Exelixis collection of P elements as described in Parks et al., 2004.

Rescue analysis

A BAC from the attB-P[acman] library (Venken et al., 2009) containing the p53RE and surrounding genomic region (CH322-118F05) was obtained from BACPAC Resources and was targeted to the first chromosome using an attP docking site (Bloomington stock 9726 with genotype *y[1] w[1118] PBac{y[+]-attP}VK00006* located at 19E7) using Φ C31 transposase. Once a transformant was recovered, it was placed into the *D2^{p53RE}* background.

RT-PCR

Embryos from *w¹¹¹⁸* (wild type) *D2^{p53RE}* and *D3^{control}* mutants were collected for 2.5 hours, aged for 2.5 hours, and either mock treated or irradiated at 40Gy followed by a 1.5 hour recovery. Embryos were dechorionated with 50% bleach for 2-3 minutes, rinsed with water, frozen in liquid nitrogen, and stored at -80°C until needed. Total RNA was isolated using Qiagen's RNeasy Kit, cDNA was generated using Bio-rad's iScript cDNA synthesis kit, and semi-quantitative PCR was carried out using Promega's GoTaq Green PCR kit.

Microarray analysis

Embryos were collected and processed as above. RNA was labeled using the Ambion MessageAmp™II-Biotin Enhanced Kit Single Round aRNA Amplification Kit and hybridized to the Affymetrix Drosophila Genome 2.0 Array and analyzed as described in the GeneChip® Expression Analysis Technical Manual.

Chromosome Conformation Capture

Tissue preparation

4-6.5 hour embryos from w^{1118} (wild type), $D2^{p53RE}$, or $p53$ mutant animals were dechorionated with 50% bleach and fixed at the interface of equal amounts of heptane and 2% formaldehyde in the presence of 50 mM HEPES pH 7.6, 100 mM NaCl, 0.1 mM Na-EDTA, 0.5 mM Na-EGTA while shaking. Embryos were washed in PBS, 0.01% Triton X-100 and 0.125 M glycine then placed in cold lysis buffer (10mM Tris pH 8.0, 10mM NaCl, 0.2% NP40, and protease inhibitors) for 15 min, transferred to a dounce homogenizer, and disrupted with 10 strokes of homogenizer. Resulting tissue was transferred to 1.5 ml tube and spun at 400g for 5 min at 4°C. Supernatant was removed, and the sample was stored at -80°C until further processed. DNA was isolated and treated as described (Hagege et al., 2007) using HindIII as the restriction enzyme of choice. First, pelleted tissue was resuspended in digestion buffer containing 0.3% SDS, incubated at 37°C for 1 hour while shaking vigorously, triton-X-100 was added to a final concentration of 2%, and cells were incubated at 37°C for 1 hour while

shaking vigorously. 400-500U of enzyme of choice (HindIII, NlaIII, NEB) was added and samples were digested overnight at 37°C while shaking vigorously. Samples were removed and SDS was added to 1.6%, incubated at 65°C for 20 minutes, and then transferred to a 50ml conical with 1X ligation buffer and 1% triton-x-100 to a total of 7mls for ligation. Samples were incubated at 37°C while shaking gently for 1 hour, at least 100U and up to 2000U T4 DNA ligase (NEB) was added, and samples were incubated at 16°C for four hours followed by 30 minutes at room temperature. 300ug of Proteinase K was added and samples were decrosslinked overnight at 65°C. Samples were removed, 300ug RNase was added, incubated at 37°C for 30 minutes and then phenol-chloroform precipitated (add 7ml phenol-chloroform, spin 15 min 2200g, remove aqueous layer, optional chloroform wash, add 7ml water, 1.5ml 2M sodium acetate, 35ml of EtOH to precipitate, put in -80 for 1 hour, spin 45 min at 4°C for 45 min, wash with 70% EtOH overnight, resuspend in 10mM Tris pH 7.5). Primers for 3C are listed below.

qPCR reagents

qPCR was done with two reagent sets. One analysis facilitated iQ™ SYBR Green Supermix by Bio-Rad. The reaction included the mix, template, and primers at a final concentration of 500 nM. The reaction was carried out on the CFX96™ Real-Time PCR Detection system by Bio-Rad. We used the 2-step real time PCR program in the manual. The second reagent was Taqman® Gene Expression Master mix by Applied Biosystems. A Taqman® Probe was designed to represent the fragment associated with the p53 response element. The sequence is 5'

TAGCTCCTCGGCGGTGCGCGCTTT 3'. The reaction was performed on the same machine using the Taqman® mix, 200 nM Taqman® Probe, 900 nM primers and template. We used the program from the Taqman® Gene Expression Master mix manual.

Determining the concentration and reference point for 3C samples

The Wizard Genomic DNA Purification kit by Promega was used to generate gDNA from the parental strain w¹¹¹⁸. The gDNA was then diluted to 200 ng/uL as a working concentration. A 5X dilution series was generated from this sample, creating 6 samples that ranged from 0.064 to 200 ng/uL. This panel of dilutions was then used to calculate the concentration of the 3C prepared samples. The primers H99-For (5' GGCTAATGACCAGATACTCTGCTATC 3') and H99-Rev (5' ACACACCGTACTAATCATGCGAGT 3') cover a 134 bp fragment that lies within the fragment harboring the p53 response element. This primer set was used for creating the internal reference values. This line of experimentation used iQ™ SYBR Green for qPCR analysis. Using the dilution series as template, the primer set for the H99 region was able to generate a standard curve. In the same qPCR run 'unknown' samples were dilutions (1:100, 1:500 and 1:2500) of the various 3C preparations. The standard curve was then used to calculate the concentration of the 3C samples. Once this value was established, all samples were diluted to the same concentration of 750 ng/uL. These diluted samples were then ran again with the gDNA dilution series and the value extrapolated was used in conjunction with the data from the looping analysis to generate a ratio that permits one to compare looping between regions.

Establishing a control DNA population for 3C analysis

To quantitate the amount of looping in the 3C samples, a reference DNA sample must be established. Each gene to be analyzed is represented in the reference DNA sample as a BAC, Table 1. These BACs were isolated and combined in equal molar ratios to create the reference sample. This reference sample then underwent the 3C methodology and was quantitated against the gDNA curve stated above. Thus generating a positive control for looping interactions and a platform for primer validation.

Analyzing the 3C samples for the presence of looping

For increased sensitivity and specificity, the Taqman technology was used for the following analysis. The reference DNA sample (3C BAC preparation) was used to create a 6X dilution series that ranges from 2.5 - 20,000 ng/uL. The constant primer was combined individually with each variable primer, Table 3. Each primer set was then used to create a standard curve from the dilution series from the 3C BAC preparation. The 3C samples were also present on this plate. This BAC-based standard curve allowed the primer set to be validated and assigned a value to that particular looping interaction. A ratio was then calculated by dividing the value assigned by the 3C BAC dilution series by the value assigned by the gDNA dilution series. These ratios were then plotted.

RESULTS

Using FRT mediated recombination (see methods), we produced tailored deletions in the Rpr region (Figure 3-1). One of these, $D2^{p53RE}$, removes the Dp53RE. Another, $D3^{control}$, deletes neighboring sequences and is used throughout our studies as a control. Flies homozygous for either deletion are viable and fertile. To examine activity from the Dp53 enhancer, we measured p53 dependent transcriptional activity in the Rpr region in 4-6.5 hour $D2^{p53RE}$ and $D3^{control}$ embryos. As previously reported by us and others (Akdemir et al., 2007; Brodsky et al., 2004), *rpr*, *hid*, and *skl* (but not *grim*) are induced in wild type (w^{1118}) but not $p53^-$ embryos after radiation challenge (Figure 3-2). In $D2^{p53RE}$ mutants, *rpr* was completely nonresponsive (Figure 3-2), whereas normal regulation of this gene occurred in $D3^{control}$ deletion animals. This result confirming that, as expected, the Dp53 enhancer regulates stimulus dependent expression of the adjacent target *in vivo*. Surprisingly, however, *hid* and *skl* were also unresponsive in $D2^{p53RE}$ animals (Figure 3-2) but showed wildtype behavior in $D3^{control}$ mutants, suggesting the Dp53RE exerts long-range regulatory effects throughout the Rpr region (note: *skl* may not be fully induced possibly due to proximity to deletion). Other genes in the Rpr region including *grim* were unaffected by the $D2^{p53RE}$ deletion (Figure 3-3). Therefore, elimination of this single response element specifically impacted stimulus dependent behavior of multiple genes over long range distances (300 kb). Hence, this *cis* element specifies coordinated regulation of Dp53 responsive genes throughout the Rpr region.

These findings were extended genome wide using expression arrays (see methods) to compare expression behavior of RIPD genes in wild type and $D2^{p53RE}$ animals. We found that at least 75% of genes previously reported using genome wide expression studies to be radiation inducible and p53 dependent (known as RIPD genes: Radiation Induced p53 Dependent) (Akdemir et al., 2007) required the Dp53 enhancer for effective induction (Table 3-1). (Akdemir et al., 2007). To verify these results, we assayed for irradiation inducible expression of a select number of these $D2^{p53RE}$ dependent RIPD genes. In the embryo, a gene designated *xrp1* (Akdemir et al., 2007) is, like *rpr*, among the most acutely responsive genes, exhibiting rapid induction within 15 minutes after exposure (Brodsky et al., 2004). Therefore, we examined *xrp1* RNA levels and found that, in contrast to wild type or $D3^{control}$ homozygous animals, this gene was strikingly unresponsive in $D2^{p53RE}$ homozygotes (Figure 3-4) despite the fact that the physical distance between *xrp1* (3R:14740690) and the p53 enhancer (3L:18396357) spans distances greater than 20 megabases (Mb) across the centromere. We similarly examined another RIPD gene, *ku80*, which resides on the second chromosome, and again, $D3$ mutants showed wild type induction after irradiation, but $D2^{p53RE}$ homozygotes did not (Figure 3-4). Together, these data indicate that a single Dp53 response element exerts control over multiple genes, some of which are physically located at great distances and not linked in *cis* to the enhancer itself.

The kinetics of upregulation of *xrp1* after irradiation are not consistent with successive cascades to promote gene expression since this gene is induced at the same rate as *rpr*. Therefore, the Dp53 enhancer could physically contact proximal and

physically distant RIPD genes through chromosomal looping. To test this possibility, we analyzed genome organization in the embryo using Chromosome Conformation Capture (3C). This method combines cross-linking, ligation, and PCR to detect chromatin contact sites *in vivo* (Dekker *et al.*, 2002). Using 3C to profile chromosome conformations in the Rpr region, we discovered numerous loops from multiple genes, including *rpr*, *hid*, and *skl*, to the Dp53 enhancer throughout this interval (Figure 3-5). These interactions were specific as no signal was detected without ligase or in the $D2^{p53RE}$ mutant background (Figure 3-6). Additionally, looping appeared similar to wild type in $D3^{control}$ animals. By shifting the constant primer to a region directly outside of the $D2^{p53RE}$ deletion, we found that Dp53 enhancer sequences are required for these loops since these shifted constant primers are eliminated in the $D2^{p53RE}$ mutant background (Figure 3-7). Together, these data indicate that the Dmp53 enhancer sequences are necessary for chromosomal looping. To more accurately define regions near *hid* that loop to the p53RE, we designed new primers based on the four base cutter NlaIII and found that we recapitulated our previously described chromosome conformation patterns. Additionally, we defined the presence of “micro” loops, or multiple regions within larger regions that loop to the p53RE (Figure 3-8).

Our data suggest that the Dp53 enhancer directs transcriptional regulation of genes in the Rpr region through chromosomal loops that generate physical interactions between the Dp53RE and tightly linked RIPD genes. We next examined whether the Dp53RE might interact with physically unlinked RIPD genes. Figure 3-9 shows that the Dp53 enhancer, which resides on the left arm of chromosome 3, interacts with multiple

locations at the *xrp1* locus, which resides on the right arm of chromosome 3. Note that all validated 3C products in figure 5 disappeared in control reactions without ligase and in samples prepared from $D2^{p53RE}$ homozygotes. Direct sequencing of PCR bands confirmed the expected product linking sequences from the Dp53RE to *xrp1* via a single HindIII site junction. Finally, we tested whether the Dp53 enhancer directly contacts *ku80*, a gene located on the second chromosome. Similar to *xrp1*, we found distinct regions of looping between the Dp53RE and *ku80* (Figure 3-9). Fine mapping of both *xrp1* and *ku80* show similar micro loops to the p53RE as throughout the *hid* region (Figure 3-10).

p53 might influence interactions between the Dp53 enhancer and distant genes. Therefore, we profiled 3C contacts in $p53^-$ animals and observed that without wild type p53, many contacts were dramatically decreased or lost all together (Figures 3-5 and 3-9). These results suggest that p53 mediates or stabilizes chromatin contacts between the Dp53 enhancer and target genes.

To determine if Dp53 enhancer mediated looping is dynamic during development, we performed 3C at different stages of embryonic, larval, and adult development. Late staged embryos (10-14 hr) showed diminished looping between the Dp53RE and contact sites in the Rpr region (Figure 3-11 and 3-12), but previously reported looping in the bithorax complex (BX-C) continued throughout development (Figure 3-11) (Lanzuolo, Roure et al. 2007). Long-distance contacts also remained intact, and like early embryos, these interactions were eliminated in animals lacking p53 (Figure 3-11, 3-13 and 3-14). Whole larval preparations did not show any indication of

p53 enhancer looping, while adult female ovaries displayed similar looping patterns to early embryos. Together, these observations indicate that chromosome structure around the Dp53 enhancer is dynamic throughout development.

To determine if the Dp53 enhancer region is sufficient to stimulate looping, we placed a rescue construct containing this element on the first chromosome (see methods) in the *D2^{p53RE}* mutant background and profiled looping contacts. Strikingly, many but not all looping contacts were restored between the p53RE and its targets, including the Reaper region, *xrp1*, and *ku80*, despite the fact that the Dp53RE was relocated to a non-native site. An example of restored looping from the Dp53RE to *ku80* is shown in Figure 3-15. These results are currently being repeated and validated. These data suggest that the Dp53RE is sufficient for looping, however positional contexts are essential for some looping structure, particularly in the Rpr region as not all loops are restored.

DISCUSSION

A long-acting p53 enhancer regulates stress responses

Here, we present evidence that a single p53 enhancer directs long-range gene expression. Using tailored deletion analysis *in vivo*, our studies show that a single p53 enhancer is essential for proper regulation of at least three canonical cell death genes in span of over 300kb. We also established that the Dp53 enhancer regulates multiple p53-dependent, radiation-induced genes up to 20Mb removed from the Rpr region or on entirely different chromosomes. This regulation appears to be mediated through chromosomal looping resulting in direct contact of the Dp53RE and the genes it regulates. The exact mechanism in which chromosomal loops are formed is not known. However, we observed looping enhancement in the presence of p53, indicating that p53 plays a role in forming or stabilizing chromosomal conformation. A recent report also indicated that in murine ES cells, Mediator and Cohesin facilitate chromosomal looping (Kagey et al., 2010) and perhaps these players, along with p53, establish the 3D chromosomal structure essential for proper gene regulation. Additional unknown binding partners of p53 may also mediate chromosomal looping and identifying if any of these partners exist at the looping structure may elucidate the mechanism in which higher order chromosomal structure is maintained.

The p53 enhancer loops to distant regions to regulate transcriptional responses after stress

Canonical cis-elements were thought to act in a linear fashion along the chromosome to regulate expression but observations driven by new technologies suggest that these regulatory regions may function at long distances mediated by chromosomal looping. These new technologies allowed us to map the 3-D structure of the chromosome, and using 3C, we identified several locations within the Rpr region that contact the p53 enhancer. More strikingly, we identified regions near both *xrp1* across the centromere and *ku80* on a different chromosome that loop to the Dp53 enhancer. Enhancers working in *trans* is not entirely novel as early geneticist E.B. Lewis described transvection in *Drosophila* in which an enhancer can interact with and control its homologous gene in *trans* (reviewed in (Duncan, 2002)). More recently, technological advances have improved our understanding of cis-element function (reviewed in (Bulger and Groudine, 2010)) and several correlative studies have suggested enhancer mediated transcriptional regulation in *trans* (as reviewed in(Williams et al., 2010)). Along these lines, our observations definitively establish that a single enhancer loops to distant genes in a functionally relevant manner, indicating that canonically defined cis-elements can act in *trans*.

Even with our strong evidence for chromosomal looping, we cannot rule out the possibility that a trans-factor functions to regulate transcription of distant p53 dependent genes. However, in a matter of 15 minutes after stress, *rpr* and *xrp1* are highly transcribed while *hid* is induced by 30 minutes(Brodsky et al., 2004). Therefore, if a

trans-factor, originating either from the $D2^{p53RE}$ location or produced as a result of Rpr expression, was acting to control long distance regulation, it would have to be transcribed, translated, and promote *xrp1* expression within 15 minutes. While this scenario could occur, it seems unlikely due to developmental time constraints. Alternatively, noncoding (nc) RNAs may be involved in regulation of distant stress-responsive genes. Recently, long ncRNAs have been shown to act similar to enhancers (Orom et al., 2010) in that they are required for proper expression of neighboring genes. A neighboring ncRNA could act to promote the expression of distant RIPD genes as part of the Dp53RE enhancer looping structure, but as of yet, we have found no evidence for this idea.

p53 enhancer looping is dynamic during development

Chromosome conformation appears dynamic during development. Early stage embryos are highly sensitive to stress, and during this time, the p53 enhancer region loops to control multiple p53 dependent, pro-apoptotic genes. However, as embryos age, they become resistant to stress-induced cell death. Likewise, we saw multiple looping contacts decrease or disappear in the Rpr region during late embryonic development which correlates to no induction of *rpr*. In this case, p53 would not be able to induce the expression of cell death genes, which may be the defining mechanism to stress-induced cell death resistance at this stage in development. Previously described looping in the BC-X region remained unaffected (as reported in (Lanzuolo et al., 2007)), and intriguingly, long-acting interaction of *ku80* and *xrp1* with the p53 enhancer remained in contact, indicating that dynamic looping is not a result of chromosome

structural break down. These data also suggest that p53 and its target, the Dp53RE, are still active in pathways distinct from cell death during late embryonic development, and perhaps p53 dedicates its activity to functions other than death. We also noted that whole larval preparations did not show evidence for Dp53RE looping. However, the abundance of different tissue types might mask looping in whole larval tissue preparations, and if assayed in a tissue specific manner, it is probable that Dp53RE looping may still be observed. Likewise, chromosome *in situ* hybridization in whole embryos or larval tissues might provide insight into chromosomal looping tissue specificity.

Ongoing aims to establish cross-chromosomal looping

We established that the p53RE is necessary for regulation of several RIPD genes and resides in a conformation that enables physical proximity to these distant genes. However, to definitely establish that the p53RE regulates these genes, we are undergoing rescue experiments to restore both looping and regulation of expression. We introduced a rescue construct containing this element on the first chromosome and placed it in the $D2^{p53RE}$ mutant background to profile looping contacts. Preliminary results suggest that this exogenous rescue fragment restores many but not all looping contacts despite the fact that the Dp53RE was relocated to a non-native site. We are currently validating these results. Additionally, we plan to test for restoration of RIPD gene regulation after irradiation. If we restore induction of *rpr*, *skl*, *hid*, *ku80*, and *xrp1*, we would have definitive evidence that the p53 enhancer works to regulate genes in both *cis* and *trans*.

PERSPECTIVES AND FUTURE DIRECTIONS

We discovered a potential role for a single p53 binding site to control transcription at great distances in *cis* and in *trans*. This potentially transformative mechanism for transcriptional control has far reaching implications. First, conventional thought places enhancers on the same chromosome as which the gene resides. Our data negates this necessity and explores the possibility that an enhancer can reside anywhere in the genome. Multiple enhancers on multiple chromosomes could finely regulate gene expression based on cell type, developmental time point, or environmental condition. Second, enhancer analysis often begins directly surrounding the gene of interest. However, if enhancers can reside on any chromosome in the genome, enhancer identification and validation methods we currently use are not sufficient. Third, presumed silent mutations and other polymorphisms detected through positional cloning throughout the genome could potentially affect distant genes if they inhibit long-acting enhancers. These are only a few of the many possible scenarios that could potentially change our understanding of enhancer action.

We have only just begun to explore the mechanism of enhancer action in *trans*. We know that chromosomal looping is essential to regulation, but the mechanism in which two distant points contact each other remains unclear. We have more finely mapped contact points between looping structures to try to provide insights on whether sequence or the 3-D structure of genomic regions play a role in chromosomal looping. However, no simple sequence or secondary structure have emerged from this brief analysis. A more in depth study of looping regions, including which proteins bind to

these regions, and fine mapping of the p53 enhancer region to determine the minimal genomic region that loops to distant genes could provide mechanistic insight into how chromatin contacts are formed in order to specify chromosomal conformations.

Using targeted deletions, we have identified a 20kb region required for looping. However, we do not currently know if the p53 binding site is sufficient, or whether more DNA sequences are required for proper looping. We currently possess various sized rescue constructs including the multimerized p53 binding site, 150bps surrounding the binding site, 2kb, 3.5kb, 3.5kb lacking the binding site, and 11kb as constructs or in animals ready to be tested for rescue of looping or regulation. These constructs would narrow the DNA region sufficient for looping and regulation, determine whether the actual p53 binding site is essential, and provide additional clues to looping mechanism.

We have validated a small number of p53 regulated targets that operate through this enhancer site. However, there are more than 20 high stringency RIPD genes throughout the genome with no validated p53 binding site. It is possible that this p53 enhancer works throughout the genome to coordinate transcription of most RIPD genes. To determine where the p53RE acts genome wide, we can turn to 4C or chromosome conformation capture on chip. This technique specifically queries a single target region and through chromosome conformation capture along with PCR amplification and tiling array hybridization, we can identify all looped targets of the p53RE. These data may define a p53 network that is activated through a single p53 binding site.

Finally, two principal questions remain to fully understand how these data could effect transcriptional regulation. 1) is enhancer function in *trans* conserved throughout

evolution and 2) do other transcription factors act this way? Once these questions are answered, we can more fully understand the nature of enhancer action in *trans*.

Most of the text and data in this chapter is in preparation for submission. All data are mine with the exception of qPCR.

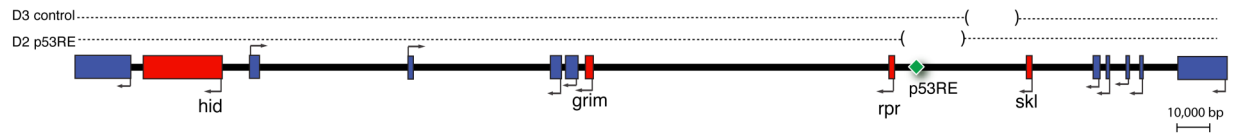


Figure 3-1. The p53 response element maps near validated stress induced pro-apoptotic genes.

Validated deletions are plotted in a schematic of the Reaper region on 3L spanning coordinates 18,150,842-18,485,841 (*Drosophila melanogaster* assembly release 5). Annotated protein coding genes are labeled in blue and pro-apoptotic genes are red. The p53 response element (noted as a green \diamond) is eliminated in the D2 mutation but remains intact in D3.

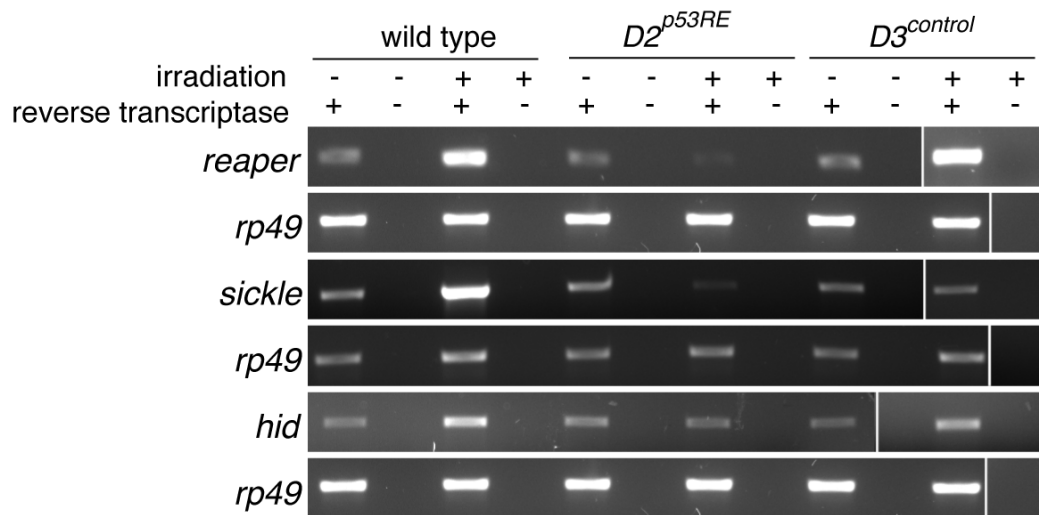


Figure 3-2. The p53 enhancer regulates stimulus-induced transcription of multiple genes in the reaper region.

Radiation-induced transcription of Rpr genes was assessed in $D2^{p53RE}$ mutants lacking a validated p53 enhancer. cDNA was generated, with or without reverse transcriptase, using total RNA isolated from irradiated or mock treated 4-6.5 hour old embryos and PCR was used to assess transcript levels. After irradiation, semi-quantitative PCR demonstrates that the p53RE regulates stimulus responsive expression of regional reaper genes (*rpr*, *skl*) as well as a more distant radiation induced transcription (*hid*) more than 215kb away. Control deletions ($D3^{control}$) remain unaffected. *rp49* is used as a loading control and was run in parallel reactions.

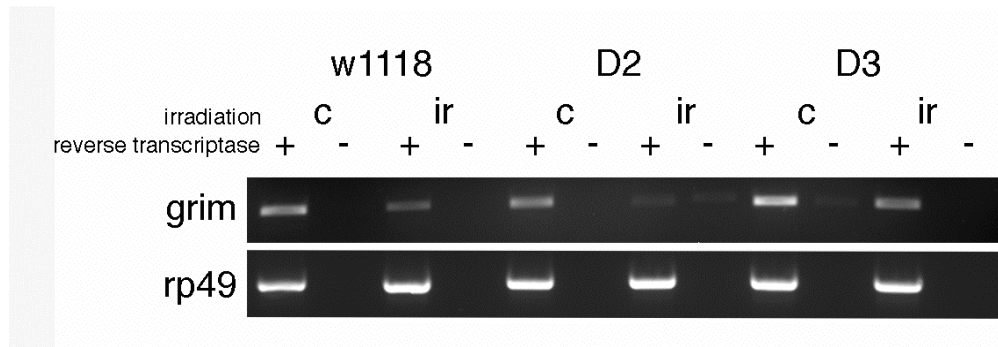


Figure 3-3. The p53 enhancer does not regulate *grim*, an unresponsive cell death gene in the Reaper region.

Unlike other IAP antagonists encoded in the Rpr region, *grim* is not induced after radiation challenge. Here, transcription of *grim* was assessed in $D2^{p53RE}$ mutants lacking a validated p53 enhancer. cDNA was generated, with or without reverse transcriptase, using total RNA isolated from irradiated (ir) or mock treated (c) 4-6.5 hour old embryos and PCR was used to assess transcript levels. After irradiation, semi-quantitative PCR demonstrates that the p53RE does not regulate canonical Reaper region genes such as *grim*, indicating that the p53RE regulates specific irradiation responsive genes. Control deletions ($D3^{control}$) also remain unaffected. *rp49* is used as a loading control and was run in parallel reactions.

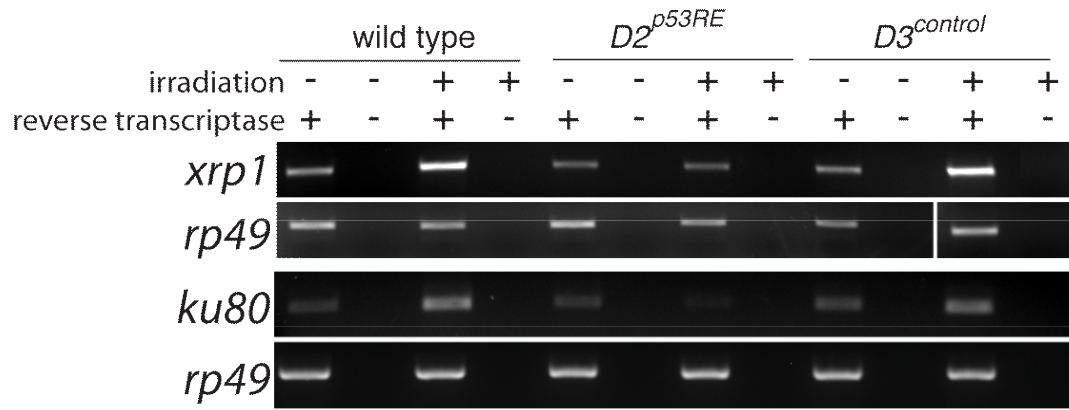


Figure 3-4. The p53 enhancer regulates stimulus-induced transcription of multiple Radiation Induced, p53 dependent (RIPD) genes outside of the reaper region.

Radiation-induced transcription of RIPD genes was assessed in *D2^{p53RE}* mutants. As in Fig 3-2, cDNA was generated, with or without reverse transcriptase, using total RNA isolated from irradiated or mock treated 4-6.5 hour old embryos and PCR was used to assess transcript levels. Transcription of a distant RIPD gene, *xrp1*, which is more than 20Mb from the p53 enhancer, is dramatically impaired after radiation. Surprisingly, the p53RE also regulates stress-induced transcription of RIPD gene Ku80 located on a different chromosome. Control deletions (*D3^{control}*) remain largely unaffected. *rp49* is used as loading control and was run in parallel reactions.

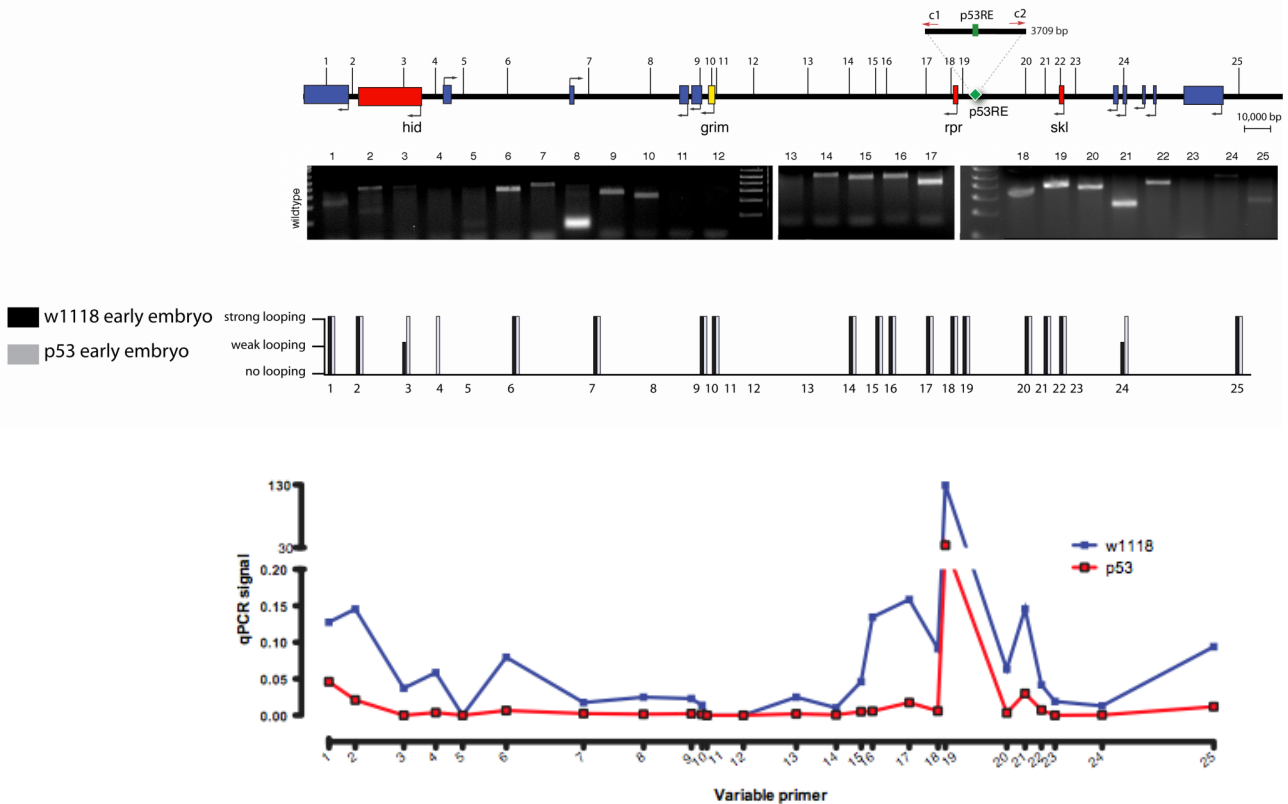


Figure 3-5. The p53 enhancer loops to multiple genes in the reaper region.

A schematic of the Reaper region including the p53 enhancer region (see insert) and radiation induced genes in red. Non-relevant genes are shown in blue, and *grim*, an unresponsive pro-apoptotic gene, is shown in yellow. Primers designed at HindIII sites used in 3C reactions are noted by numbers. Below, ethidium bromide stained gels display 3C reactions. Regions that loop to the p53RE show a positive PCR band, and these positive bands are graphically represented below with present or absent calls based on band intensity. Numbers refer to primers labeled in schematic. Note that regions near *Hid*, *Grim*, *Reaper*, and *Sickle* loop to the p53RE. Signal from qPCR 3C reactions (generated by Melissa O'Neal) is also plotted with wild type in blue and p53 in red. Note differences between p53 and wild type looping, indicating p53 influences looping.

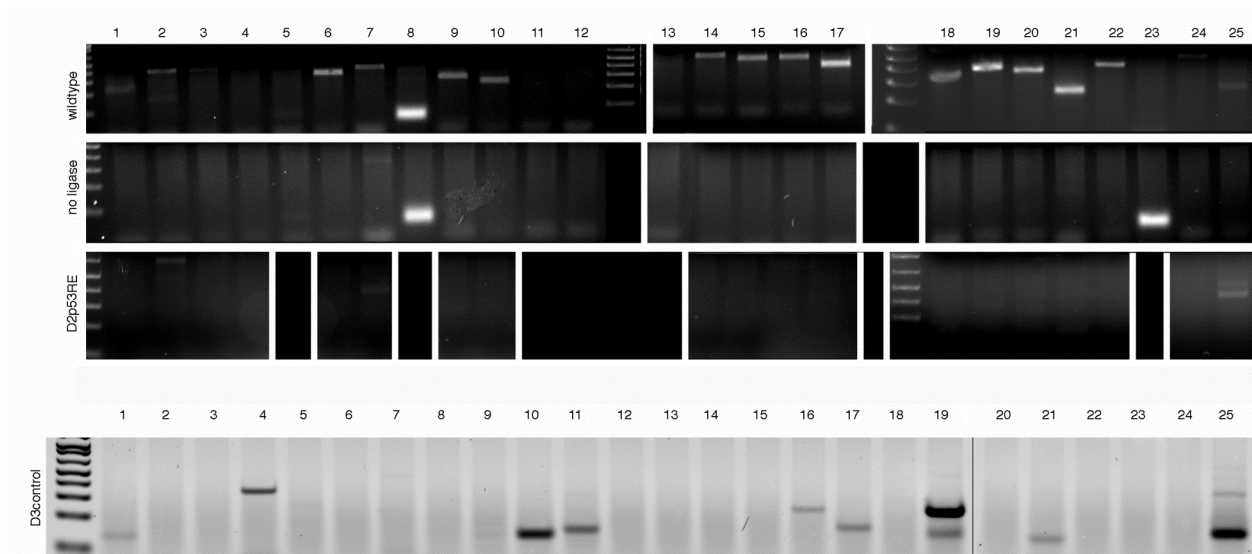


Figure 3-6. 3C looping to the p53RE is validated and specific.

Semi-quantitative PCR in wild type 4-6.5 hour embryos shows regions that contact the p53RE. Numbers correspond to primers located at regions indicated in Figure 3-5. PCRs for chromosomal looping (top gel image) are specific shown by the absence of PCR bands in the no ligase control and the $D2^{p53RE}$ mutant background. Chromosomal looping still occurs in the control $D3^{control}$ mutation, suggesting that $D3^{control}$ does not affect chromosomal structure.

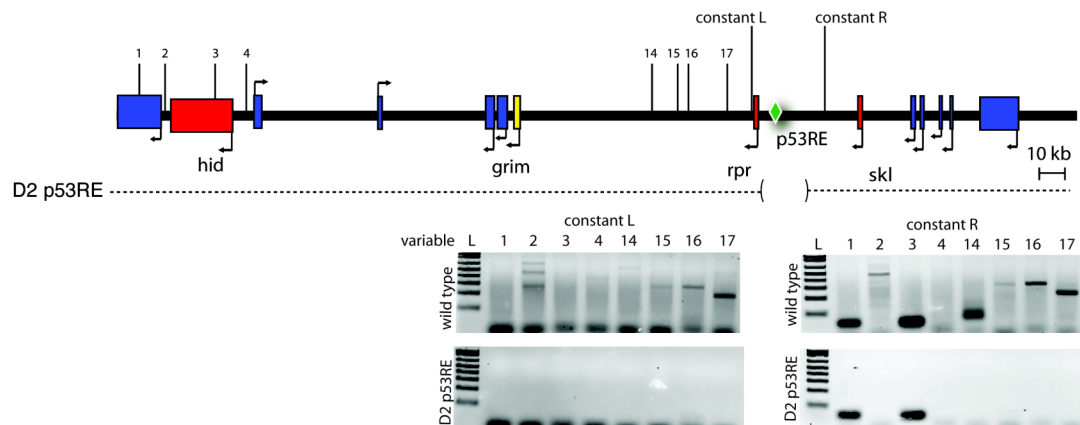


Figure 3-7. The p53 enhancer is necessary for looping

To test whether the p53 enhancer is necessary for chromosomal looping, constant primers were shifted to regions directly outside the $D2^{p53RE}$ deletion and were used in 3C reactions with a subset of variable primers. A schematic of the Rpr region is shown with primers indicated as numbers (same as in Figure 3-5) and constant primers noted near the p53RE. Constant primers L (normally variable primer 18) and R (normally variable primer 20) were used in 3C reactions with primers 1-4 and 14-16. In wild type animals (top panels) some looping occurs between the shifted constant primers and variable primers indicated. However, in $D2^{p53RE}$ mutant animals, these loops are absent, indicating that the p53 enhancer region is necessary for looping. Note that constant L and constant R are directly outside the $D2^{p53RE}$ deletion.

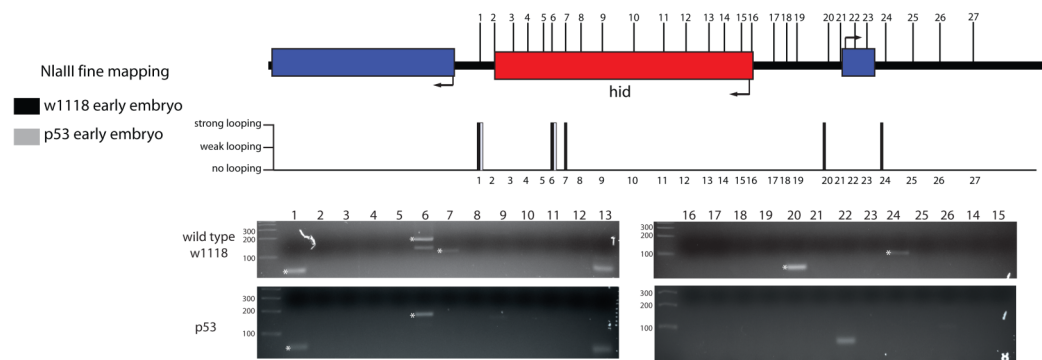


Figure 3-8. Fine mapping of looping contacts between the p53RE and Hid locus.

A schematic of Hid with primers designed to NlaIII cut sites (indicated with numbers) that were used in 3C reactions to map looping to the p53RE. Below is a graphical representation of NlaIII looping patterns with present or absent calls based on band intensity of ethidium bromide stained gels below. Four independent regions at the hid locus contact the p53RE and some are dependent upon p53. Note that these fine mapping loops recapitulate HindIII 3C reaction loops. Shino Murakami and Gianella Garcia-Hughes produced these data with my guidance.

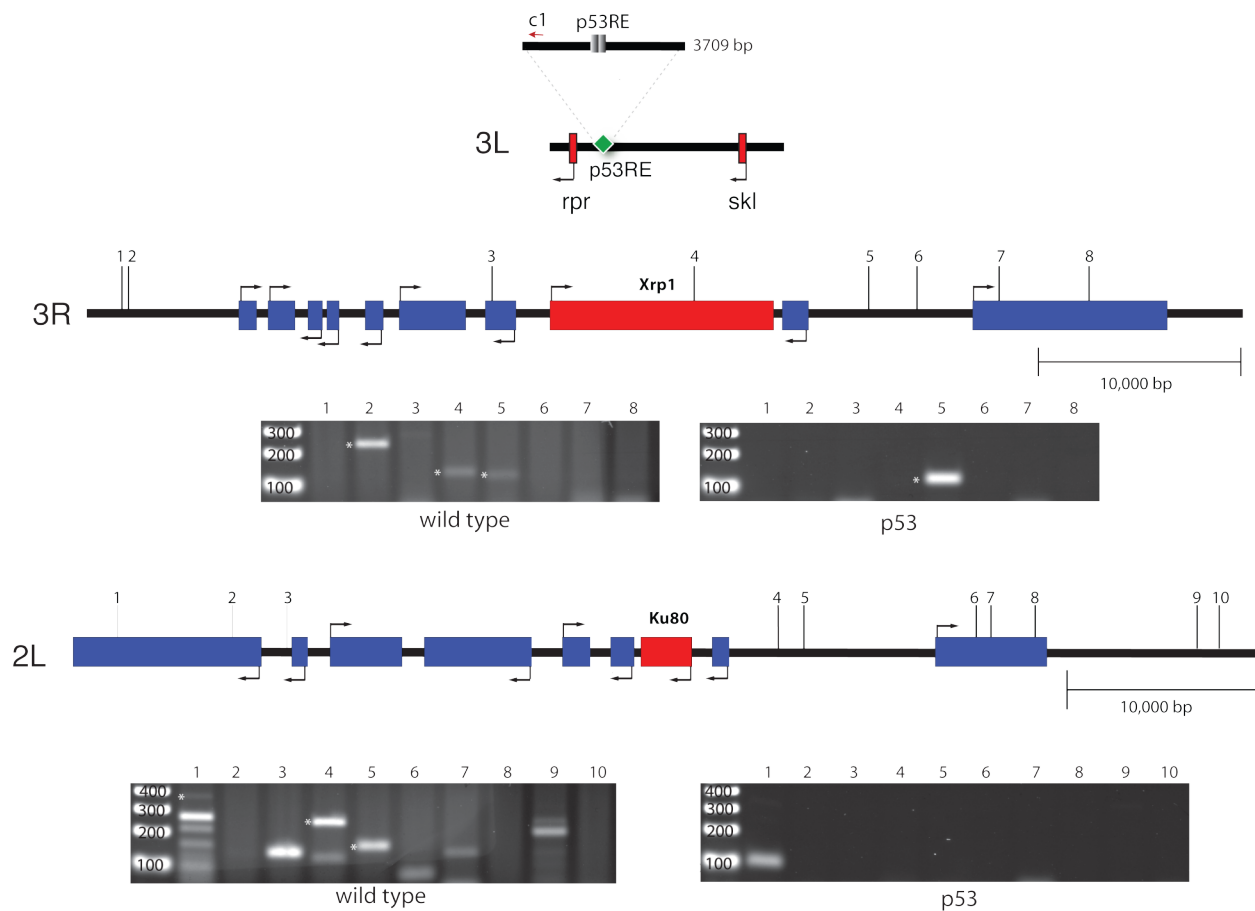


Figure 3-9. The p53 enhancer loops to multiple Radiation Induced, p53 dependent (RIPD) genes outside of the Reaper region.

A schematic of the *xrp1* and *ku80* regions with the p53 enhancer region (see insert). RIPD genes are shown in red, and non-relevant genes are shown in blue. To detect looping contacts between the p53 enhancer region and distant sites on 3R and 2L. The constant primer c1 was used in conjunction with labeled primers (see methods for sequences) designed at HindIII sites indicated with numbers throughout these regions in 3C reactions. Analysis of chromatin isolated from wild type (*w¹¹¹⁸* on left) and *p53*-animals are shown. Authentic bands demonstrating long-distance chromatin contacts are indicated by *. The p53RE loops to *xrp1* sequences near primers 2 and 4 in wild type animals but not in *p53* mutants. Looping to region 5 at *xrp1* is unaffected by *p53* status. The p53RE also loops to *ku80* at primer locations 1, 4, and 5 (noted by *) in wild type but not in *p53* mutant animals. Bands shown without asterisks are smaller than expected size.

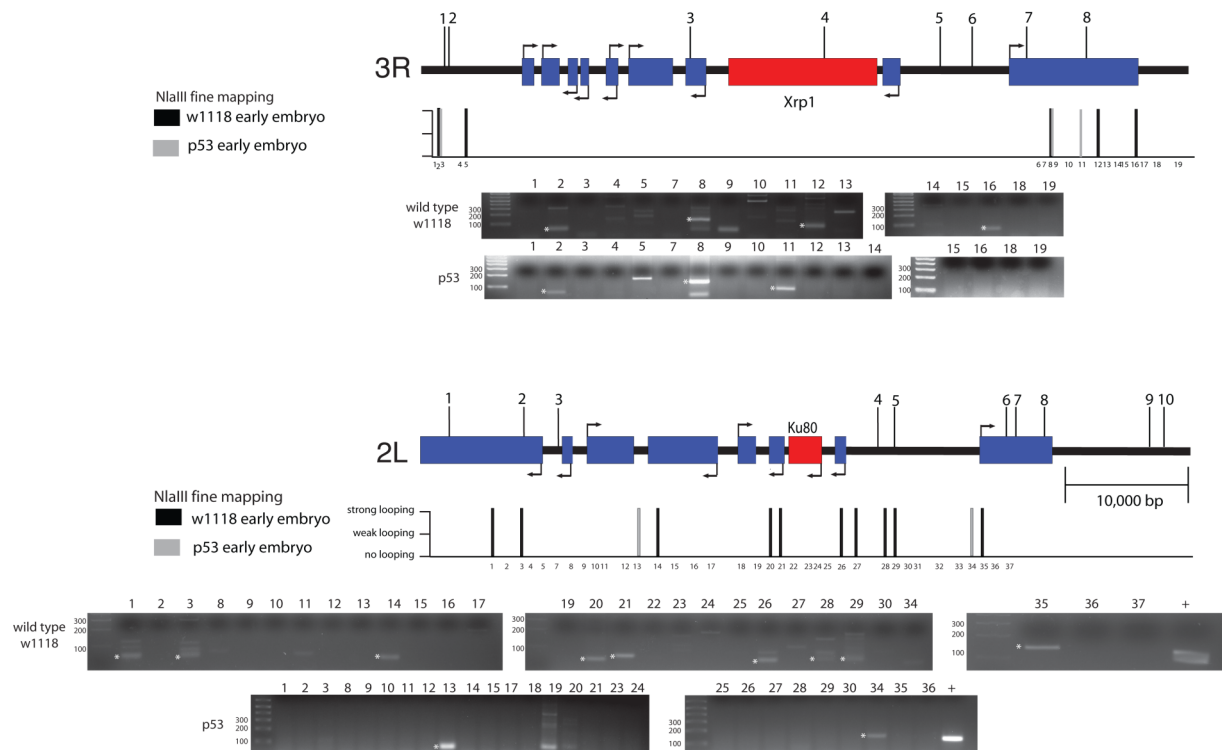


Figure 3-10. Fine mapping of looping contacts between the p53RE and distant loci *xrp1* and *ku80*.

A schematic of *xrp1* and *ku80* with primers designed to NlaIII cut sites that were used in 3C reactions to map looping to the p53RE. Below is a graphical representation of NlaIII looping patterns with present or absent calls based on band intensity on gels. Positive bands are indicated with an asterisk. Note that these fine mapping loops recapitulate HindIII 3C reaction loops. Shino Murakami and Gianella Garcia-Hughes produced these data with my guidance.

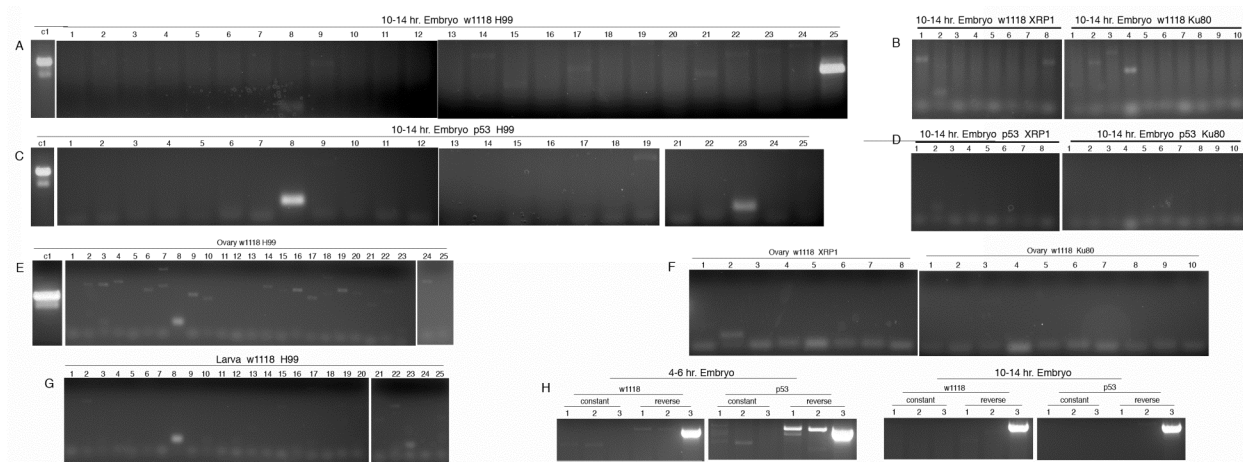


Figure 3-11. p53RE looping is developmentally dynamic.

Semi-quantitative PCR shows H99 chromosomal looping in late stage embryos (A, 10-14 hr) is severely diminished while completely absent in p53 mutant animals (C). Distant looping is retained to XRP1 and Ku80 in late stage embryos (B) but is dependent upon p53 (D). However, some looping around a previously reported BX-C appears unaffected (H), suggesting that all chromosomal structures forming looping are not eliminated. Adult female ovaries (E) show similar cis-looping patterns to early stage embryos but long-distance looping appears eliminated (F) while whole larval preparations (G) show no or severely diminished looping to genes in the Reaper region. Primers in the H99 region correspond to numbers annotated in Figure 3-5 while primers near XRP1 or Ku80 correspond to numbers in Figure 3-9 near XRP1 or Ku80. C1 is an internal control for the p53RE constant region. Shino Murakami generated this data with my guidance.

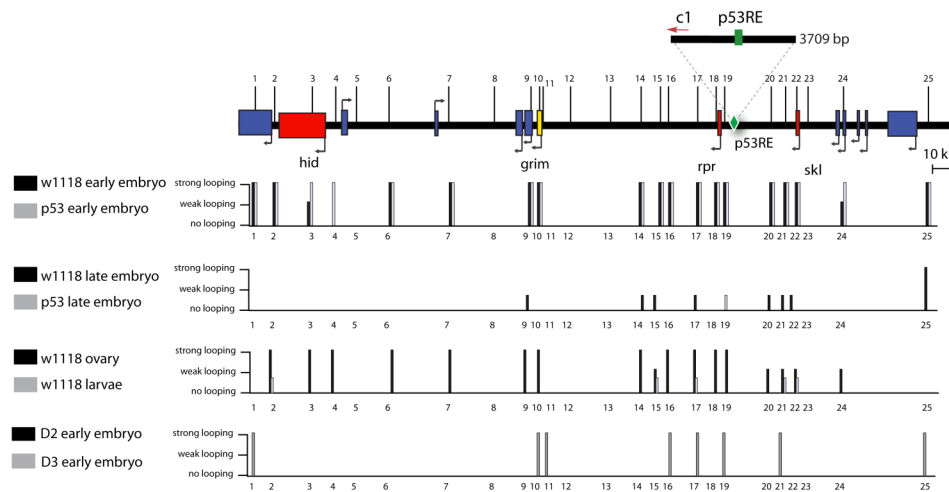


Figure 3-12. Reaper region looping is developmentally dynamic.

A schematic of the Rpr region with primers labeled and a graphical representation of Figure 3-11. Present or absent calls are based on band intensity. *D3^{control}* loops differ from wild type, but overall looping architecture remains the same.

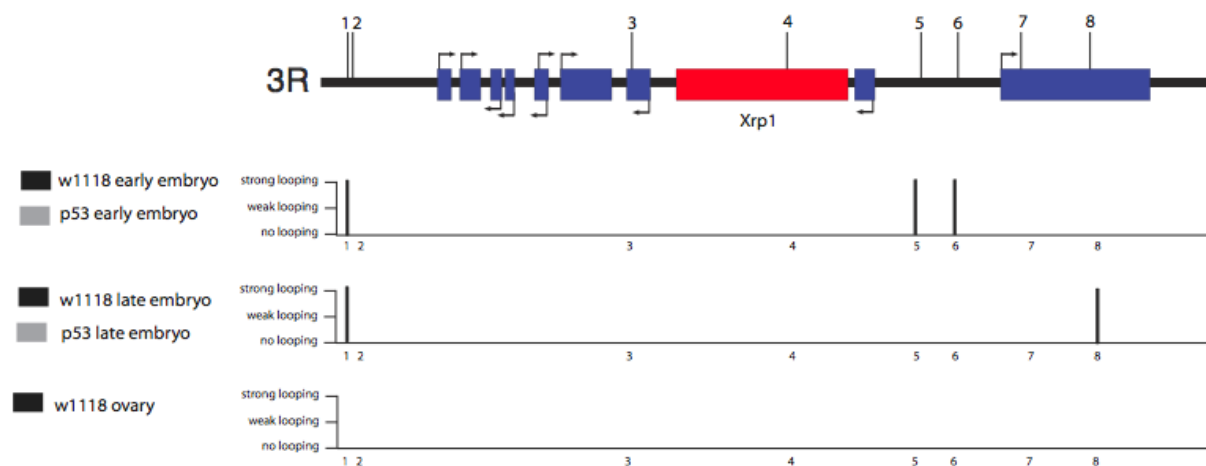


Figure 3-13. XRP1 region looping is developmentally dynamic.

A schematic of the Xrp1 region with primers labeled. Below are graphical representations of Figure 3-11. Present or absent calls are based on PCR band intensity.

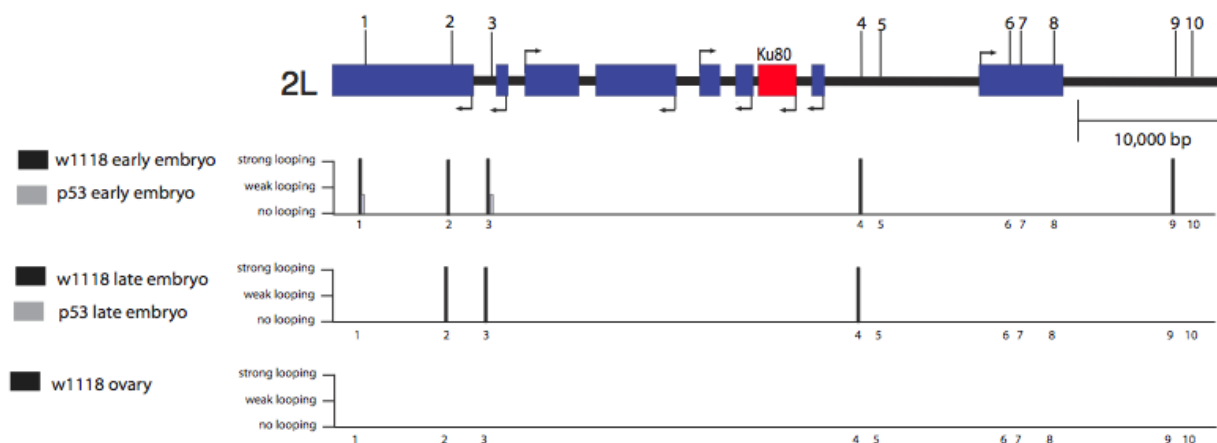


Figure 3-14. Ku80 region looping is developmentally dynamic.

A schematic of the Ku80 region with primers labeled. Below are graphical representations of Figure 3-11. Present or absent calls are based on PCR band intensity.

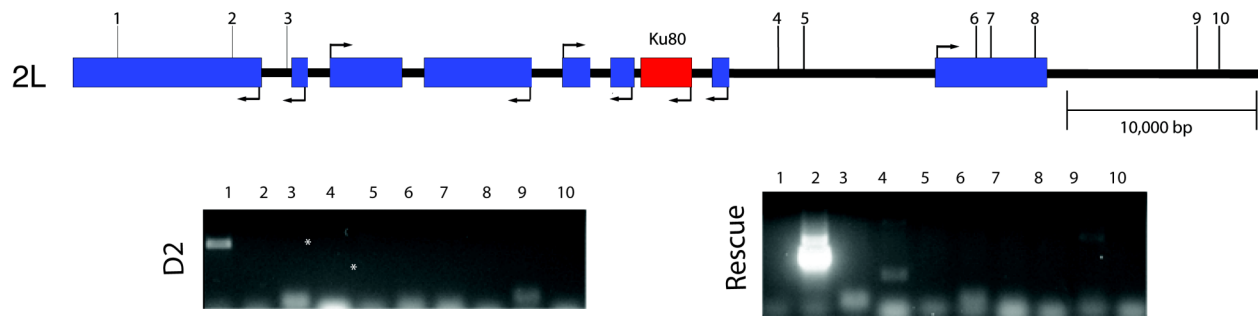


Figure 3-15. An exogenous rescue construct restores looping to the Ku80 region in $D2^{p53RE}$ mutants.

A schematic of *ku80* with primers designed to HindIII sites labeled with numbers. 3C reactions were carried out in $D2^{p53RE}$ mutant background (left) or $D2^{p53RE}$ mutants containing an exogenous rescue construct (right). $D2$ mutants show no looping between the p53RE and *ku80* while the rescue construct restores looping to regions around primer 2. These results are now being repeated and validated.

RIPD genes	Fold change (log2) D2IR VS WIR	Change p-value
rpr	-6.3	0.999998
skl	-6.2	0.999998
pyd	-2.8	0.999998
halo	-2.5	0.999975
Xrp1	-2.5	0.999998
eiger	-2.3	0.999998
CG12194	-2.3	0.999998
hid	-2.3	0.999998
spook	-2	0.999998
Corp	-1.8	0.999998
Pka-C3	-1.7	0.999998
CG15479	-1.7	0.999998
Gst D5	-1.4	0.999963
CG13204	-1.2	0.999998
CG18596	-1.1	0.999998
CG6272	-1.1	0.999998
CG9836	-0.9	0.999998
CG1555	-0.8	0.999284
mus205	-0.8	0.999998
eIF6	-0.6	0.999624
cul-2	-0.4	0.999997
CG1718	-0.3	0.999966

CG6171	0.4	0.000247
mus210	0.5	0.00001
CG12171	1.4	0.000002
CG11897	1.8	0.000002
RnrL	NC	0.052964
mre11	NC	0.5
CG5664	NC	0.5
escl	NC	0.5

Table 3-1. Affymetrix array data indicates RIPD genes require the p53RE for regulation

Affymetrix arrays were used to assay expression of wild type and $D2^{p53RE}$ RNA levels after ionizing radiation. The above are high stringency RIPD genes, their fold change when comparing irradiated D2 animals to irradiated wild type (w^{1118}) animals. 75% of RIPD genes require the p53RE for proper regulation after irradiation, with *rpr* and *skl* most dramatically affected.

Primers	Sequence
<i>grim</i> fwd	CGC TGC TGA TCT CGA AGG ATA TCT GAA
<i>grim</i> rev	AAG ACT TAA AGT GCA AGC AGT GAA TGG
<i>sickle</i> fwd	CGC ATG GAA TCT TAG CCA CAT ATT GCT
<i>sickle</i> rev	GAG AGA ATG AGC GAG ACA GTG ACA GAG A
<i>reaper</i> fwd	TTGCGATGGCTTGCGATATTTGCC
<i>reaper</i> rev	GTGTGCGCCAGCAACAAAGAACTA
<i>xrp1</i> fwd	AGCAACTACTCAGCCAGCTCCAGCTG
<i>xrp1</i> rev	TTCGTCCAAAGCGTAATC
<i>ku80</i> fwd	GGACGAATTACTTGCGGAAA
<i>ku80</i> rev	CGAGACTGAGGGCGTACTTC
<i>dark</i> fwd	CGCTATTGACTAGCTGCTGCTTGCTACCACCAC
<i>dark</i> rev	TTGAGAGCTCTCTAAACGTTCTGGAGCCCGCTG
<i>hid</i> fwd	CAGCCGCAACCACATCCGTCATAT
<i>hid</i> rev	TGGCAGACTGGATTATTGCTGCTG
<i>rp49</i> fwd	ACAAATGTGTATTCCGACCAGG
<i>rp49</i> rev	ATGACCATCCGCCAGCATACA

Table 3-2. Primer sequences used in RT-PCR reactions

BAC ID	gene	BAC ID	gene
CH321-80L05	<i>hid</i>	RP98-4F07	<i>Rpr</i> , p53RE, <i>grim</i>
CH321-74N02	<i>ku80</i>	CH321-90P12	<i>skl</i>
RP98-44N12	<i>xrp1</i>		
CH321-61B11	<i>hid</i>		

Table 3-3. BACs used to verify 3C primer pairs

Variable Primers **Sequence**

BC-X1	AAC ACT AGA CAA TAA CAC GCA AGG CGG C
BC-X2	ACG GAT ACG TCC GCC ATT GAA ATT CAA
BC-X3	CAT CTG CAA CAT CTG CAT ATT CGC ATT
xrp1	ACG TTT CGG ATT GGA GAT TGA GAA GTG G
xrp2	AAT AAC AGC AAC ATC ACT CAT ACG CAA G
xrp3	CAT TCA ATA TCT GCT GGA ATG TGG GTG A
xrp4	CAT TTC CCA CCT GAT GGC GCA GTT AAG A
xrp5	GAT AAG AAC ACT GCA CAG TTG TTA ATG GC
xrp6	GAG AGC GGT CAA TTA GGG AGT TTC ATC G
xrp7	AGA TAG AGT GAA ATG AGA ATG CAG GAG A
xrp8	CGC CTT TGT GTG ATA TTT GCC ATA GAC A
h991	CTC GAC TCC ATT TAG GTA TTC GGA TAG C
h992	AGG TTA ACA TAA TTG CCC AGC CTG GTG C
h993	ACT CTT TGC TTG TGG TTT TCG TTA TTG C
h994	ACA CTT ACT CGC ATT TAT CTC GGC TGA C
h995	ATA GTA TAG ACT CTC CAG ACT TCG GCA CG
h996	ATT CTA ACG CAC ACT CGG ACA TCC AGA A
h997	TAA CAA TGC GTG AAG TTT GTC GCC GCT T
h998	CCT TAC ACA ATC GTC TGA CAA CTG ACA A
h999	TGG TCA GAT TTG GGA ACT TCA CTT GTC T
h9910	TGG AAC CAC TAA CCC GCT TTC AAG TTA A
h9911	TAA CAA TGC CGA GCT GCC AGT TCT GTT

h9912	GCA AGA CAC GGC TCA GAT AGA TTT CTA CT
h9913	AGG TGA TAG GTG ATA CTG TGC TTG TTA C
h9914	TTG GTT TCC ATG AGC ATA AGC GTC CAG T
h9915	TTC AGT CGA GGC TTA ATG AAC AGT CTT G
h9916	TCC AGT CCA GTC CAT TGT TTG CCA TCA T
h9917	ACG CAA TTT ATC GGG AAA GTT TCG CAA G
h9918	CAA GGA AGA GTT CCG TTC CAT TTC TTG A
h9919	GTG CTC GGG TCA TTA ACT CAC TCT CCT A
h9920	GCT ACA CTT CTT TGA AGA ACA CAA TCG C
h9921	AGA CTT GGC AGC ATT AGC AAG GCA AAC A
h9922	TTA GAC GTG ACC TTG ACC AAT TTC CTG T
h9923	GGA GAC TAA GCT ACC TAC GTG AAT CTG A
h9924	GCC AGG TGG TGC CAT TAA TTG TAC ATA G
h9925	TAT CCC ATC AGT TAC CAA CGC AAT CAC G
ku801	TAA TTA GTT TGG TCA GGG CTG CGG AGG A
ku802	AAG AAC AGA GCG TGA GAA AGC GAG ACG
Ku803	AAC CAC AAT CCA CTC TCA ATC TCC AGC T
Ku804	CTA ATG ACA TTT GTG TGC CGT TGC AGA CA
Ku805	TGG TCG AGT ATT ATT GTG CGG ATC TCT A
Ku806	ACA GAT GAG CTT CGA GTA CAA CAT TCA G
Ku807	GGT TTG TGC AGA TGA GGT GGA CAA ATC TG
Ku808	CGA GGA TTC CAA GGC ATA CGA GGT TAT C
Ku809	TCT TAA AGT TCG GTA ACT TGG CTC GCT T

Ku8010	CGA GTT CAA ACT GGT TTT AAT CCC TGA TTC
--------	---

Constant primers	Sequence
Reverse h99 Constant	CAA TTA ATG AGT AAC AGA AGC GGA GAA CTC AC
h99 constant	GGC TAA TGA CCA GAT ACT CTG CTA TCC G
h99 reverse	AAG CTG ACA ACT CTC GTG AGT CCA TTG G
reverse BC-X constant	TAA CTG ACT GAA ATC CGA CAT CCC AAT CG
BC-X constant	TTG AAA CAG CAA CCC TAG TGT GAG TGT A

Table 3-4. Primer sequences used in 3C reactions

BIBLIOGRAPHY

Abbott, M.K., and Lengyel, J.A. (1991). Embryonic head involution and rotation of male terminalia require the *Drosophila* locus head involution defective. *Genetics* 129, 783-789.

Abrams, J.M. (1999). An emerging blueprint for apoptosis in *Drosophila*. *Trends in Cell Biology* 9, 435-440.

Adams, J.M., and Cory, S. (2002). Apoptosomes: engines for caspase activation. *Curr Opin Cell Biol* 14, 715-720.

Akdemir, F., Christich, A., Sogame, N., Chapo, J., and Abrams, J.M. (2007). p53 directs focused genomic responses in *Drosophila*. *Oncogene* 26, 5184-5193.

Akdemir, F., Farkas, R., Chen, P., Juhasz, G., Medved'ova, L., Sass, M., Wang, L., Wang, X., Chittaranjan, S., Gorski, S.M., *et al.* (2006). Autophagy occurs upstream or parallel to the apoptosome during histolytic cell death. *Development* 133, 1457-1465.

Ashkenas, J., Muschler, J., and Bissell, M.J. (1996). The extracellular matrix in epithelial biology: shared molecules and common themes in distant phyla. *Dev Biol* 180, 433-444.

Barolo, S., Castro, B., and Posakony, J.W. (2004). New *Drosophila* transgenic reporters: insulated P-element vectors expressing fast-maturing RFP. *Biotechniques* 36, 436-440, 442.

Bellotto, M., Bopp, D., Senti, K.A., Burke, R., Deak, P., Maroy, P., Dickson, B., Basler, K., and Hafen, E. (2002). Maternal-effect loci involved in *Drosophila* oogenesis and embryogenesis: P element-induced mutations on the third chromosome. *The International journal of developmental biology* 46, 149-157.

Bertone, P., Stolc, V., Royce, T.E., Rozowsky, J.S., Urban, A.E., Zhu, X., Rinn, J.L., Tongprasit, W., Samanta, M., Weissman, S., *et al.* (2004). Global Identification of Human Transcribed Sequences with Genome Tiling Arrays. *Science* (New York, NY).

Birney, E., Stamatoyannopoulos, J.A., Dutta, A., Guigo, R., Gingeras, T.R., Margulies, E.H., Weng, Z., Snyder, M., Dermitzakis, E.T., Thurman, R.E., *et al.* (2007).

Identification and analysis of functional elements in 1% of the human genome by the ENCODE pilot project. *Nature* **447**, 799-816.

Brodsky, M.H., Nordstrom, W., Tsang, G., Kwan, E., Rubin, G.M., and Abrams, J.M. (2000). *Drosophila* p53 binds a damage response element at the reaper locus. *Cell* **101**, 103-113.

Brodsky, M.H., Weinert, B.T., Tsang, G., Rong, Y.S., McGinnis, N.M., Golic, K.G., Rio, D.C., and Rubin, G.M. (2004). *Drosophila melanogaster* MNK/Chk2 and p53 regulate multiple DNA repair and apoptotic pathways following DNA damage. *Mol Cell Biol* **24**, 1219-1231.

Broihier, H.T., and Skeath, J.B. (2002). *Drosophila* homeodomain protein dHb9 directs neuronal fate via crossrepressive and cell-nonautonomous mechanisms. *Neuron* **35**, 39-50.

Bulger, M., and Groudine, M. (2010). Enhancers: the abundance and function of regulatory sequences beyond promoters. *Dev Biol* **339**, 250-257.

Carninci, P., Kasukawa, T., Katayama, S., Gough, J., Frith, M.C., Maeda, N., Oyama, R., Ravasi, T., Lenhard, B., Wells, C., *et al.* (2005). The transcriptional landscape of the mammalian genome. *Science (New York, NY)* **309**, 1559-1563.

Celniker, S.E., Dillon, L.A., Gerstein, M.B., Gunsalus, K.C., Henikoff, S., Karpen, G.H., Kellis, M., Lai, E.C., Lieb, J.D., MacAlpine, D.M., *et al.* (2009). Unlocking the secrets of the genome. *Nature* **459**, 927-930.

Cheng, J., Kapranov, P., Drenkow, J., Dike, S., Brubaker, S., Patel, S., Long, J., Stern, D., Tammana, H., Helt, G., *et al.* (2005). Transcriptional Maps of 10 Human Chromosomes at 5-Nucleotide Resolution. *Science (New York, NY)*.

Chew, S.K., Akdemir, F., Chen, P., Lu, W.J., Mills, K., Daish, T., Kumar, S., Rodriguez, A., and Abrams, J.M. (2004). The apical caspase dronc governs programmed and unprogrammed cell death in *Drosophila*. *Dev Cell* **7**, 897-907.

Chou, T.B., and Perrimon, N. (1996). The autosomal FLP-DFS technique for generating germline mosaics in *Drosophila melanogaster*. *Genetics* **144**, 1673-1679.

Christich, A., Kauppila, S., Chen, P., Sogame, N., Ho, S.I., and Abrams, J.M. (2002). The Damage-Responsive *Drosophila* Gene sickle Encodes a Novel IAP Binding Protein Similar to but Distinct from reaper, grim, and hid. *Curr Biol* **12**, 137-140.

Chureau, C., Chantalat, S., Romito, A., Galvani, A., Duret, L., Avner, P., and Rougeulle, C. (2010). Ftx is a non-coding RNA which affects Xist expression and chromatin structure within the X-inactivation center region. *Human molecular genetics*.

D'Orazi, G., Cecchinelli, B., Bruno, T., Manni, I., Higashimoto, Y., Saito, S., Gostissa, M., Coen, S., Marchetti, A., Del Sal, G., *et al.* (2002). Homeodomain-interacting protein kinase-2 phosphorylates p53 at Ser 46 and mediates apoptosis. *Nat Cell Biol* 4, 11-19.

Danial, N.N., and Korsmeyer, S.J. (2004). Cell death: critical control points. *Cell* 116, 205-219.

Dekker, J., Rippe, K., Dekker, M., and Kleckner, N. (2002). Capturing chromosome conformation. *Science (New York, NY)* 295, 1306-1311.

del Peso, L., Gonzalez, V.M., Inohara, N., Ellis, R.E., and Nunez, G. (2000). Disruption of the CED-9 center dot CED-4 complex by EGL-1 is a critical step for programmed cell death in *Caenorhabditis elegans*. *Journal of Biological Chemistry* 275, 27205-27211.

Di Stefano, V., Blandino, G., Sacchi, A., Soddu, S., and D'Orazi, G. (2004). HIPK2 neutralizes MDM2 inhibition rescuing p53 transcriptional activity and apoptotic function. *Oncogene* 23, 5185-5192.

Di Stefano, V., Mattiussi, M., Sacchi, A., and D'Orazi, G. (2005). HIPK2 inhibits both MDM2 gene and protein by, respectively, p53-dependent and independent regulations. *FEBS Lett* 579, 5473-5480.

Dorstyn, L., Mills, K., Lazebnik, Y., and Kumar, S. (2004). The two cytochrome c species, DC3 and DC4, are not required for caspase activation and apoptosis in *Drosophila* cells. *J Cell Biol* 167, 405-410.

Dorstyn, L., Read, S., Cakouros, D., Huh, J.R., Hay, B.A., and Kumar, S. (2002). The role of cytochrome c in caspase activation in *Drosophila melanogaster* cells. *J Cell Biol* 156, 1089-1098.

Duncan, I.W. (2002). Transvection effects in *Drosophila*. *Annu Rev Genet* 36, 521-556.

Erkner, A., Roure, A., Charroux, B., Delaage, M., Holway, N., Core, N., Vola, C., Angelats, C., Pages, F., Fasano, L., *et al.* (2002). Grunge, related to human Atrophin-like proteins, has multiple functions in *Drosophila* development. *Development* 129, 1119-1129.

Garner, _____ W.s.
http://innovationswmededu/research/instrumentation/higher_pages/inst_doc_about.html.

Hagege, H., Klous, P., Braem, C., Splinter, E., Dekker, J., Cathala, G., de Laat, W., and Forne, T. (2007). Quantitative analysis of chromosome conformation capture assays (3C-qPCR). *Nat Protoc* 2, 1722-1733.

Hao, Z., Duncan, G.S., Chang, C.C., Elia, A., Fang, M., Wakeham, A., Okada, H., Calzascia, T., Jang, Y., You-Ten, A., *et al.* (2005). Specific ablation of the apoptotic functions of cytochrome C reveals a differential requirement for cytochrome C and Apaf-1 in apoptosis. *Cell* 121, 579-591.

Hengartner, M.O., Ellis, R.E., and Horvitz, H.R. (1992). *Caenorhabditis elegans* gene *ced-9* protects cells from programmed cell death. *Nature* 356, 494-499.

Hofmann, T.G., Moller, A., Sirma, H., Zentgraf, H., Taya, Y., Droge, W., Will, H., and Schmitz, M.L. (2002). Regulation of p53 activity by its interaction with homeodomain-interacting protein kinase-2. *Nat Cell Biol* 4, 1-10.

Huarte, M., Guttman, M., Feldser, D., Garber, M., Koziol, M.J., Kenzelmann-Broz, D., Khalil, A.M., Zuk, O., Amit, I., Rabani, M., *et al.* (2010). A large intergenic noncoding RNA induced by p53 mediates global gene repression in the p53 response. *Cell* 142, 409-419.

Igaki, T., Kanda, H., Yamamoto-Goto, Y., Kanuka, H., Kuranaga, E., Aigaki, T., and Miura, M. (2002). Eiger, a TNF superfamily ligand that triggers the *Drosophila* JNK pathway. *Embo J* 21, 3009-3018.

Jacobson, M.D., Weil, M., and Raff, M.C. (1997). Programmed Cell death in Animal Development. *Cell* 88, 347-354.

Jaklevic, B.R., and Su, T.T. (2004). Relative contribution of DNA repair, cell cycle checkpoints, and cell death to survival after DNA damage in *Drosophila* larvae. *Curr Biol* 14, 23-32.

Jin, S., Martinek, S., Joo, W.S., Wortman, J.R., Mirkovic, N., Sali, A., Yandell, M.D., Pavletich, N.P., Young, M.W., and Levine, A.J. (2000). Identification and characterization of a p53 homologue in *Drosophila melanogaster*. *Proc Natl Acad Sci U S A* 97, 7301-7306.

Johnson, S.A., and Milner, J. (1987). The final stages of wing development in *Drosophila melanogaster*. *Tissue Cell* 19, 505-513.

Johnstone, O., Deuring, R., Bock, R., Linder, P., Fuller, M.T., and Lasko, P. (2005). Belle is a *Drosophila* DEAD-box protein required for viability and in the germ line. *Dev Biol* 277, 92-101.

Kagey, M.H., Newman, J.J., Bilodeau, S., Zhan, Y., Orlando, D.A., van Berkum, N.L., Ebmeier, C.C., Goossens, J., Rahl, P.B., Levine, S.S., *et al.* (2010). Mediator and cohesin connect gene expression and chromatin architecture. *Nature* 467, 430-435.

Kapranov, P., Cawley, S.E., Drenkow, J., Bekiranov, S., Strausberg, R.L., Fodor, S.P., and Gingeras, T.R. (2002). Large-scale transcriptional activity in chromosomes 21 and 22. *Science (New York, NY)* 296, 916-919.

Katayama, S., Tomaru, Y., Kasukawa, T., Waki, K., Nakanishi, M., Nakamura, M., Nishida, H., Yap, C.C., Suzuki, M., Kawai, J., *et al.* (2005). Antisense transcription in the mammalian transcriptome. *Science (New York, NY)* 309, 1564-1566.

Kerr, J.F.R., and Harmon, B.V. (1991). Definition and incidence of apoptosis: an historical perspective. In *Apoptosis: the molecular basis of cell death* (New York, Cold Spring Harbor Laboratory Press), pp. 5-29.

Kerr, J.F.R., Wyllie, A.H., and Currie, A.R. (1972). Apoptosis: a basic biological phenomenon with wide ranging implications in tissue kinetics. *Br J Cancer* 26, 239-257.

Kiger, J.A., Jr., Natzle, J.E., Kimbrell, D.A., Paddy, M.R., Kleinhesselink, K., and Green, M.M. (2007). Tissue remodeling during maturation of the *Drosophila* wing. *Dev Biol* 301, 178-191.

Kim, Y.H., Choi, C.Y., Lee, S.J., Conti, M.A., and Kim, Y. (1998). Homeodomain-interacting protein kinases, a novel family of co-repressors for homeodomain transcription factors. *J Biol Chem* 273, 25875-25879.

Kimura, K., Kodama, A., Hayasaka, Y., and Ohta, T. (2004). Activation of the cAMP/PKA signaling pathway is required for post-ecdysial cell death in wing epidermal cells of *Drosophila melanogaster*. *Development* 131, 1597-1606.

Kosman, D., Small, S., and Reinitz, J. (1998). Rapid preparation of a panel of polyclonal antibodies to *Drosophila* segmentation proteins. *Dev Genes Evol* 208, 290-294.

Kroemer, G., and Martin, S.J. (2005). Caspase-independent cell death. *Nat Med* 11, 725-730.

Kuida, K., Haydar, T.F., Kuan, C.Y., Gu, Y., Taya, C., Karasuyama, H., Su, M.S.S., Rakic, P., and Flavell, R.A. (1998). Reduced Apoptosis and Cytochrome C-Mediated Caspase Activation in Mice Lacking Caspase 9. *Cell* 94, 325-337.

Kuida, K., Zheng, T.S., Na, S.Q., Kuan, C.Y., Yang, D., Karasuyama, H., Rakic, P., and Flavell, R.A. (1996). Decreased apoptosis in the brain and premature lethality in cyp32-deficient mice. *Nature* 384, 368-372.

Kuranaga, E., Kanuka, H., Igaki, T., Sawamoto, K., Ichijo, H., Okano, H., and Miura, M. (2002). Reaper-mediated inhibition of DIAP1-induced DTRAF degradation results in activation of JNK in *Drosophila*. *Nature Cell Biology* 4, 705-710.

Lanzuolo, C., Roure, V., Dekker, J., Bantignies, F., and Orlando, V. (2007). Polycomb response elements mediate the formation of chromosome higher-order structures in the bithorax complex. *Nat Cell Biol* 9, 1167-1174.

Lawrence, P.A. (1992). *The making of a fly: the genetics of animal design* (London, Blackwell Scientific Publications).

Lee, J.H., Lee, E., Park, J., Kim, E., Kim, J., and Chung, J. (2003). In vivo p53 function is indispensable for DNA damage-induced apoptotic signaling in *Drosophila*. *FEBS Lett* 550, 5-10.

Li, P., Nijhawan, D., Budihardjo, I., Srinivasula, S.M., Ahmad, M., Alnemri, E.S., and Wang, X.D. (1997). Cytochrome c and datp-dependent formation of apaf-1/caspase-9 complex initiates an apoptotic protease cascade. *Cell* 91, 479-489.

Lindsley, D.L., and Zimm, G.G. (1992). *The genome of Drosophila melanogaster* (San Diego, Academic Press).

Lu, W.J., and Abrams, J.M. (2006). Lessons from p53 in non-mammalian models. *Cell Death Differ* 13, 909-912.

Lu, W.J., Chapo, J., Roig, I., and Abrams, J.M. (2010). Meiotic recombination provokes functional activation of the p53 regulatory network. *Science* (New York, NY) 328, 1278-1281.

Luchnik, A.N., Hisamutdinov, T.A., and Georgiev, G.P. (1988). Inhibition of transcription in eukaryotic cells by X-irradiation: relation to the loss of topological constraint in closed DNA loops. *Nuc Acids Res* **16**, 5175-5190.

Luebke, K.J., Balog, R.P., Mittelman, D., and Garner, H.R. (2002). Digital Optical Chemistry: A Novel System for the Rapid Fabrication of Custom Oligonucleotide Arrays. In *Microfabricated Sensors, Application of Optical Technology for DNA Analysis*, A.U.a.W.T.L. Richard Kordal, ed. (American Chemical Society Publications).

Manak, J.R., Dike, S., Sementchenko, V., Kapranov, P., Biemar, F., Long, J., Cheng, J., Bell, I., Ghosh, S., Piccolboni, A., *et al.* (2006a). Biological function of unannotated transcription during the early development of *Drosophila melanogaster*. *Nature genetics* **38**, 1151-1158.

Manak, J.R., Dike, S., Sementchenko, V., Kapranov, P., Biemar, F., Long, J., Cheng, J., Bell, I., Ghosh, S., Piccolboni, A., *et al.* (2006b). Biological function of unannotated transcription during the early development of *Drosophila melanogaster*. *Nat Genet*.

Menendez, D., Inga, A., and Resnick, M.A. (2009). The expanding universe of p53 targets. *Nat Rev Cancer* **9**, 724-737.

Muro, I., Berry, D.L., Huh, J.R., Chen, C.H., Huang, H., Yoo, S.J., Guo, M., Baehrecke, E.H., and Hay, B.A. (2006). The *Drosophila* caspase Ice is important for many apoptotic cell deaths and for spermatid individualization, a nonapoptotic process. *Development* **133**, 3305-3315.

Nordstrom, W., Chen, P., Steller, H., and Abrams, J.M. (1996). Activation of the reaper gene during ectopic cell killing in *drosophila*. *Developmental Biology* **180**, 213-226.

Oh, S.W., Kingsley, T., Shin, H.H., Zheng, Z., Chen, H.W., Chen, X., Wang, H., Ruan, P., Moody, M., and Hou, S.X. (2003). A P-element insertion screen identified mutations in 455 novel essential genes in *Drosophila*. *Genetics* **163**, 195-201.

Ollmann, M., Young, L.M., Di Como, C.J., Karim, F., Belvin, M., Robertson, S., Whittaker, K., Demsky, M., Fisher, W.W., Buchman, A., *et al.* (2000). *Drosophila* p53 is a structural and functional homolog of the tumor suppressor p53. *Cell* **101**, 91-101.

Orom, U.A., Derrien, T., Beringer, M., Gumireddy, K., Gardini, A., Bussotti, G., Lai, F., Zytynicki, M., Notredame, C., Huang, Q., *et al.* (2010). Long noncoding RNAs with enhancer-like function in human cells. *Cell* **143**, 46-58.

Parks, A.L., Cook, K.R., Belvin, M., Dompe, N.A., Fawcett, R., Huppert, K., Tan, L.R., Winter, C.G., Bogart, K.P., Deal, J.E., *et al.* (2004). Systematic generation of high-resolution deletion coverage of the *Drosophila melanogaster* genome. *Nat Genet* 36, 288-292.

Peters, M., DeLuca, C., Hirao, A., Stambolic, V., Potter, J., Zhou, L., Liepa, J., Snow, B., Arya, S., Wong, J., *et al.* (2002). Chk2 regulates irradiation-induced, p53-mediated apoptosis in *Drosophila*. *Proc Natl Acad Sci U S A* 99, 11305-11310.

Petruk, S., Sedkov, Y., Riley, K.M., Hodgson, J., Schweisguth, F., Hirose, S., Jaynes, J.B., Brock, H.W., and Mazo, A. (2006). Transcription of bxd noncoding RNAs promoted by trithorax represses Ubx in cis by transcriptional interference. *Cell* 127, 1209-1221.

Potts, P.R., Singh, S., Knezek, M., Thompson, C.B., and Deshmukh, M. (2003). Critical function of endogenous XIAP in regulating caspase activation during sympathetic neuronal apoptosis. *The Journal of cell biology* 163, 789-799.

Raney, B.J., Cline, M.S., Rosenbloom, K.R., Dreszer, T.R., Learned, K., Barber, G.P., Meyer, L.R., Sloan, C.A., Malladi, V.S., Roskin, K.M., *et al.* ENCODE whole-genome data in the UCSC genome browser (2011 update). *Nucleic acids research* 39, D871-875.

Rinn, J.L., Euskirchen, G., Bertone, P., Martone, R., Luscombe, N.M., Hartman, S., Harrison, P.M., Nelson, F.K., Miller, P., Gerstein, M., *et al.* (2003). The transcriptional activity of human Chromosome 22. *Genes Dev* 17, 529-540.

Rinn, J.L., Kertesz, M., Wang, J.K., Squazzo, S.L., Xu, X., Brugmann, S.A., Goodnough, L.H., Helms, J.A., Farnham, P.J., Segal, E., *et al.* (2007). Functional demarcation of active and silent chromatin domains in human HOX loci by noncoding RNAs. *Cell* 129, 1311-1323.

Rodriguez, A., Oliver, H., Zou, H., Chen, P., Wang, X.D., and Abrams, J.M. (1999). Dark is a *Drosophila* homologue of Apaf-1/CED-4 and functions in an evolutionarily conserved death pathway. *Nature Cell Biology* 1, 272-279.

Rogulja-Ortmann, A., Luer, K., Seibert, J., Rickert, C., and Technau, G.M. (2007). Programmed cell death in the embryonic central nervous system of *Drosophila melanogaster*. *Development* 134, 105-116.

Roy, S., Ernst, J., Kharchenko, P.V., Kheradpour, P., Negre, N., Eaton, M.L., Landolin, J.M., Bristow, C.A., Ma, L., Lin, M.F., *et al.* (2010). Identification of Functional Elements

and Regulatory Circuits by *Drosophila* modENCODE. *Science* (New York, NY) **330**, 1787-1797.

Salvesen, G.S., and Abrams, J.M. (2004). Caspase activation - stepping on the gas or releasing the brakes? *Lessons from humans and flies. Oncogene* **23**, 2774-2784.

Shin, J., Bossenz, M., Chung, Y., Ma, H., Byron, M., Taniguchi-Ishigaki, N., Zhu, X., Jiao, B., Hall, L.L., Green, M.R., *et al.* (2010). Maternal Rnf12/RLIM is required for imprinted X-chromosome inactivation in mice. *Nature* **467**, 977-981.

Shoemaker, D.D., Schadt, E.E., Armour, C.D., He, Y.D., Garrett-Engle, P., McDonagh, P.D., Loerch, P.M., Leonardson, A., Lum, P.Y., Cavet, G., *et al.* (2001). Experimental annotation of the human genome using microarray technology. *Nature* **409**, 922-927.

Sogame, N., Kim, M., and Abrams, J.M. (2003). *Drosophila* p53 preserves genomic stability by regulating cell death. *Proc Natl Acad Sci U S A* **100**, 4696-4701.

Stolc, V., Gauhar, Z., Mason, C., Halasz, G., van Batenburg, M.F., Rifkin, S.A., Hua, S., Herreman, T., Tongprasit, W., Barbano, P.E., *et al.* (2004). A gene expression map for the euchromatic genome of *Drosophila melanogaster*. *Science* (New York, NY) **306**, 655-660.

Su, Y.C., Treisman, J.E., and Skolnik, E.Y. (1998). The *Drosophila* Ste20-related kinase misshapen is required for embryonic dorsal closure and acts through a JNK MAPK module on an evolutionarily conserved signaling pathway. *Genes Dev* **12**, 2371-2380.

Thibault, S.T., Singer, M.A., Miyazaki, W.Y., Milash, B., Dompe, N.A., Singh, C.M., Buchholz, R., Demsky, M., Fawcett, R., Francis-Lang, H.L., *et al.* (2004). A complementary transposon tool kit for *Drosophila melanogaster* using P and piggyBac. *Nat Genet* **36**, 283-287.

Vaux, D.L., and Korsmeyer, S.J. (1999). Cell death in development. *Cell* **96**, 245-254.

Vegh, M., and Basler, K. (2003). A genetic screen for hedgehog targets involved in the maintenance of the *Drosophila* anteroposterior compartment boundary. *Genetics* **163**, 1427-1438.

Venken, K.J., Carlson, J.W., Schulze, K.L., Pan, H., He, Y., Spokony, R., Wan, K.H., Koriabine, M., de Jong, P.J., White, K.P., *et al.* (2009). Versatile P[acman] BAC libraries for transgenesis studies in *Drosophila melanogaster*. *Nat Methods* **6**, 431-434.

Vousden, K.H., and Lu, X. (2002). Live or let die: the cell's response to p53. *Nat Rev Cancer* 2, 594-604.

Vousden, K.H., and Prives, C. (2005). P53 and prognosis: new insights and further complexity. *Cell* 120, 7-10.

Vousden, K.H., and Prives, C. (2009). Blinded by the Light: The Growing Complexity of p53. *Cell* 137, 413-431.

White, K., Grether, M., Abrams, J.M., Young, L., Farrell, K., and Steller, H. (1994). Genetic Control of Programmed Cell Death in *Drosophila*. *Science* (New York, NY) 264, 677-683.

Williams, A., Spilianakis, C.G., and Flavell, R.A. (2010). Interchromosomal association and gene regulation in trans. *Trends Genet* 26, 188-197.

Wolff, T., and Ready, D.F. (1991). Cell death in normal and rough eye mutants of *Drosophila*. *Dev Biol* 113, 825-839.

Wyllie, A.H., Kerr, J.F.R., and Currie, A.R. (1980). Cell death: the significance of apoptosis. *Int Rev Cytol* 68, 251-306.

Xu, D., Li, Y., Arcaro, M., Lackey, M., and Bergmann, A. (2005). The CARD-carrying caspase Dronc is essential for most, but not all, developmental cell death in *Drosophila*. *Development* 132, 2125-2134.

Xu, J., Xin, S., and Du, W. (2001). *Drosophila* Chk2 is required for DNA damage-mediated cell cycle arrest and apoptosis. *FEBS Lett* 508, 394-398.

Xu, P., Vernooy, S.Y., Guo, M., and Hay, B.A. (2003). The *Drosophila* MicroRNA Mir-14 Suppresses Cell Death and Is Required for Normal Fat Metabolism. *Curr Biol* 13, 790-795.

Yin, V.P., and Thummel, C.S. (2005). Mechanisms of steroid-triggered programmed cell death in *Drosophila*. *Semin Cell Dev Biol* 16, 237-243.

Yoshida, H., Kong, Y.Y., Yoshida, R., Elia, A.J., Hakem, A., Hakem, R., Penninger, J.M., and Mak, T.W. (1998). Apaf1 Is Required For Mitochondrial Pathways of Apoptosis and Brain Development. *Cell* 94, 739-750.

Yu, X., Wang, L., Acehan, D., Wang, X., and Akey, C.W. (2005). Three-dimensional Structure of a Double Apoptosome Formed by the *Drosophila* Apaf-1 Related Killer. *J Mol Biol.*

Yu, X., Wang, L., Acehan, D., Wang, X., and Akey, C.W. (2006). Three-dimensional structure of a double apoptosome formed by the *Drosophila* Apaf-1 related killer. *Journal of molecular biology* *355*, 577-589.

Yuan, J., and Horvitz, H.R. (1992). The *Caenorhabditis elegans* cell death gene *ced-4* encodes a novel protein and is expressed during the period of extensive programmed cell death. *Development* *116*, 309-320.

Zhang, Q., Yoshimatsu, Y., Hildebrand, J., Frisch, S.M., and Goodman, R.H. (2003). Homeodomain interacting protein kinase 2 promotes apoptosis by downregulating the transcriptional corepressor CtBP. *Cell* *115*, 177-186.

Zhang, S., Xu, L., Lee, J., and Xu, T. (2002). *Drosophila* atrophia homolog functions as a transcriptional corepressor in multiple developmental processes. *Cell* *108*, 45-56.